ulm university universität

uulm

Ulm University | 89069 Ulm | Germany

Faculty of Natural Sciences

Institute of Organic Chemistry III
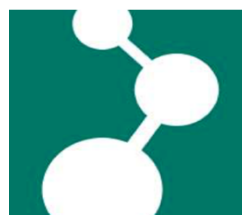
Master thesis

Adapting the properties of redox-active polydopamine thin films using different monomers

Sruthi Sunder

MS Advanced Materials - Universität Ulm

Synthesis of Macromolecules - Max Planck Institute for Polymer Research

Submitted in April 2019

First Reviewer: Prof. Dr. Tanja Weil

Second Reviewer: Dr. Katrin Wunderlich

Ph.D. Mentors: Sean Harvey, Tommaso Marchesi

TABLE OF CONTENTS

ACKNOWLEDGEMENTS

Standing on the shoulders of giants, contributing to scientific research and generating logical data would be nearly impossible without the help of human connections such as those with my mentors, peers and the support of friends and family. I would like to start by acknowledging Prof. Dr. Tanja Weil at the Max Planck Institute for Polymer Research for hosting me in her research group during my master thesis, as well as for her valuable expertise and input during all group meetings and discussion sessions. I thank Dr. Katrin Wunderlich for her patience and the guidance she provided me with at every step of the way, ensuring that my thesis was a truly enriching, smooth, and knowledge-filled experience. My appreciation goes out to the valuable encouragement given to me by Sean Harvey, Tommaso Marchesi, Lisa Hüeske and Xu Ning, keeping in mind all the formal and informal discussions that helped shape several ideas and to put my thesis into gear. I thank the technicians and staff at the MPIP who provided me with insightful training for operating several instruments during the course of my experiments and likewise, thank them for the measurements that contributed to the data presented in my thesis. Leaving out several colleagues from the MPIP who interacted with me in informal discussions all through my time there would make this list incomplete. This thesis would also have been impossible without the support from my course lecturers at Ulm University, Ulm and especially in providing me with the background knowledge that equipped me to do my thesis. Helping level my theoretical knowledge with practical knowledge was truly useful in all aspects of my ongoing work. This list would be incomplete without gratitude for my family back home who very much shaped the support I needed throughout my thesis – I am truly grateful for them endlessly reassuring my motivation to work to the best of my abilities. I thank my parents, my younger sister and my grandparents and relatives abroad who were always there for me. Orienting myself towards this novel topic would have been difficult without various authors, unpublished and published, whom I thank for providing me with valuable data and insight into the window into the world of polymer science, photocatalysis and clean energy. I dedicate this work to my late grandparents.

ABSTRACT

Polydopamine-derived systems have found great potential applications that are distributed across the fields of materials science, biomedicine, energy, environmental science, and clean engineering applications like hydrogen generation through photocatalytic water-splitting (PWS). As a sacrificial reagent to be used in hybrid systems with PDA + CdSe@CdS sensitizers for PWS, polydopamine has catechol and quinone moieties in a pH- dependent redox equilibrium with each other that allows self-regulation and protection of the sensitizers. In this thesis, an attempt was made to adapt the properties of the polydopamine sacrificial layer by extending the parameters and conditions used for polydopamine thin film synthesis by electropolymerization to other homopolymer films synthesized from different monomers: 3-amino-L-tyrosine, p-phenylenediamine and serotonin. CV studies with PDA + ALT (3:1) and PDA + p-PDA (3:1) films showed that the oxidation and reduction potentials adapted the electrochemical response of PDA to varying pH environments (in the range 4.6-7.3) and that the peak separation values ΔE_{ps} depend on the scan rate (ϑ) at which they are analyzed with lower ϑ being ideal to prevent electrode fouling effects. These monomers incorporate aromatic amino groups into PDA behaving similarly to n-dopants for an intrinsic semiconductor and could potentially increase electron mobility, charge carrier concentration and electron-hole recombination time. Several films synthesized were characterized using cyclic voltammetry, ATR-FTIR, AFM, and XPS. The copolymer systems PDA + p-PDA (3:1) and PDA + ALT (3:1) present promising features for use in PWS and could also be extended to applications such as pH sensing. The novel electron systems of these copolymers present possibilities for tuning the electron transfer characteristics, π electron delocalization and electron recombination time in the sacrificial layer of the hybrid systems. This property can be extended for use of these copolymers in conjunction with Organic Field Effect Transistors, or for creating devices using lithographic techniques for biosensing applications.

Keywords: Polydopamine, copolymerization, cyclic voltammetry, materials science

LIST OF ABBREVIATIONS

5-HT: 5-hydroxytryptamine/serotonin

AD: Aromatic diamines

ADC: Analog to Digital Converter

AFM: Atomic Force Microscope/Microscopy)

ALT/p-ALT: Polyaminotyrosine

ATR -FTIR: Attenuated Total Reflection Fourier Transform IR Spectroscopy

BFC: Biofuel Cell

C.B.: Conduction Band

C.E.: Counter Electrode

CV: Cyclic Voltammetry

DA: Dopamine

DFT: Density Functional Theory

E-T: Everhart- Thornley

EDX: Energy Dispersive X-ray spectroscopy

HEPES: (4-(2-hydroxyethyl)-1-piperazineethanesulfonic acid

HOMO: Highest Occupied Molecular Orbital

LUMO: Lowest Unoccupied Molecular Orbital

NHE: Normal Hydrogen Electrode

p-PDA: Polyphenylenediamine

p-Ser: Polyserotonin

PB: Phosphate buffer

PDA: Polydopamine

R.E.: Reference Electrode

S.D: Standard Deviation

SAM: Self-assembled Monolayers

SEM: Scanning Electron Microscopy

Tris – Tris(hydroxymethyl)aminomethane

V.B.: Valence Band

W.E.: Working Electrode

XPS: X-ray photoelectron spectroscopy

STRUCTURE OF THE THESIS

Note: An executive summary of the data in this thesis can be found in Section 4.6.

Chapter 1: Introduction provides an insight into the basics of the photocatalytic water-splitting (PWS) (section 1.1) process and parameters that contribute towards its optimization. It explains the introductory details of polydopamine (section 1.2), its structure and synthesis methods as well as basic details of the monomers used in the project work (sections 1.3 - 1.5). The chapter enumerates several synthesis and characterization techniques used in this thesis (section 1.6) such as electropolymerization, cyclic voltammetry, profilometry, AFM, ATR-FTIR, XPS, SEM, EDX and contact angle measurements. The working principles behind the instruments used as well as their setups are given in this chapter to supplement the characterization results provided later.

Chapter 2: Motivation and Objectives explains a brief history of work leading up to the work in this thesis (section 2.1) as well as the reasons for the use of polydopamine in PWS and several monomers put forward in the introduction. It provides reasons for the novelty of the thesis and using literature-based examples, lists the long-term and experimental aims of this thesis keeping in mind that the goal is to adapt the redox-active polydopamine thin film for use in photocatalytic water-splitting (section 2.2).

Chapter 3: Experimental Section provides information about the techniques, materials, and methods used in gathering data for this thesis. It details the techniques for preparation of homopolymers (section 3.1) PDA, p-ALT, p-PDA and p-Ser as well as copolymers prepared using PDA and other monomers by electropolymerization (section 3.2). The chapter briefly states the instruments used with their manufacturer details along with information about sample preparation for characterization techniques and the methodology used in the characterization of the samples (see section 3.3). The software and hardware used in each case is listed as well.

Chapter 4: Results and Discussion provides data and detailed analysis obtained from experiments performed as well as literature review at appropriate points for understanding and critically evaluating the results. The cyclic voltammograms, characterization images, as well as

a summary of the viability and errors from the experiments, are provided in a detailed manner. Section 4.1 gives an insight into reproducibility of p-Ser, p-PDA, and p-ALT homopolymer films using PDA as a reference. It also provides data for copolymer films produced in conjunction with PDA and summarizes the thickness, roughness and reproducibility data for all thin films produced. In section 4.2, the influence of scan rate on the oxidation/reduction potentials as well as the peak currents at pH ~ 7 is reported for the PDA (reference), PDA + p-PDA (3:1) and PDA + ALT (3:1) films. The influence of pH on the oxidation and reduction potentials of PDA (reference), PDA + p-PDA (3:1), PDA + ALT (3:1) is examined and compared with PDA + p-PDA (1:1) and PDA + ALT (10:1) along with further data for p-Ser using cyclic voltammetry in section 4.3. A breakdown of critical parameters that can influence experimental results and accuracy as well as the sources of error is provided here. Data from further characterization techniques such as contact angle measurements, ATR-FTIR in the reflection mode and XPS are provided in Sections 4.1.3, 4.1, and 4.5, for a comparison between different polymer films studied.

Chapter 5: Conclusion and Outlook provides a summary of the work performed in this thesis. It lists out scope for improvement and future experiments. This chapter also provides a brief outlook for applications made possible from the findings in this master thesis.

Chapter 6: Appendix provides supporting information about experiments that provided preliminary data that presents scope for future work as well as unsuccessful trials that prompted changes to experimental methods which were reported in the experimental section.

1   INTRODUCTION

Polydopamine-derived systems have found great potential applications that are distributed across the fields of material science, biomedicine, energy, environmental science, and clean engineering applications like hydrogen generation through photocatalytic water-splitting (PWS). This section comprises the basic concepts and background for the methodology and experiments used throughout the thesis and relevant scientific equations and formulas.

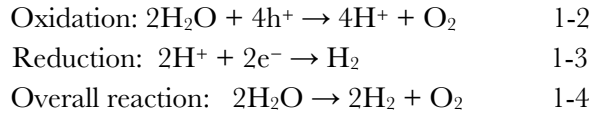## 1.1   Photocatalytic water-splitting

As of 2013, worldwide energy consumption was estimated at ~ 60,000 TWh per year [1] and this figure is expected to at least double by 2050. Thus, a clean, alternative affordable energy source that reduces our dependence on fossil fuels being the primary source of energy remains the need of the hour. Sustainable hydrogen production is one such candidate since it is carbon free. Presently, though 95% of commercial hydrogen is produced from non-renewable sources (such as fossil fuels), PWS offers a "green" alternative [2]. Also called artificial photosynthesis, in this process hydrogen (H_2) and oxygen (O_2) are produced from water by utilizing the energy of light. The process is cyclic and non-polluting since: 1) solar energy is the primary energy source, 2) water is largely available on the earth's surface, and 3) the combustion of H_2 in air reproduces water.

1.1.1   Process

The general schematic representation of the process is given in Figure 1.1 [3]. The catalyst usually comprises of a semiconductor/semiconductor-like material with a LUMO (Lowest Unoccupied Molecular Orbital) or C.B. (Conduction Band) and HOMO (Highest Occupied Molecular Orbital) or V.B. (Valence Band) separated by a bandgap (E_g) with energy in the order of a few eV [2]. The process by which water-splitting occurs can be divided into four steps as shown in Figure 1.1: (1) photon absorption with the condition that:

$$h\nu > E_g \qquad\qquad \text{1-1}$$

where $h\nu$ represents the energy of photons and E_g is the band gap of the photocatalyst (2) charge separation of photoelectrons into the conduction band and holes remaining behind in the valence band, (3) charge transport by migration from bulk to the catalyst surface and the following (4) oxidation, reduction and overall reactions at the catalyst surface:

$$\text{Oxidation: } 2H_2O + 4H^+ \rightarrow 4H^+ + O_2 \qquad \text{1-2}$$
$$\text{Reduction: } 2H^+ + 2e^- \rightarrow H_2 \qquad \text{1-3}$$
$$\text{Overall reaction: } 2H_2O \rightarrow 2H_2 + O_2 \qquad \text{1-4}$$

The overall reaction is endothermic and results in the increase of Gibbs free energy by 238 kJ mol^{-1} [4].
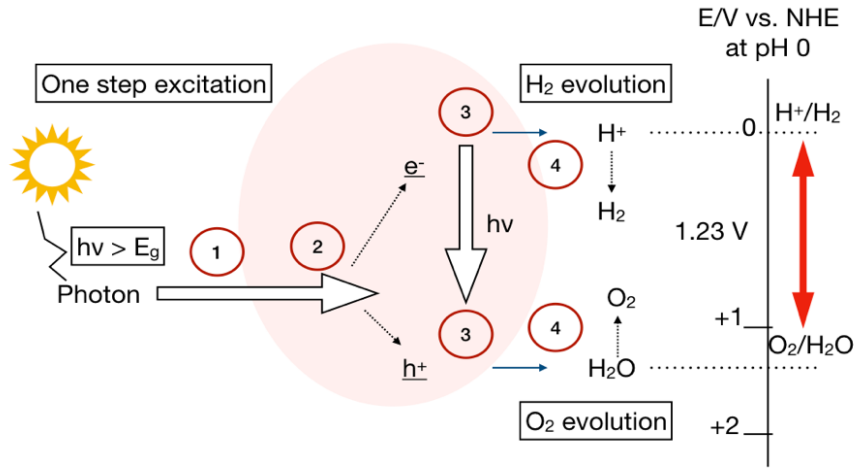

Figure 1.1 General schematic for the PWS process; own figure, adapted from [3]

1.1.2 Optimization

Two main parameters must be taken into account to optimize this process: the band structure of the photocatalyst and the efficiency of the reaction [5]. Thermodynamically, the process is more favourable if $2.42 \text{ eV} \leq E_g \leq 3.2 \text{ eV}$ [6], where E_g is the band gap of the photocatalyst. For the process of hydrogen reduction, the following condition should be met:

$$V_{(CB)} < V_{(H)} \qquad \text{1-5}$$

where $V_{(CB)}$ is the potential of the conduction band and $V_{(H)}$ is the potential of H$_2$ evolution. Since both values are negative, this implies that $V_{(CB)}$ should be more negative than $V_{(H)}$ (0 V versus NHE (Normal Hydrogen Electrode) at pH 0). Similarly:

$$V_{(VB)} > V_{(O_2)} \qquad \text{1-6}$$

where $V_{(VB)}$ is the potential of the valence band and $V_{(O_2)}$ is the potential of O$_2$ evolution. Here, both are positive hence $V_{(VB)}$ should be more positive than $V_{(O_2)}$ (+1.23 V versus NHE at pH 0). Recombination of the electrons and holes should also be prevented by extending charge carrier lifetime to avoid loss of energy in the form of heat or phonon generation. Lastly,

photocorrosion of photocatalysts can reduce the activity of the system over time and must be prevented [7],[8]. Often, various sacrificial reagents such as inorganic salts and organics can be added to the photocatalytic system to control the charge recombination process and improve quantum efficiency [9].

1.2 Polydopamine

Dopamine (DA) is a compound present in the body as a neurotransmitter and a precursor of other biochemical bodily compounds. A mussel adhesive protein inspired molecule, dopamine has also been reported by Lee et al. [10] to serve as a multifunctional polymer coating capable of adhesion onto almost any solid surfaces without surface pre-treatment. Polydopamine (PDA) is a dopamine derived synthetic eumelanin polymer formed by the oxidation of dopamine. It can be easily synthesized by exposing dopamine (3,4-dihydroxyphenylethylamine) to air in basic aqueous buffer solutions and has widely been used to coat metals, oxides and ceramics among other substances [10].

1.2.1 Structure

Although PDA is a widely studied polymer, its structure is still under discussion; though it has been proposed that it is composed of dihydroxyindole, indoledione, and DA units, which are assumed to be covalently linked. Figure 1.2 shows the proposed structures of polydopamine as provided in literature [11]. The structure of polydopamine is suggested as consisting of (a,b) homopolymers of indoles (c) possessing a connection between the monomer units occurring not only via the benzo moiety but also via the pyrrole fragment (f,g) primary C−C bond connecting DA (h) indole moieties in various oxidation states (i) and two fused indole rings forming PDA.
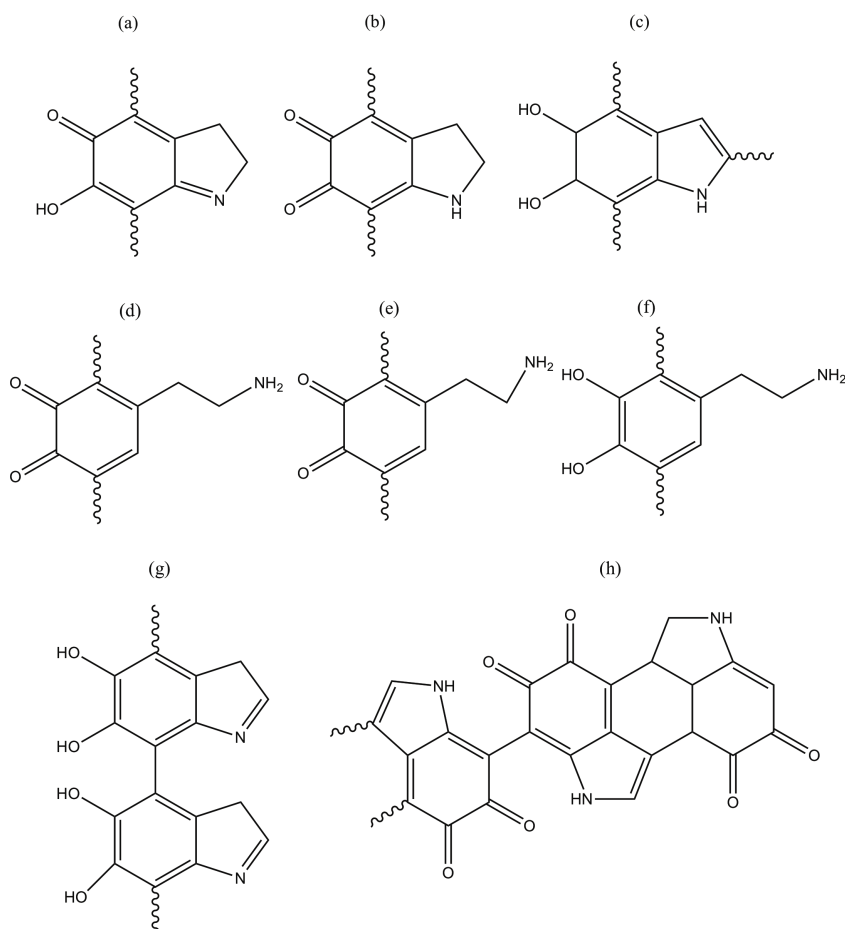
Figure 1.2 Proposed structures of polydopamine according to literature; redrawn and adapted from [11]

1.2.2 Synthesis

DA is commercially available as dopamine hydrochloride and can be oxidized using an oxidizing agent and self-polymerize under mild conditions in an alkaline environment. The polymerization process is indicated by a change from colourless to light brown to dark brown which is characteristic of PDA formation. The intensity of the color (and hence the film thickness) is dependent on the polymerization time [12]. The suggested mechanism of polymerization and the structure of PDA most widely used in literature is shown in Figure 1.3. The deposition rate of self-polymerized PDA is very low (for example, by dip coating) and self-polymerization of DA under alkaline condition would result in the formation of nano/microparticulate aggregates of PDA in solution, which greatly increase surface roughness [13]. The oxidation of DA to dopaminequinone is considered the foundational step in polydopamine formation [14]. This step follows a redox reaction scheme, which can be

performed electrochemically [15] with precise control over the redox reactions, under neutral conditions using fixed scan voltages, number of cyclic sweeps and scan rate.
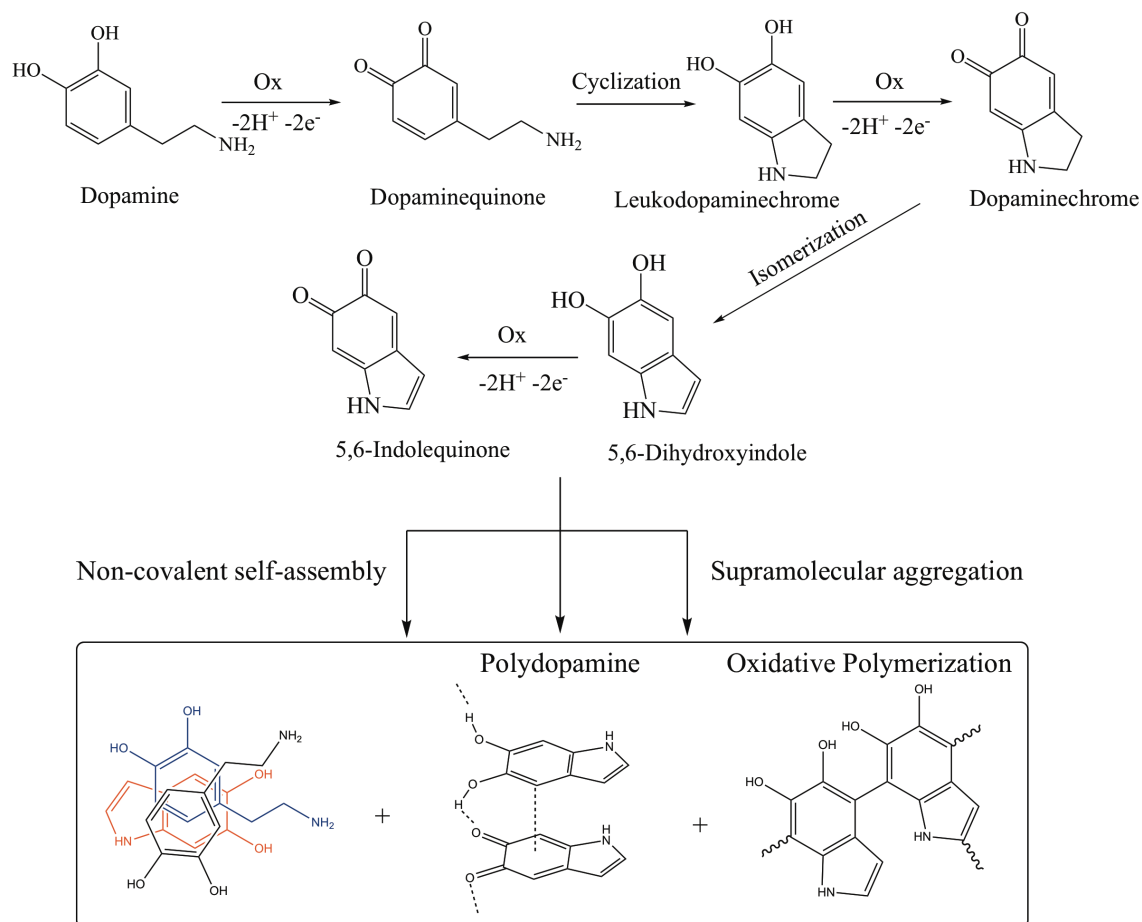

Figure 1.3 Proposed mechanism of polydopamine formation and final structures formed; redrawn and adapted from [14]

It has been reported that DA monomer concentration directly affects film thickness, the rate of film deposition and roughness during electropolymerization [14],[16]. Also, increasing the oxygen concentration of the solution leads to a significant decrease in roughness as compared to that observed with oxygenation due to exposure to air [17]. It is known that the different functional groups in polydopamine can react with many molecules, and thus allow the post-modification of the surface. Under slightly basic conditions or after thermal treatment at 150 ° C, the catechol which group is oxidized to a quinone, becomes electrophilic and highly reactive towards nucleophiles such as thiols and amines and easily at room temperature via can react Schiff's reaction and/or Michael addition [18],[19] as shown in Figure 1.4.
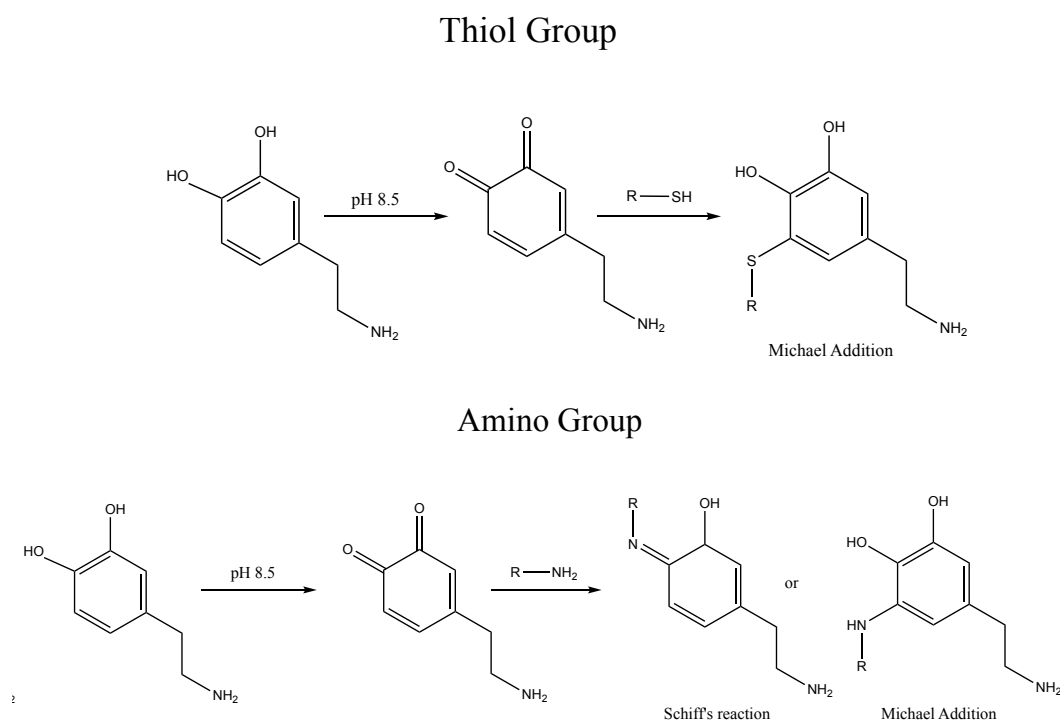
Thiol Group

Michael Addition

Amino Group

Schiff's reaction   Michael Addition

Figure 1.4 Chemical reactions of the Thiol group and Amino group with PDA at basic pH; redrawdn and adapted from [18],[19]

1.3   P-phenylene diamine

P-phenylenediamine or benzene-1,4-diamine with chemical formula $C_6H_4(NH_2)_2$ is a non-biodegradable, precursor for the polymerization of Kevlar commercially used in hair dyes. It differs by aniline by only a single additional -NH_2 group and can be recognized in solution as it turns dark purple on exposure to air [20]. The structure of the monomer is shown in Figure 1.5. Shape control of the pure polyphenylenediamine (p-PDA) polymer has been studied widely in literature using different synthetic conditions under UV irradiation including the formation of nanoneedles, almond-like microstructures and star-shaped patterns [21]. The oxidative polymerizations of aromatic diamines (AD) for example in this case, into p-PDA occurs via oxidation of one or both amino groups in the structure [22]. The advantages of using such aromatic diamines include: the variability of electroconductivity and multifunctionality due to one free amino group per repeat unit on the polymers [23]. The polymer form also shows increased resistivity in comparison to polyaniline which is more widely studied [24]. p-PDA can be chemically or electrochemically deposited on surfaces or particles can be incorporated in sensors such as glucose sensors [25], peroxide sensors [26] or nitrophenol sensors. Its use as a redox active environment for photocatalysis has not yet been explored and is studied in this thesis for the first time [27].
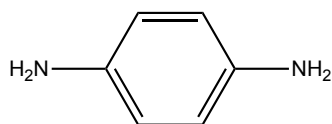
Figure 1.5 Structure of p-phenylenediamine

1.4   3-amino-l-tyrosine

3-amino-L-tyrosine with chemical formula $C_9H_{12}N_2O_3$ is a biodegradable derivative of the non-essential amino acid tyrosine which acts as a precursor for DA in the body. The structure of the monomer is shown in Figure 1.6. It was first discovered in the milk protein casein (hence the name tyrosine as "tyros" in Greek means cheese) and has been used in the biosynthesis of a thermally sensitive chemiluminescent polymer called diazo-luminomelanin used in microwave dosimetry research [28] and also as a competitive inhibitor of mushroom tyrosinase due to its similarity in structure with tyrosine [29]. It was chemically synthesized as an extension of the tyrosine structure by reducing the nitro group of 3-nitrotyrosine to an amino group, using sodium hydrosulfite [30]. Tyrosine, like DA has been shown to successfully polymerize under synthetic conditions to form melanin-like materials [10]. However, the same process using an amino-group containing tyrosine-based derivative with electropolymerization to form polyaminotyrosine (ALT/p-ALT) is yet to be studied. A promising feature of this monomer is that like DA, it was also reported [31] to be redox-active.
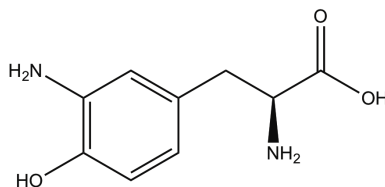

Figure 1.6 Structure of 3-amino-L-tyrosine

1.5   Serotonin

Serotonin (5-hydroxytryptamine, 5-HT) was discovered in 1951 in blood, peripheral tissues and the nervous system as a vasoconstrictor and monoamine neurotransmitter [32]. The structure of serotonin in monomer form is shown in Figure 1.7. It consists of an indole ring with a hydroxide group on the fifth C atom, and a carboxyl-amide side chain and contains one amino group that is connected to an aromatic ring by a two-carbon chain ($-CH_2-CH_2-$). The advantage of studying serotonin over other polymer hybrid systems (for example p-PDA) is its biocompatibility and biodegradability. Earlier studies related to Alzheimer's patients have shown that serotonin can form highly ordered structures in an oxidative environment [33]. Under basic environments (pH ~ 9.5) it can self-assemble into monodisperse polyserotonin (p-Ser) nanoparticles, and this technique has been studied earlier for use as potential

nanoplatforms in biomedical applications [34]. It was also reported in the same study that p-Ser shows four times reduced adhesion properties on Au substrates in comparison with PDA.
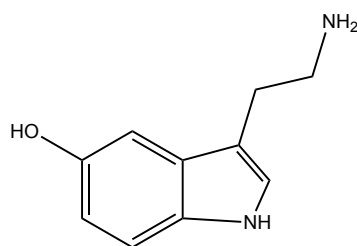
Figure 1.7 Structure of serotonin

1.6   Synthesis and characterization techniques

1.6.1   Electropolymerization and cyclic voltammetry (CV)

Electropolymerization or electro-initiated polymerization is the process in which electrolysis is used to initiate the polymerization process with one or more monomers being polymerized on a conducting surface. It is different from electrolysis in that the amount of the monomer polymerized does not have to be in a stoichiometric ratio with the amount of current passed. The formation of a polymer can be initiated electrochemically hence, the presence of an initiator and its removal after polymerization is not a concern here. The initiators of polymerization can include [35] the monomer molecules, supporting electrolyte ions, solvent molecules, and impurities in the system or any species added to the reaction medium. The yield, molecular weight, and molecular weight distribution can also be controlled. The process functions due to interactions between the reaction medium and the electrode surface and thus, parameters such as the applied potential and current, scan rate and the number of voltage cycles applied (in case of cyclic sweep) must be controlled. The applied potential should be sufficient to oxidize the monomer and polymerize it, but not too high so that it does not cause metal dissolution or induce corrosion. However, since the mechanisms are poorly understood, there is an inherent possibility of poor-quality coatings and reproducibility reported in literature [36] and care must be taken to report reproducibility of results.

Consider a chemical system where no redox couple is present. The potential form shown in Figure 1.8 is applied to the system for obtaining a voltammogram [37]. Initially, there is a sharp rise in current because of a sharp change in the scan rate v. The current then reaches a steady state as the voltage constantly varies. Reversing the scan voltage causes the resultant current to change sign, and it goes to 0 as the scan is stopped. This is repeated for several cycles as per requirement in cyclic voltammetry to allow observations to the system over time, where a voltammogram or the V-I characteristics of a cyclic voltage sweep applied to an electrolyte are obtained.
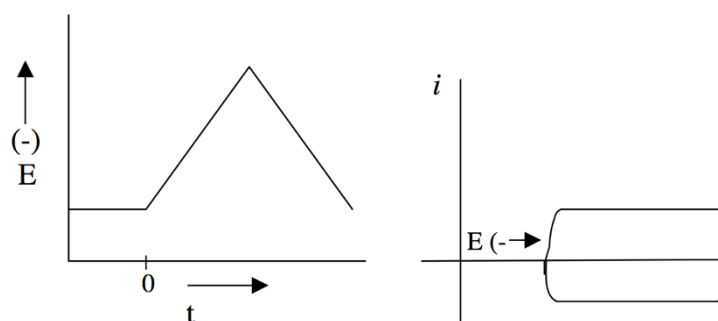

Figure 1.8 Schematic explanation of a cyclic voltammetry experiment in the absence of a redox couple [37]

An example of the same recorded in the presence of a redox couple according to IUPAC convention is shown in Figure 1.9 (a). The x-axis represents an applied voltage (V) and the y-axis represents the resulting current. The arrow above the "duck diagram" (called so due to its shape) represents the direction in which it must be read.
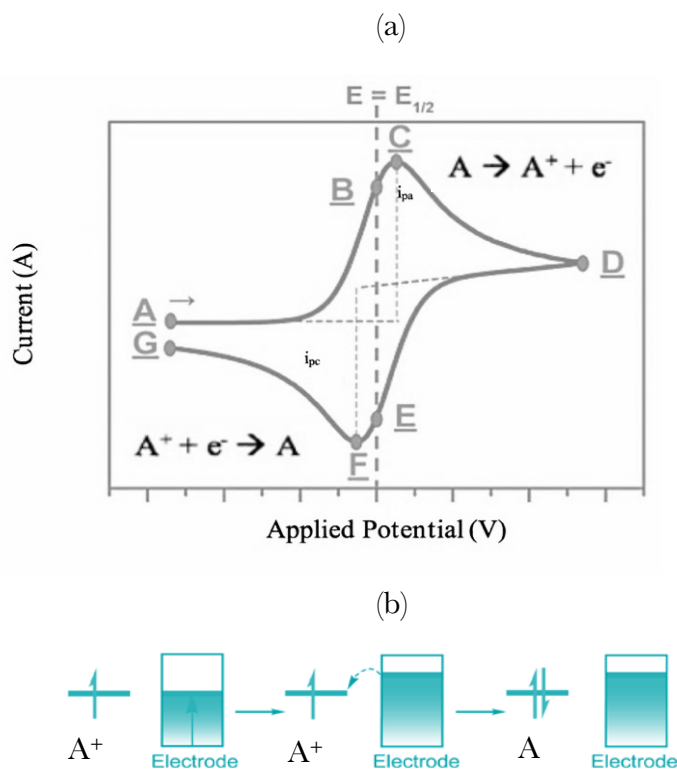
(a)

(b)

Figure 1.9 (a) Typical cyclic voltammogram (b) electron transfer process occurring at the W.E.; adapted from [35]

A circuit diagram and schematic representation of the electrochemical cell used for electropolymerization is given in Figure 1.10 (a) [38]. The circuit is comprised of an electrochemical cell, an adjustable voltage source (V_S), an ammeter (A_M) and a voltmeter (V_M). Three electrodes used in the cell are the working electrode (W.E.), the reference electrode (R.E.), and the counter electrode (C.E.). The source voltage (V_S) for the electropolymerization is applied between the working electrode and the counter electrode. The voltmeter measures the potential (E) between the R.E. and the W.E., and the overall voltage (V_S) is adjusted to maintain this potential. The ammeter (A_M) measures resulting current (i) flowing to or from the W.E.
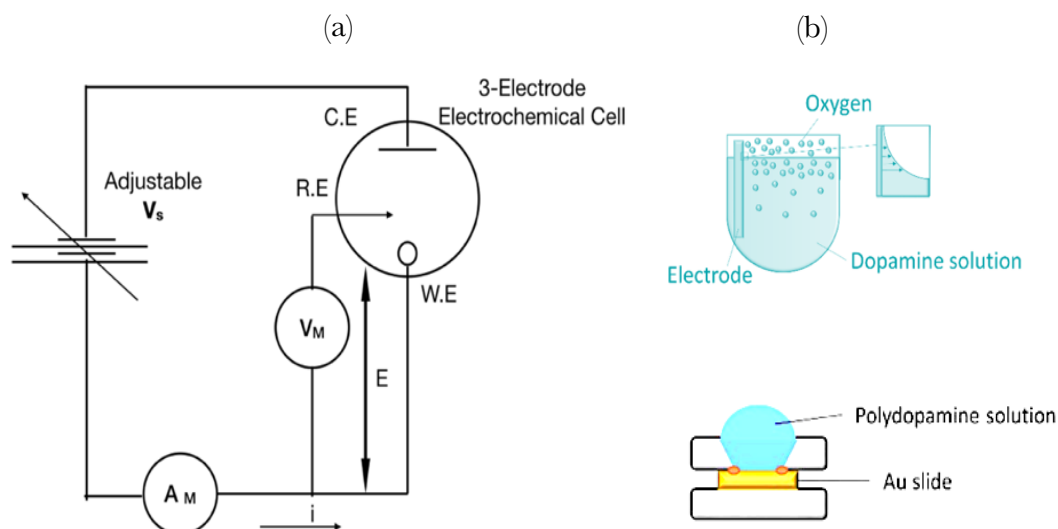
Figure 1.10 (a) Circuit diagram for 3-electrode setup used in electropolymerization and cyclic voltammetry (CV) (own figure adapted from [38]) (b) vertical (top) and horizontal configurations for electropolymerization

The setup is possible in two ways: (i) a horizontal setup and (ii) vertical setup as shown in Figure 1.10 (b) where the substrate is either dipped in the reaction medium or placed on a horizontal surface, held in place after which a few drops of the electrochemical solution is added. The differences in the abilities of these two methods in producing polydopamine thin films have been studied earlier and horizontal cells are found to produce somewhat more homogenous thin films with circular, thick edges [39]. The reaction medium consists of the following:

 i. Solvent: An appropriate solvent would show high mutual solubility with a monomer and low solubility with the polymer formed from a monomer such that film formation is preferred to dissolution. Usually, water is used.

ii. Supporting electrolyte: Ideally, this possesses a high ionic concentration as it serves to increase the conductivity in the reaction medium. This would allow migration of ions from bulk to the surface of the substrate.

iii. Substrate: An ideal substrate does not show any chemical reaction with the solvent or the solute species. It must not undergo corrosion or redox reactions at the voltages to be applied to the solvent or before electrolysis is complete.

The R.E., usually an Ag/AgCl chloride electrode, is non-polarizable and currentless, near the W.E. (made of a noble metal such as Au/Pt) due to an Ohmic drop due to the resistance of the solution between both electrodes. It has a 3 M KCl salt bridge to prevent contamination of the

electrolyte. For simplicity, consider a compound AX where A is more easily reducible. At the W.E. the following reduction reaction occurs:

$$A^+ + e^- \rightarrow A \qquad\qquad \text{1-7}$$

The reaction occurs because the LUMO of A^+ is at a lower energy than the HOMO of the W.E. as shown in Figure 1.9 (b). The peaks for oxidation and reduction in the diagram can be explained by considering the equilibrium between the species A and A^+ described by the Nernst equation:

$$E = E^0 + \frac{RT}{nF}\ln\frac{(Ox)}{(Red)} \qquad\qquad \text{1-8}$$

Where E is the potential of the electrochemical cell, E^0 is the standard potential of a species, $\frac{(Ox)}{(Red)}$ represents the relative activities of the species being oxidized and reduced in the reaction medium at equilibrium, R is the universal gas constant, F is Faraday's constant, n is the number of electrons and T is the temperature. Applying the equation to the one-electron reaction described in:

$$E = E^{0\prime} + \frac{RT}{F}\ln\frac{[A^+]}{[A]} \qquad\qquad \text{1-9}$$

Where activities are replaced by the concentration of the species [A] and [A+], E^0 is replaced by the formal potential $E^{0\prime}$ and n becomes 1. The species A present at the electrode surface is oxidized to A+ as the applied potential is more positive. As the potential varies from point A to point D, [A] is steadily depleted near the electrode as it is oxidized to increase [A+]. At point C, where the peak anodic current or oxidation peak current $(i_{(p.a)})$ is observed with corresponding oxidation potential $E_{(ox)}$, the current is controlled by the presence of additional [A] transported via diffusion from the bulk solution. The volume of the solution at the surface of the electrode containing the oxidized A is called the diffusion layer and continues to grow throughout the scan. This slows down mass transport of A to the electrode. Thus, while more negative potentials are applied, the rate of diffusion of A from the bulk solution to the electrode surface reduces, causing in a decrease in the resulting current as the voltage is scanned (C → D). When the switching potential (D) is reached, the scan direction is reversed, and the potential

is scanned in the other direction resulting in a peak cathodic current $(i_{(p.c)})$ with corresponding reduction potential E (red). At points B and E, the concentrations of species A^+ and A at the electrode surface are equal, following the Nernst equation, $E = E_{1/2}$. This corresponds to the halfway potential between the peaks C and F and can be used to estimate the $E^{0\prime}$ for a reversible electron transfer. While the concentration of A^+ at the electrode surface is depleted, the concentration of A at the electrode surface increases and vice-versa, satisfying the Nernst equation. Diffusion of the analyte to and from the electrode causes the peak separation. The scan rate inversely affects the size of the diffusion layer and thus directly affects the current as shown by the Randles-Sevcik equation [40]:

$$i_p = 0.466nFAC^O(\frac{nFvD_0}{RT})^{1/2} \qquad \text{1-10}$$

the peak current i_p increases linearly with the square root of the scan rate v (V s^{-1}), where n is the number of electrons transferred in the redox reaction, A (cm^2) is the electrode surface area, D_0 (cm^{2}s^{-1}) is the diffusion coefficient of the oxidized species, and C^0(mol cm^{-3}) is the bulk concentration of the analyte. The peak separation voltage ΔEps is given by:

$$\Delta Eps = E \text{ (ox)} - E \text{ (red)} \qquad \text{1-11}$$

Where E (ox) is the oxidation potential and E (red) is the reduction potential. If the half width of the peak separation in the forward scan is 59 mV at 25°C (ideal case), the reduction process is completely reversible and indicates a one-electron process where electron transfer is faster than mass transport given by [41]:

$$\Delta Eps = \frac{59}{n} \qquad \text{1-12}$$

Where n is the number of electrons involved in the redox process. When the peak separation is greater than 59 mV it implies a quasi-reversible system, and one with novel properties from a one-electron reversible system [42] and the loss of an Ohmic drop [43]. It indicates that the electron-transfer process occurs at the same rate as mass transport. The peak separation ΔEps is also influenced by the presence of alkali metals, hence the choice and concentration of supporting electrolyte as mentioned above should be noted. For an irreversible system electron transfer is slower than mass transport.

1.6.2 Profilometry

Profilometry is used to extract topographical information about a surface (morphology, thickness, surface roughness etc.). The setup of a profilometer consists of a movable sample stage and detector. The stylus can scan the sample in x, y and z directions (3D). The typical resolution of such a profilometer depends on the scan rate and signal sampling rate but is much higher in the y-direction (height). The variations in the topography of the sample impart a force onto the stylus and this gets converted by a transducer into an analog electrical signal. This signal is then converted into a digital signal by an analog to digitall converter (ADC). This is shown with the profilometer setup in Figure 1.11 (a) and (b) [44].
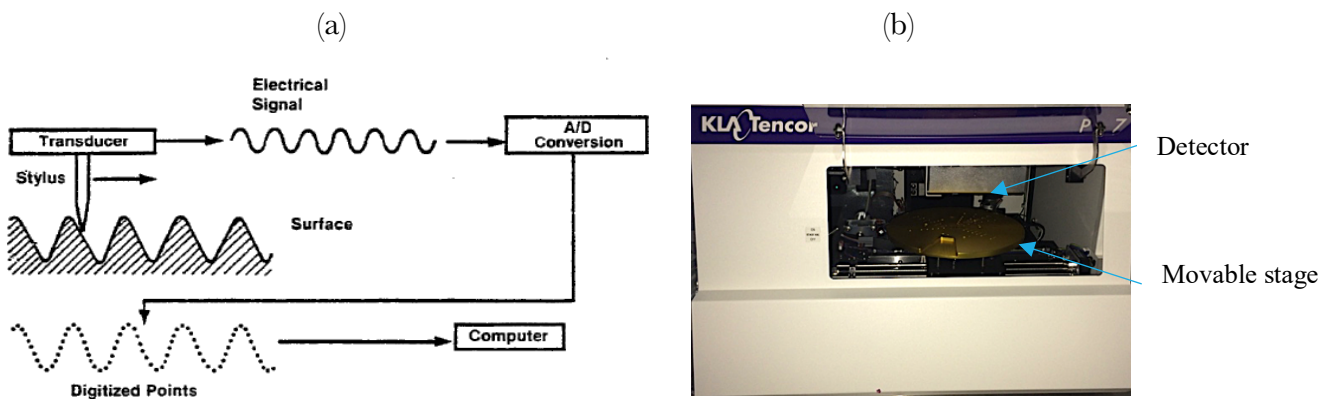
(a)   (b)

Figure 1.11 (a) Block diagram for a profilometer [44] (b) actual profilometry setup

1.6.3 Atomic Force Microscopy (AFM)

The Atomic force microscopy (AFM) was invented by Binnig, Quate, and Gerber in 1986 [45]. Atomic force microscopy can provide topographic information down to Angstrom level and is hence useful for studying the thin films explored in this thesis. Its setup consists of a sharp probe made of a piezoelectric crystal chosen according to the sample under study (in this thesis, an OTESPA cantilever of 300 kHz was used). The probe is attached to a flexible cantilever that is movable under applied mechanical forces. The movement occurs at an angle of inclination proportional to the intensity of the force which is measured by deflecting a laser beam off a split photodiode. This detected movement is then converted to an electric signal similar to the profilometer. This is depicted in Figure 1.12 (a) [45]. Thus, both devices work on the principle of piezoelectricity since a force applied along a particular direction (say, x) causes a deflection in a perpendicular direction (say, y) and this produces a current in a direction transverse to both (z). The AFM can be operated in several modes, however, in this report only (soft) tapping mode was used where the cantilever assembly is made to oscillate over the sample at the

resonant frequency of the cantilever. The mechanical resonance frequency ω_o of a cantilever beam is:

$$\omega_o = \sqrt{\frac{k_p}{m_{eff}}} \qquad\qquad 1\text{-}13$$

where the effective mass m_{eff} is dependent on the mass distribution and geometry of the AFM probe and k_p is the effective stiffness of the probe. This is a useful mode since it prevents damage to the sample and the probe. The cantilever oscillation amplitude is maintained constant by a feedback loop which is software-assisted. When the tip passes over a bump in the surface, the cantilever has less spatial freedom to oscillate and the amplitude of oscillation decreases. Conversely, when the tip passes over a depression, the cantilever has greater spatial freedom to oscillate and the amplitude increases (approaching the maximum free air amplitude). This concept is used to extract thickness profiles of several samples in this project. The oscillation amplitude of the tip is measured by the detector and input to the controller electronics. The digital feedback loop then adjusts the tip-sample separation to maintain a constant amplitude and force on the sample.
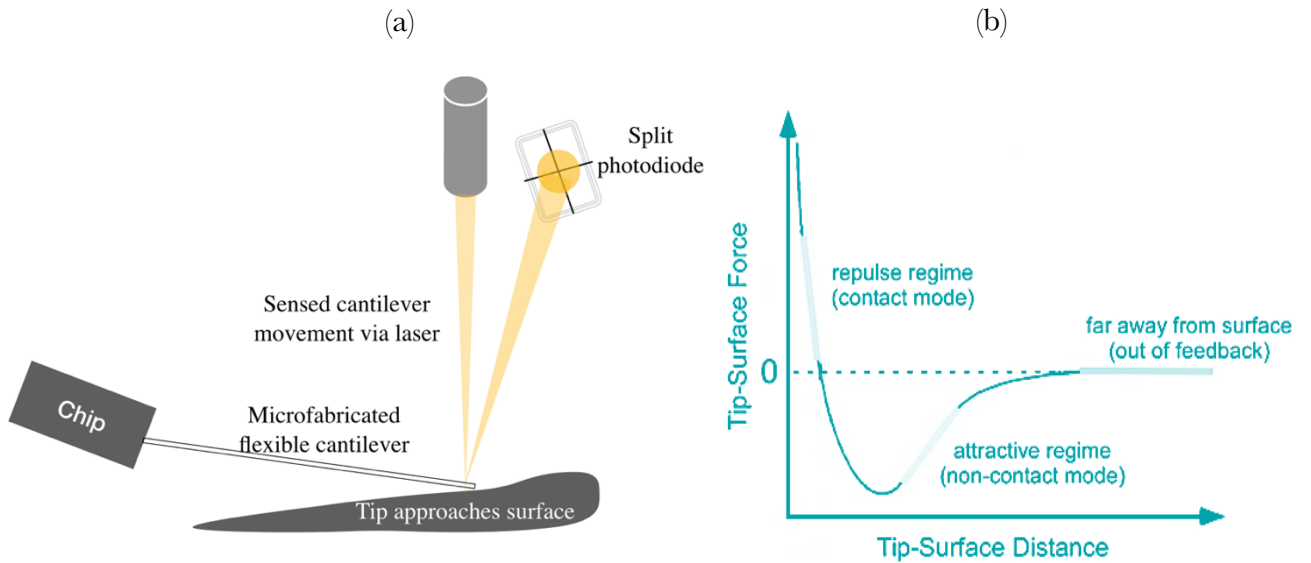

Figure 1.12 (a) Schematic of an AFM setup, redrawn and modified [45] (b) Lenard Jones potential representing the interaction between probe and sample in AFM analysis [46]

The interaction between the probe and sample can be explained by the Lenard-Jones potential equation and curve shown in Figure 1.12 (b) [46]:

$$V_{LJ}(r) = \frac{A}{r^{12}} + \frac{B}{r^6} \qquad\qquad 1\text{-}14$$

where A and B are constants and r represents distance between particles of the probe and sample. At shorter distances between the probe and sample ($\sim$ a few Angstroms) repulsive forces dominate due to exchange interactions between their overlapping molecular orbitals. At longer distances, attractive forces dominate. The forces can have van der Waals nature due to induced polarization between atoms of the probe and sample, electrostatic interactions caused by localized charges and magnetic interactions by dipoles present.

1.6.4 Attenuated Total Reflection Fourier Transform IR Spectroscopy (ATR -FTIR)

Infrared spectroscopy is a powerful tool for the characterization of polymers based on the absorption of radiation in the infrared wavelength range due to the molecular vibrations of the functional groups contained in the polymer chain. This technique has limited sensitivity since most of the radiation transmitted through a sample as a function of wavenumber does not interact with the open slits of the detector and hence, analyzing the thin films could prove challenging. The schematic is shown in Figure 1.13 [47]. The FT-IR setup uses a Michelson interferometer consisting of two mirrors and a beam splitter. The beam splitter reflects half the incident radiation from a source to a stationary mirror and transmits the rest to a moving mirror. Radiation is then reflected by the sample and by the two mirrors to the beam splitter where the amplitudes of the waves are combined either destructively or constructively to form an interferogram which is created at the detector. The interferogram is Fourier-transformed from time into the frequency spectrum. This technique has several distinct advantages since it can scan the infrared spectrum constantly throughout its optical range quickly with a moderate resolution. It can measure al1 wavelengths simultaneously with a high signal-to-noise ratio and this would be useful when differentiating the background of the substrate from the sample surface signal used in this project. The interferometer has no slit or grating and has a high throughput [47].
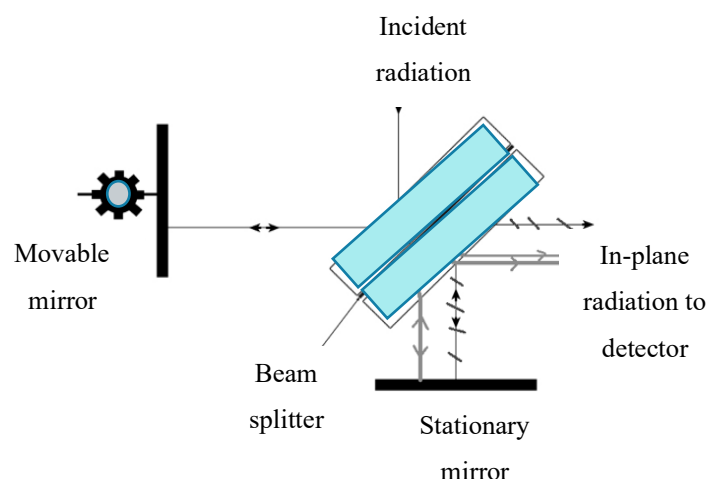
Figure 1.13Schematic of an ATR-FTIR setup redrawn and adapted from [47]

1.6.5   X-ray photoelectron spectroscopy (XPS)

X-ray photoelectron spectroscopy (XPS) was developed during 1954-70 by K. Siegbahn and his research group [48]. XPS is a surface sensitive technique due to the short mean free path of the excited electrons (several nm), where the sample is irradiated with x-rays and the energy distribution of the emitted photoelectrons is recorded. The analysis of the measured spectra can give information on the composition of the sample and the chemical bonding of the atoms within. The spectroscope shown in Figure 1.14 [49] consists of a dual anode x-ray source, a hemispherical energy analyzer, and a channeltron detector. The whole system is evacuated at a pressure of 10^{-8} to 10^{-9} mbar. The x-rays generated in the x-ray source are directed to the sample and some of the photoelectrons generated in the sample that can escape are analyzed in the hemispherical analyzer. The ion gun can be used to sputter away layers of the sample in order to depth profile the sample composition. The interaction of x-ray with matter can produce photoelectron emission where an x-ray photon liberates an electron in one of the various orbitals of the chemical compound under test. Depending on the experimental setup and the photon energy $h\nu$, these electrons can be either absorbed in the valence band or they can leave the atom as free electrons with kinetic energy E_k where:

$$E_k = h\nu - E_{BE} \qquad\qquad 1\text{-}15$$

Where E_{BE} is the ionization energy or binding energy of electrons in the orbital. The exact binding energy for an electron in an atom depends not only on the orbital of the electron but also on the chemical environment of the atom. The energy of an electron in an atomic orbital is determined by the Coulomb interaction with the other electrons and the attractive potential

17

of the nucleus. Any change in the chemical environment of the element will involve a spatial redistribution of the valence electrons, creating a different potential as seen by a core electron. This results in a change in the binding energies or a chemical shift. This process is shown in Figure 1.15 (a).
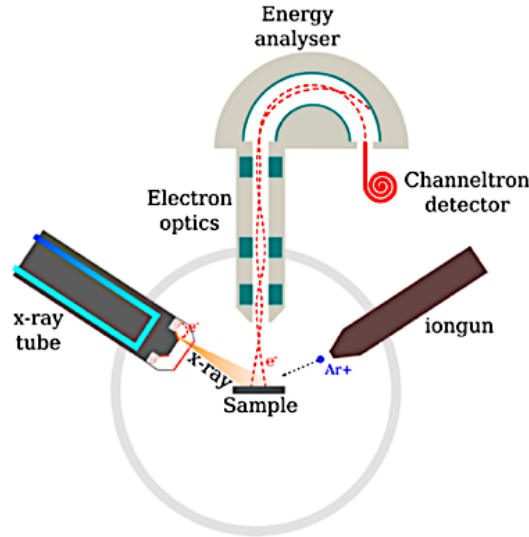

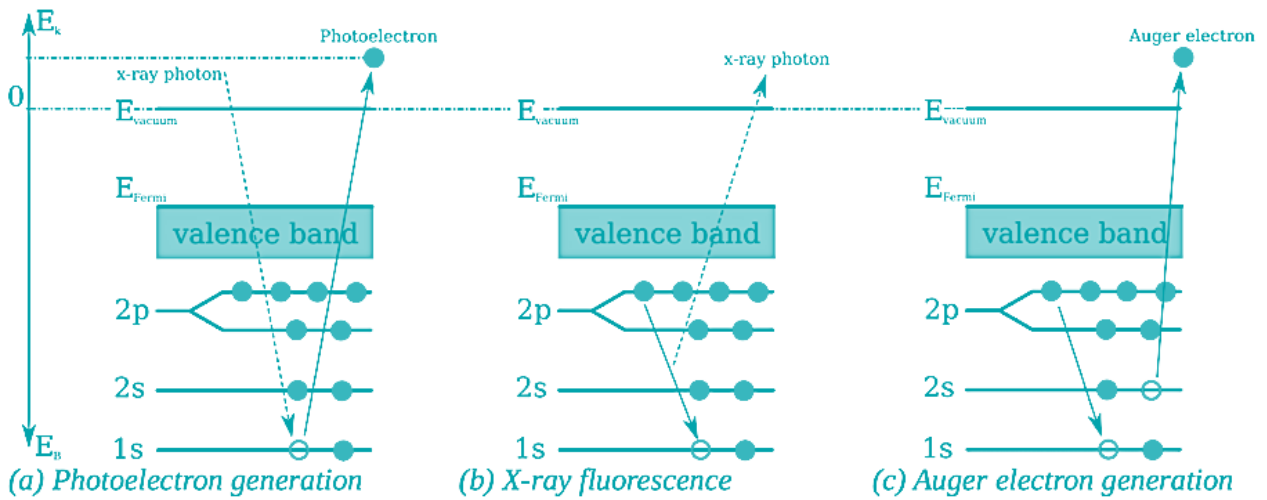*Figure 1.14 Schematic of an X-ray photoelectron spectroscope [49]*

Figure 1.15 Excitation and relaxation processes occurring in x-ray irradiated matter adapted from [50]

After an electron is emitted from an inner orbital of the atom a cation vacancy is left behind. An electron from an outer orbital undergoes relaxation and fills the empty inner orbital. The excess energy is released either by the emission of an x- ray photon (x-ray fluorescence) shown in Figure 1.15 (b) or by the ejection of a second photoelectron Figure 1.15 (c) (Auger electron emission).

1.6.6 Characterization using electron interactions

A Scanning Electron Microscope (SEM) works on the principle of using accelerated electrons from a suitable source, directed through a series of electromagnetic lenses and deflectors onto the surface of a charged sample in order to gain information about morphology and chemical contrast [51]. The image obtained from SEM depends upon several parameters such as scan speed, source voltage, intrinsic characters such as conductivity of the sample and so on and these can be fixed or tuned during the scans.
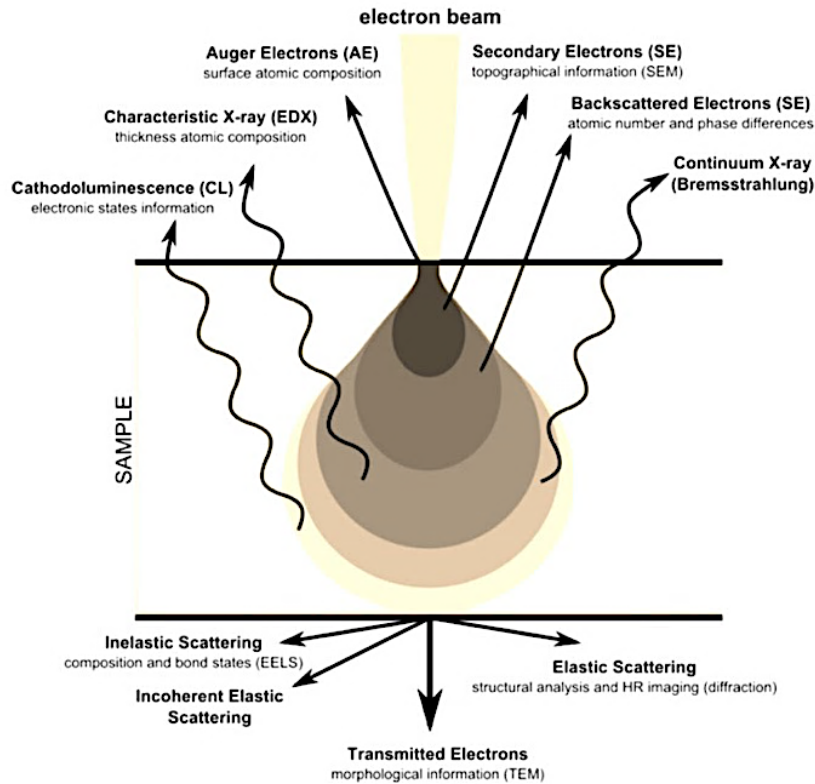
Figure 1.16 Information obtained from a sample by SEM based on the interaction volume of an electron targeting it [51]

There are three main detectors in an SEM [52]: Everhart- Thornley (E-T), in-line Detector and Backscattered Electron detector. The E-T detector primarily collects SEs and low-energy BSEs, also some high-energy BSEs are detected, which gives channeling contrast. In addition, the SEs (SEs created by BSEs leaving the sample) also contribute to the channeling contrast. The inline detector is placed in the electron column. This detector has better contrast because the collection solid angle for high-energy BSEs is larger for this detector. More SE2 electrons are collected by the in-lens detector than the E-T detector. The disadvantage is that the in-lens SE detector is very surface sensitive and is more prone to contamination. The backscattered

electron detector has high grain orientation contrast is due to the high collection efficiency of the high-energy BSEs, which carry the channeling contrast information. Figure 1.16 [51] shows the interaction volume of the channeled electrons in the sample in order to produce different types of electrons and the resulting effect on the image information one can obtain. EDX or Energy dispersive X-ray analysis/spectroscopy [52] is based on the principle of detecting X-ray emissions caused due to transitions of electrons between K, L and M shells in the atoms of the sample under analysis. For example, an inner K shell electron can get knocked out and either an L or M shell electron can take its place. This results in an emission of X-rays which then go to a detector or analyzer and get displayed as the K_α and K_β lines in the X-ray spectrum. When there is such a transition from the M to L shell, we get L lines of the X-ray spectrum. There can also be noise in the spectrum due to Bremsstrahlung radiations from decelerated electrons. An image of these transitions can be seen in Figure 1.17 [52].
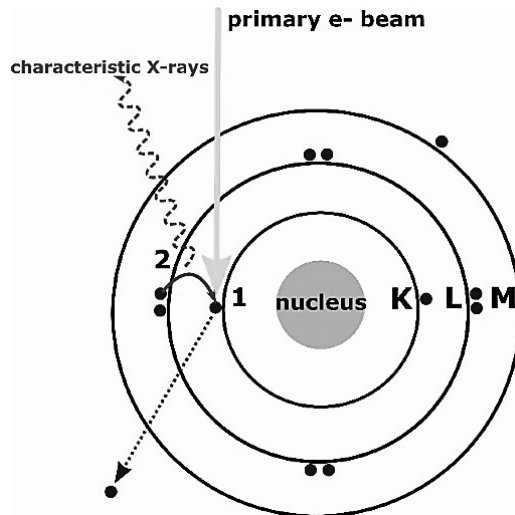
Figure 1.17 Basic principle of EDX [52]

The samples are mounted on the sample stage using a sticky carbon pad and focused to get a clear image. The energy used is 2.5 times the electron energy mentioned in the reference periodic table for stimulating the emission of a particular element. This increases the probability to knock out an electron from the element's electron shell. However, a major limitation exists for samples with ultrathin surfaces which reduces the interaction volume.

1.6.7   Static Contact Angle: Sessile Drop Method

Static contact angle measurements are used to find the hydrophilicity of a sample surface by applying a drop of water onto the solid sample and analyzing its angle θ with respect to the

surface using a goniometer. The setup of the contact angle measurement instrument is shown in Figure 1.18. A high-resolution camera is placed in the line of sight of the sample stage, where the sample is placed. Above the sample, a syringe with a needle controlled by the software is allowed to drop water onto the surface of the sample at a chosen rate (here 20 µL/min is used). The contact angles are then measured by contour fitting that is performed by the software on the captured image of the droplet on the sample surface.
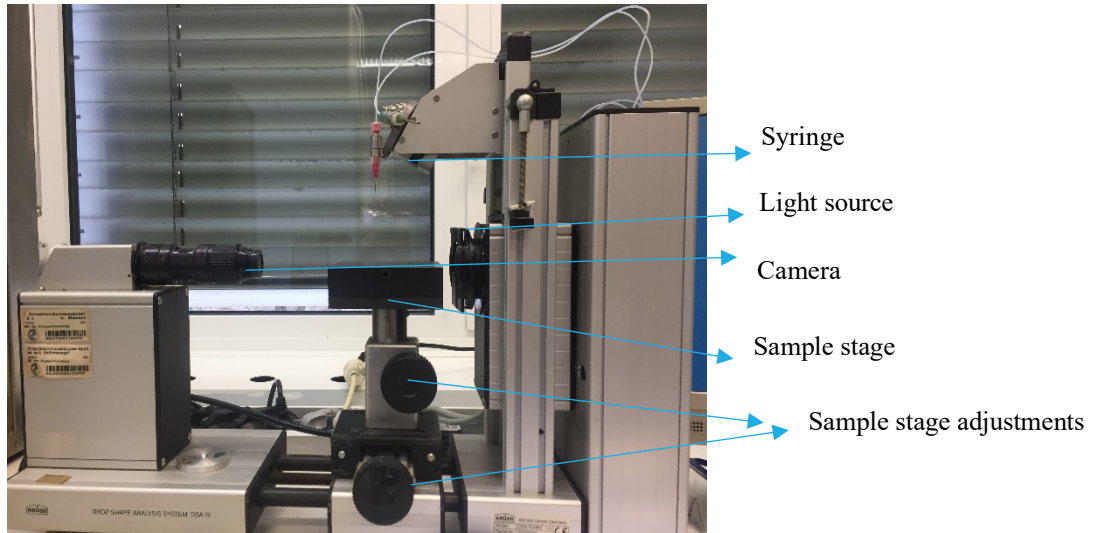
Figure 1.18 Instrument setup for sessile drop method contact angle measurement

The contact angle signifies the extent of wettability and hence hydrophilicity of the surface as shown in Figure 1.19. This is due to the surface tension of the liquid σ_l (e.g. water), the interfacial tension between the liquid and solid sample σ_{sl} and the free energy at the surface of the solid sample σ_s. These parameters are related to the contact angle by Young's equation given as [53]:

$$\sigma_s = \sigma_{sl} + \sigma_l.cos\theta \qquad\qquad 1\text{-}16$$

where θ is the angle shown in Figure 1.19 (b) between the liquid-solid interface.

(a)

(b)

$\theta < 90°$ => hydrophilic

$\theta > 90°$ => hydrophobic
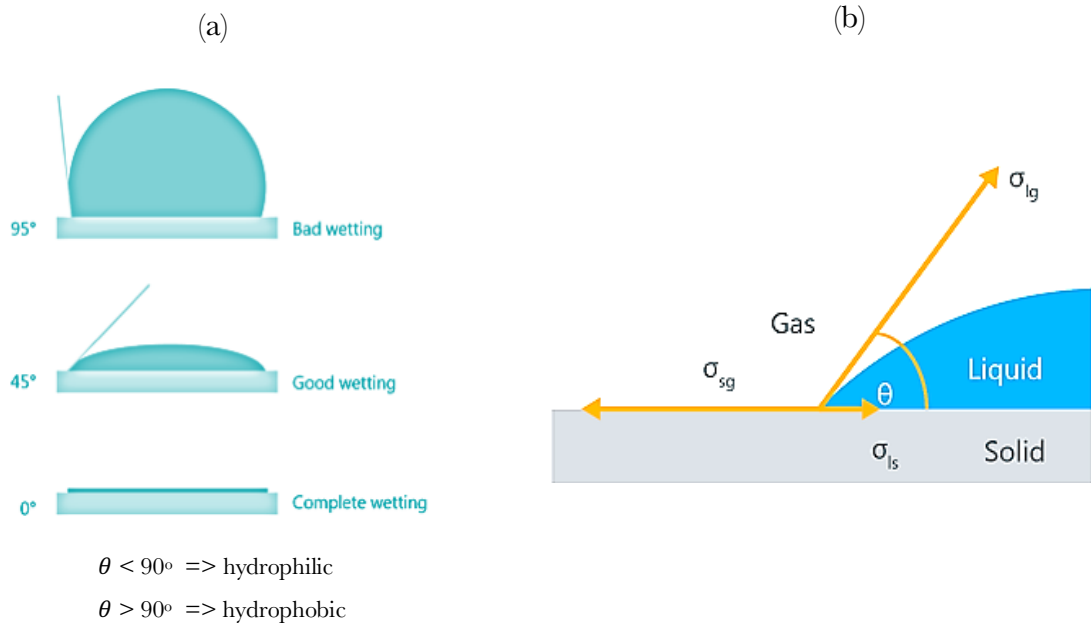
Figure 1.19 Criteria for good wettability and hydrophilicity of a surface (b) reference for explaining Young's equation adapted from [53]

2   MOTIVATION AND OBJECTIVES

2.1   Brief history and long-term goals of the project

This work is part of a project in cooperation with Dr. Maria Wächtler, Leibniz Institute for photonic technologies, Jena, CATALIGHT, Ulm and AK Weil, MPIP Mainz for water-splitting in photocatalytically active thin films. In earlier studies relevant to this project, polydopamine thin films were electropolymerized on conducting substrates, embedded with randomly distributed CdSe@CdS dot-in-rod nanostructured sensitizers and characterized [54]. An ideal setup with the sensitizers embedded and vertically aligned in the polydopamine thin film is shown in Figure 2.1. The effect of doping with Au nanoparticles after embedding these sensitizers was also studied [39]. The sensitizers can also be functionalized using metal nanoparticles (e.g. Co-complexes) that act as catalytic reaction centers. A method was also developed to strip the polydopamine films from the conducting substrate and transfer them to other substrates (that do not necessarily have conducting properties) for characterization and other purposes. Similar to the general process of PWS mentioned in the Introduction, upon absorption of light by the sensitizer, electron-hole pairs are generated, followed by charge carrier transport, separation, and localization in the CdSe seed and nanoparticle reaction centers (for electrons and holes respectively). The band gap of the combined CdSe@CdS structures correspond closely with the oxidation and reduction potentials of water; thus, catalyzing both water-splitting half reactions and stabilizing them through the electron-hole pairs generated.
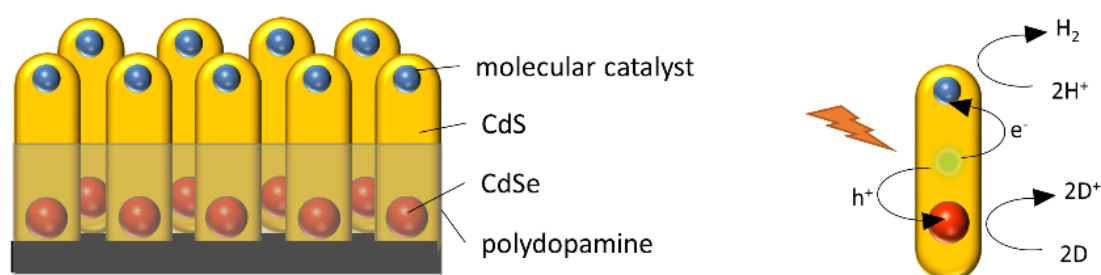

Figure 2.1 Structure of polydopamine hybrid system for PWS

2.1.1   Why Polydopamine?

Despite their potential photocatalytic activity, the structures mentioned above are subject to photodegradation and instability over time, which can be solved by embedding them in a redox active, light-stable material such as polydopamine. Structurally, polydopamine consists of

amphiprotic groups: hydroxyl and amino as well as reversible redox phenolic quinone groups [18],[55]. Though the precise molecular structure of polydopamine is relatively unknown [11], the catechol and quinone moieties of polydopamine co-exist in a pH-dependent redox equilibrium as shown in Figure 2.2, with their relative concentrations being dependent on the voltage at which the electropolymerization process is stopped [56]. The catechol moieties dominate under acidic pH while quinone moieties dominate under alkaline pH. The presence of quinone enables the self-regulation of photocatalytic activity since it intercepts the recombination process between the excited electrons in the sensitizer and the holes in the catalytic reaction center. The reducing catechol moieties would help quench residual photogenerated holes thus protecting the sensitizer from photooxidation and degradation. Hence, it is evident that the redox potential of the active polymer environment plays a vital role in supporting the water-splitting reactions occurring in the sensitizers and tuning the same (reducing the band gap) using copolymerization with different light stable monomer systems could be the next step in the investigation. PDA thin films can be a platform for secondary surface-mediated reactions, to synthesize self-assembled monolayers (SAM), grafted polymer coatings etc. [57],[58]. Applicability to many materials with complex shapes, and versatility, including surface functionalization, catalyst, soft-lithography, Li-ion batteries, among others [18],[59] provides motivation for further adapting PDA thin films.
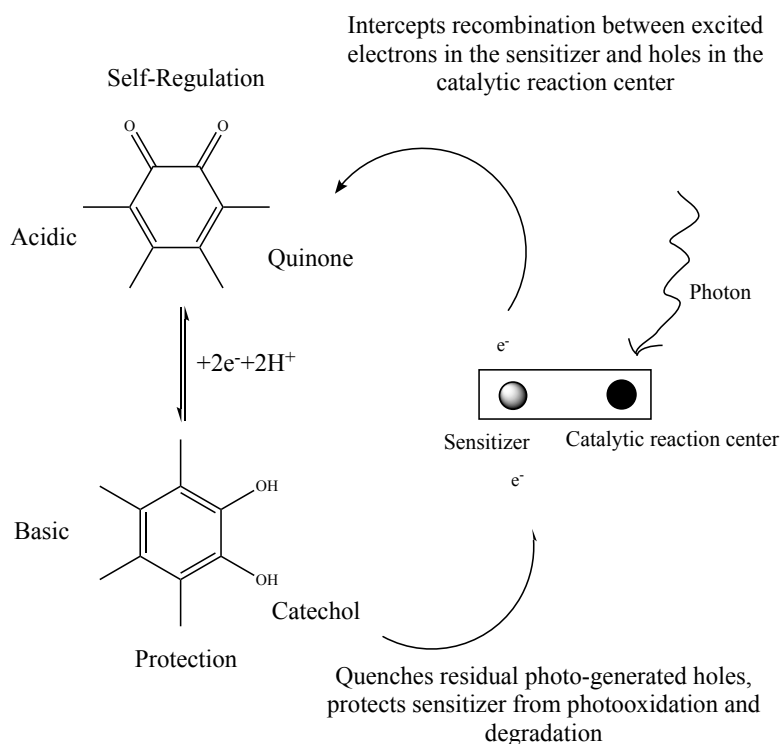
Figure 2.2 Quinone-catechol equilibrium based on pH

2.2   Objectives, novelty, and scope of the project

The objectives of this project include: modifying the redox-active polydopamine environment using new polymer and copolymer thin films with light-stable monomers that 1. can tune the pH response of the organic/inorganic hybrid materials for water reduction and 2. optimize and adjust the redox potentials between the polymeric films and sensitizers. The systems produced should ideally show long term stability, be reproducibly synthesized, have high performance in the pH range 4.0-7.0 with 4 being close to the pKa value [60] of PDA. The systems should have a high quantum yield (> 80%) to reach the efficiency necessary for a viable device, and act as a smart material with pH switching capability for photocatalytic hydrogen production. Though the pH-dependent redox potential behaviour of pure DA and polydopamine on glassy carbon electrodes has been studied earlier [61] the same has no precedent to the best of the author's knowledge in literature for polydopamine on an Au substrate with low scan rate conditions of cyclic voltammetry or copolymers of polydopamine. The data in literature will be used as a reference to ensure that experimental data produced here is reliable. Preparation of these copolymer films via electropolymerization has not been explored yet to the best of the author's knowledge. Also, thin film formation using different monomers and the possibility of a system where PDA is replaced other homopolymer films is yet to be explored further. Though PDA has several advantages as mentioned earlier for use in PWS, it has several limitations:

1. There is no evidence in literature that redox response of the PDA film can be tuned within a set pH environment for example, by tuning electropolymerization parameters such as end voltage [39] though some evidence exists for PDA-related systems being pH active [62]

2. By extension, the electron-hole recombination time and thus quantum efficiency of PDA is not adaptable as a standalone system

3. Though vast literature is available on PDA, the same is limited for studies of redox properties of copolymers of PDA, as well as other monomers, especially those produced by electropolymerization.

2.2.1   Adapting the redox-active polydopamine environment

As depicted in Figure 2.3 (a), the oxidation potential of PDA can be tuned between 0-1 V vs. NHE at a specified value of pH. Ambrico et. al suggested that the electrical properties of PDA could be chemically tuned through oxidative copolymerization of DA with a comonomer that has an aromatic amine functional group.
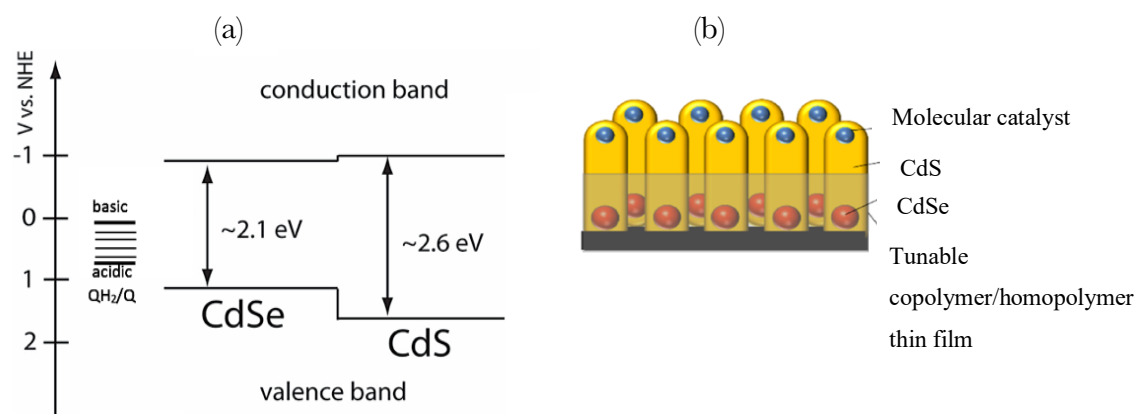
Figure 2.3 (a) Band diagram of CdSe@CdS nanostructure compared with PDA [63], [64]and (b) modified proposal of the polydopamine hybrid system

Comonomers to be used for this study include 3-amino-L-tyrosine and para-phenylenediamine which can incorporate aromatic amines and electron donating groups thus shifting redox potential [65], increase the ability to prevent electron-hole recombination and thus quantum efficiency of the sacrificial electron layer. This principle will be used to extend the study of pH-dependency and pH-switching capability to polydopamine copolymer systems with p-phenylenediamine and 3-amino-L-tyrosine. The amine groups in both being electron donating would be conjugated with the catechol/quinone moiety of DA thus extending π-electron delocalization as well as the electron mobility in the copolymer. This occurs due to a shift in the Fermi level of PDA towards its conduction band resulting in a doping effect similar to an n-type semiconductor thus also changing the band gap between its HOMO and LUMO levels. Para-phenylenediamine (p-PDA) and 3-amino-L-tyrosine (ALT) can both be considered suitable comonomers for the polymerization with PDA for tuning its electrochemical characteristics since they both [65]:

1) possess an aromatic amine function for covalent coupling with DA under the oxidation conditions required for its polymerization
2) are easily oxidized for incorporating the amine group to ensure efficient interaction with the oxidized DA system for polymerization
3) possess solubility properties that enable better film formation ability for copolymer film formation with DA

Ambrico et. al further suggested that the use of these monomers to copolymerize PDA could result in an increase in electron mobility and concentration in the polydopamine matrix as they were used for n-doping of polydopamine for hybrid semiconductor organoelectronics [65].

Investigations will be carried out using varying monomer ratios between polydopamine and the two comonomers to produce homogenous, reproducible thin films. Serotonin and 3-amino-L-tyrosine will also be used as new homopolymer systems for comparison with polydopamine. The possibility of reproducibly synthesizing an upscaled polyserotonin (p-Ser) thin film using a low concentration of monomer will be explored. Though p-Ser film formation has been reported in literature and reported as forming reactive species which adsorb irreversibly on the electrode surface resulting in fouling through the formation of an insoluble polymer-like by-product [66],[67] no studies are available (to the best of knowledge) about its oxidation/reduction dependence in different pH environments for photocatalytic applications. The abundant amino groups in its structure are promising for the purpose of chemical modification and studying its properties in PWS has not been explored to the best of the author's knowledge. Film formation using electropolymerization for 3-amino-L-tyrosine will also be attempted in this work for the first time (to the best of the author's knowledge). Thus, the experimental goals of this thesis can be summarized as follows:

1) Film formation of homopolymers with p-phenylenediamine, 3-amino-L-tyrosine and serotonin

2) Copolymer film formation between DA and three other monomers: p-phenylenediamine, 3-amino-L-tyrosine and serotonin using electropolymerization

3) Testing the adaptability of DA + p-phenylenediamine (PDA + p-PDA) and DA + 3-amino-L-tyrosine copolymers (PDA + ALT) and polyserotonin to different pH environments by evaluating variation in oxidation and reduction potentials, peak separation voltage and peak currents between the systems using cyclic voltammetry

4) Characterization of the systems for physical characteristics and chemical structural differences using various qualitative techniques

Thus, differences in functionality, including electrochemical, and surface properties of these modified systems polydopamine thin films and copolymer films will be investigated by cyclic voltammetry, profilometry, contact angle studies, and AFM. When the copolymerization of the films is achieved and optimized, they will be characterized using techniques such as XPS, ATR-FTIR, and SEM for comparison with PDA. Lastly, the possibility of adapting the properties of PDA to different pH environments will be evaluated. Using the knowledge presented in the Introduction, several experiments were designed and implemented to meet the objectives enumerated in the next section. The concepts were also used to support the motivation for this

thesis. The scientific formulas presented were also used for analysis of the experimental data presented in the Results and Discussion section.

3   EXPERIMENTAL SECTION

Preparation of Au slides: Au substrates (Sigma Aldrich, thickness 1000 Å) were cut to size using a diamond cutter and measuring grid. All used slides were cleaned using a Piranha solution of basic pH prepared using H_2O_2 (14.3 g, 34.5% -36.5%) dissolved in MilliQ water (6.7 g) and KOH (56 mg, 1.0 mmol) in a glass beaker. The gold substrates are inserted in it for several hours overnight and further purified before use in an argon plasma cleaner (Harrick) at a pressure of 2 mbar for 10 minutes.

3.1   Preparation of various homopolymers

All samples powders were weighed using a Mettler Todeo microbalance. A phosphate buffer of pH 6.9 prepared using 0.0053 M sodium phosphate dibasic heptahydrate with 0.0047 M Sodium phosphate monobasic monohydrate in MilliQ water, was used as the solution for each monomer/monomer mixture with an Au W.E., Au C.E., and Ag/AgCl (3.5 M KCl bridge) R.E. to prepare each film. The phosphate buffer solution was degassed with N_2 gas for 10 mins each time before and for 10 mins after the addition of each monomer/monomer mixture. The horizontal cell setup is shown in Figure 3.1.

3-amino-L-tyrosine homopolymer: 2 mg of 3-amino-L-tyrosine was dissolved in 6 mL in PB pH 6.9, bubbled under N_2 gas for 10 minutes and electropolymerized using a horizontal cell with the following parameters: Lower Vertex: - 0.5 V; Upper Vertex: 0.5 V; Number of scans: 8; Scan rate: 0.01 V/s; Step: 0.00244 V.

P-phenylenediamine homopolymer: 1.7 mg p-phenylenediamine was dissolved in 7 mL in PB pH 6.9, bubbled under N_2 gas for 10 minutes and electropolymerized using a horizontal cell and Nova software with the following parameters: Lower Vertex: - 0.5 V; Upper Vertex: 0.5 V; Number of scans: 8; Scan rate: 0.01 V/s; Step: 0.00244 V.

Serotonin homopolymer: Attempts were made to electropolymerize serotonin using two Methods. Method I: 10 mg of serotonin HCl was dissolved in 10 mL in PB pH 6.9, bubbled under N_2 gas for 10 minutes and electropolymerized using a horizontal cell with the following parameters: Lower Vertex: - 0.5 V; Upper Vertex: 0.5 V; Number of scans: 15; Scan rate: 0.01 V/s; Step: 0.00244 V.

Method II: serotonin films were electropolymerized using 0.5 mM Serotonin in 0.1 M NaCl and 5mM HEPES (pH ~ 6) using the following parameters: Lower Vertex: - 0.8 V; Upper Vertex: 0.8 V; Number of scans: 15; Scan rate: 0.01 V/s; Step: 0.00244 V. The number of scans and scanning voltage limits were increased in comparison with previous experiments to increase the chances of film formation based on past studies relating the number of cycles used to film thickness [39]. A summary of the chemicals and respective amounts used for the preparation of different films is shown in Table 3.1-1.

Table 3.1-1 Summary of synthesis data for various films prepared by electropolymerization

Sample	Monomer used	Weights/ratios used (g)/(mol)
PDA (reference)	Dopamine HCl (Sigma Life Science MW: 189.64 g/mol)	10 mg in 10 mL in PB pH 6.9 5.3 mM
p-PDA	1, 4, para-phenylenediamine (Sigma Aldrich MW: 108.14 g/mol)	1.7 mg in 7 mL in PB pH 6.9 2.2 mM
p-ALT	3-amino-L-tyrosine dihydrochloride hydrate (Sigma Aldrich MW: 287.14 g/mol)	1.2 mg in 6 mL in PB pH 6.9 0.7 mM
p-Ser	Serotonin HCl (Alfa Aesar, MW: 212.67 g/mol	Method 1: 10 mg Serotonin HCl in 10 mL PB pH 6.9
		Method 2: 0.5 mM Serotonin in HEPES buffer pH 5.5
PDA + p-PDA	Dopamine HCl (Sigma Life Science) + para-phenylenediamine (Sigma Aldrich)	Molar ratios: 1:1, 4:3, 3:1, 10:1
PDA + ALT	Dopamine HCl (Sigma Life Science) + 3-amino-L-tyrosine (Sigma Aldrich)	Molar ratios 1:1 4:3, 3:1,10:1
PDA + p-Ser	Dopamine HCl (Sigma Life Science) + Serotonin HCl (Alfa Aesar, MW: 212.67 g/mol	Molar ratios 1:1, 2:1, 3:1 and 10:1

3.2   Preparation of PDA and its copolymers

Polydopamine and copolymer films were prepared using a horizontal electropolymerization setup on an Au substrate (approximately 25 x 25 mm) using the following parameters kept constant: Lower Vertex: - 0.5 V; Upper Vertex: 0.5 V; Number of scans: 8; Scan rate: 0.01 V/s; Step: 0.00244 V. A phosphate buffer of pH 6.9 prepared using 0.0053 M sodium phosphate dibasic heptahydrate with 0.0047 M Sodium phosphate monobasic monohydrate in MilliQ water, was used as the solution for each monomer/monomer mixture with an Au W.E.,

Au C.E. and Ag/AgCl (3.5 M KCl bridge) R.E. to prepare each film. The phosphate buffer solution was degassed with N_2 gas for 10 mins each time before and for 10 mins after the addition of each monomer/monomer mixture. The horizontal cell setup is shown in Figure 3.1. Caution was maintained to ensure that the electrodes do not directly touch each other or the Au substrate surface, but only the monomer solution within the confines of the O-ring. In case of errors in measurements, the execution of the program was stopped on the software and the power source switched off, as stopping the data acquisition does not necessarily stop the flow of current through the setup.
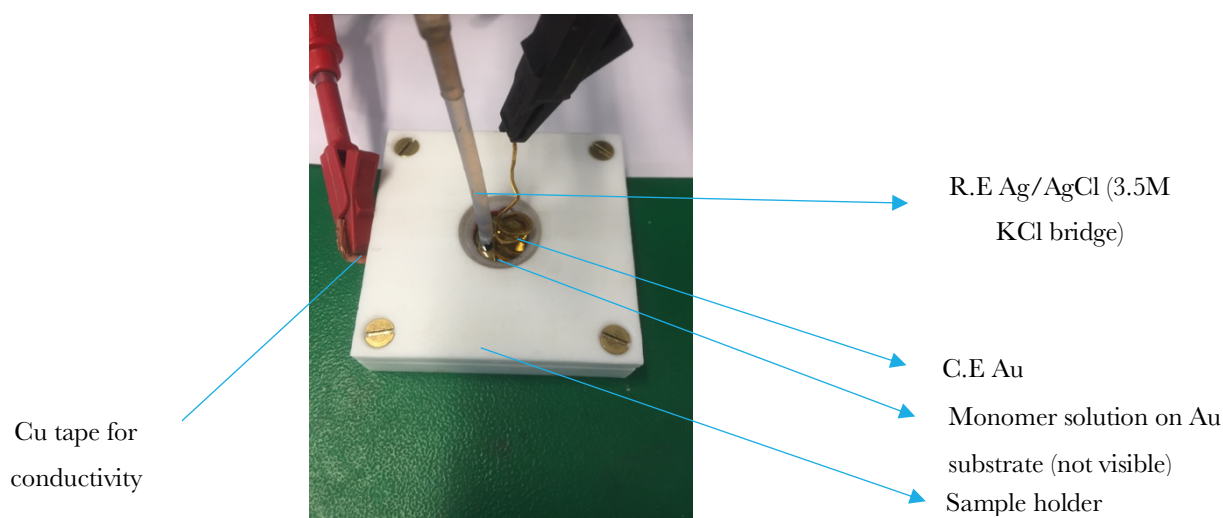
Figure 3.1 Actual setup for electropolymerization experiments

The synthesized films are rinsed with MilliQ water and then dried with N_2 gas. The films were synthesized at least twice each time to check for reproducibility. The ratio of dopamine HCl to monomers p-phenylenediamine and 3-amino-L-tyrosine was varied with decreasing amounts of the second monomers. Similarly, copolymer films of DA with serotonin were polymerized using horizontal electropolymerization setup on an Au substrate using the following parameters: Lower Vertex: - 0.5 V; Upper Vertex: 0.5 V; Number of scans: 8; Scan rate: 0.01 V/s; Step: 0.00244 V. The amount of dopamine HCl to monomer serotonin HCl used was varied using the molar ratios 1:1, 2:1, 3:1 and 10:1.

3.3   Characterization

3.3.1   Cyclic Voltammetry

All thin films for characterization by cyclic voltammetry were copolymerized using horizontal electropolymerization setup directly after their synthesis to ensure the O-ring is in the same position using the following constant parameters in the Nova software: Lower Vertex: - 0.5 V; Upper Vertex: 0.5 V; Number of scans: 8; Scan rate: 0.01 V/s; Step: 0.00244 V. Phosphate buffers of pH values 4.6, 5.6, 6.9 and 7.3 were used as the medium for cyclic voltammetry for a comparison of the system's response to different environments. A summary of the chemicals and respective amounts used for the preparation of the phosphate buffers is listed in Table 3.3-1. Appropriate amounts of disodium hydrogen phosphate and sodium dihydrogen phosphate were dissolved in MilliQ water in a laboratory flask and adjusted with the MP220 pH meter (Mettler Toledo) to the required pH with NaOH (5.0 M) and HCl (1.0 M)

Table 3.3-1 Summary of synthesis data for phosphate buffers of varying pH

Target pH	Amount of sodium phosphate dibasic	Amount of sodium phosphate monobasic
4.6	0.0032 M	0.1002 M
5.6	0.0049 M	0.0951 M
6.9	0.0534 M	0.0466 M
7.3	0.0754 M	0.0246 M

The CV characterization for all samples was performed phosphate buffers using following parameters: Lower Vertex: - 0.5 V; Upper Vertex: 0.5 V; Number of scans: 4; Scan rate: 0.01 V/s; Step: 0.00244 V. The number of scans and scan voltages were chosen such that the system would reach equilibrium for electron transfer but does not endanger removal of the film. A Pt electrode was used as the C.E. The procedure was repeated once for each trial to test reproducibility and to estimate standard deviation.

3.3.2   Surface physical properties

AFM: The PDA films were prepared by electropolymerization on a gold plate as described earlier. To determine the thickness of the films by AFM, the films were scratched with a plastic pipette tip and washed with MilliQ water before measurement. Since the lower layer appears predominantly flat, it was assumed that only the polymer layer in each case was removed [39].

For the measurements, an atomic force microscope (Bruker Dimension Fast Scan Atomic Force Microscope) in the Peak Force Quantitative Nano Mechanical mapping mode (QNM) was used with air as the medium. A silicon cantilever (Bruker OTESPA-R3) having a spring constant of 2 N/m and a resonant frequency of 70 kHz was used. To evaluate the thickness and roughness of the films Gwyddion software version 2:47 and Nano Scope Analysis Version 1.50 were used. The roughness used from the software is the mean roughness over a fixed area selected. The inclination of the profiles obtained was corrected with the lowest part of the height scale set to 0 nm. Then, the thickness of the PDA-films was determined by tracing an image of the boundary between the PDA film and the scratch and measuring the difference in height between the two planes. Some of the measurements were performed by Sean Harvey and Tommaso Marchesi and some are the author's own.

Profilometry: The sample preparation was carried out as for atomic force microscopy. A scratch in the polymer films was made with a plastic pipette tip, to avoid scratching the Au layer underneath as could occur with a metallic syringe needle. The measurements were carried out on the KLA-Tencor Stylus Profiler model P7. The following parameters were used: scan speed 20 μm/s, sampling rate 100 Hz, applied force 2 mg. All graphs were plotted using Origin 2017 graphing software and Python programming.

3.3.3 Qualitative chemical species analysis

XPS spectra: The XPS measurements were performed by Hao Lu, Gabriele Herrmann and Leon Praedel using monochromatic Al K_α^- Radiation with an energy of 1486.7 eV using a takeoff angle of 90°. Various polymer films were examined on gold plates and a pure gold plate was used as reference from previous measurements submitted by Jolanta Szelwicka [39]. An Au reference for the samples was not available for thickness computations.

FTIR: FTIR analysis of various thin films was performed in the reflection and transmission mode. A pure Au substrate was used for background measurement. The scans on each sample are performed 2000 times over 4 stages. This is to ensure a reduction in CO_2 and H_2O peaks from the atmosphere by increased purging of the sample analysis chamber with N_2 gas. FTIR measurements performed in the reflection mode were done along with Tommaso Marchesi.

4   RESULTS AND DISCUSSION

4.1   Thin film synthesis by electropolymerization

4.1.1   Serotonin, 3-amino-L-tyrosine and p-phenylenediamine homopolymers

Figure 4.1 shows the first cycle for the electropolymerization of PDA as a reference for understanding the cyclic voltammograms of the other homopolymer films. During the first positive scan, two oxidation peaks (a1) at +0.3 V and (a2) at -0.2 were observed, which can be attributed to the oxidation of the DA leading to dopaminequinone. Dopaminequinone undergoes several chemical reactions and electrochemical transformations, which then leads to the formation of PDA. Li et al. proposed an "ECECEE" mechanism that involves 5,6-indolequinone as the polymerizable species [68], [69].
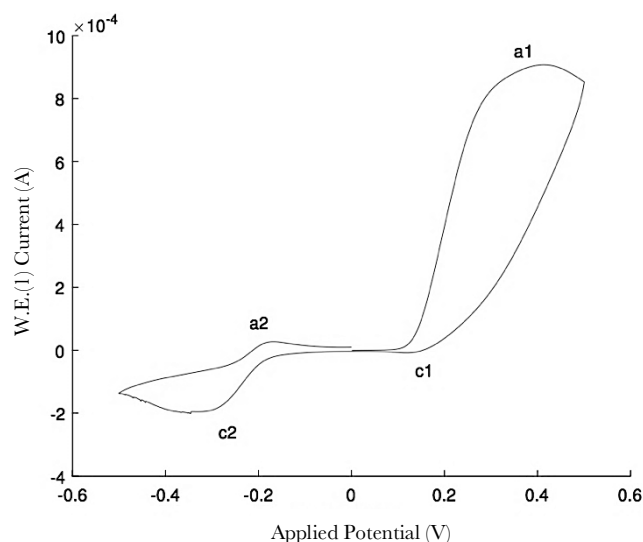
Figure 4.1 Cyclic voltammogram of polydopamine formation showing critical peaks; adapted from [68],[69]

In the subsequent reverse scan, two reduction peaks c1 and c2, were observed at +0.1 V and -0.3 V, respectively. According to the "ECECEE" mechanism, these reduction peaks (c1 and c2) can be attributed to the reduction of leucodopaminechrome and dopaminechrome, respectively. During the cycle by cycle scans, the continuous drop in electrode activity due to the formation of PDA passivating layers is shown by the continuous decrease of the peak currents of peak (a1) and peak (a2). However, the peak currents of (a2) and (c1) remain relatively constant. This behavior demonstrates the fouling of the electrode by the PDA layers as it grows with each successive scan [70]. It must be noted that the porosity of the polydopamine coatings could increase with the pH of the dopamine solution used to produce the film thus the pH of

the buffer used was checked regularly to ensure it was close to nearly 7. Figure 4.2 (a) shows the cyclic voltammograms over 8 cycles for the electropolymerization of homopolymer PDA.
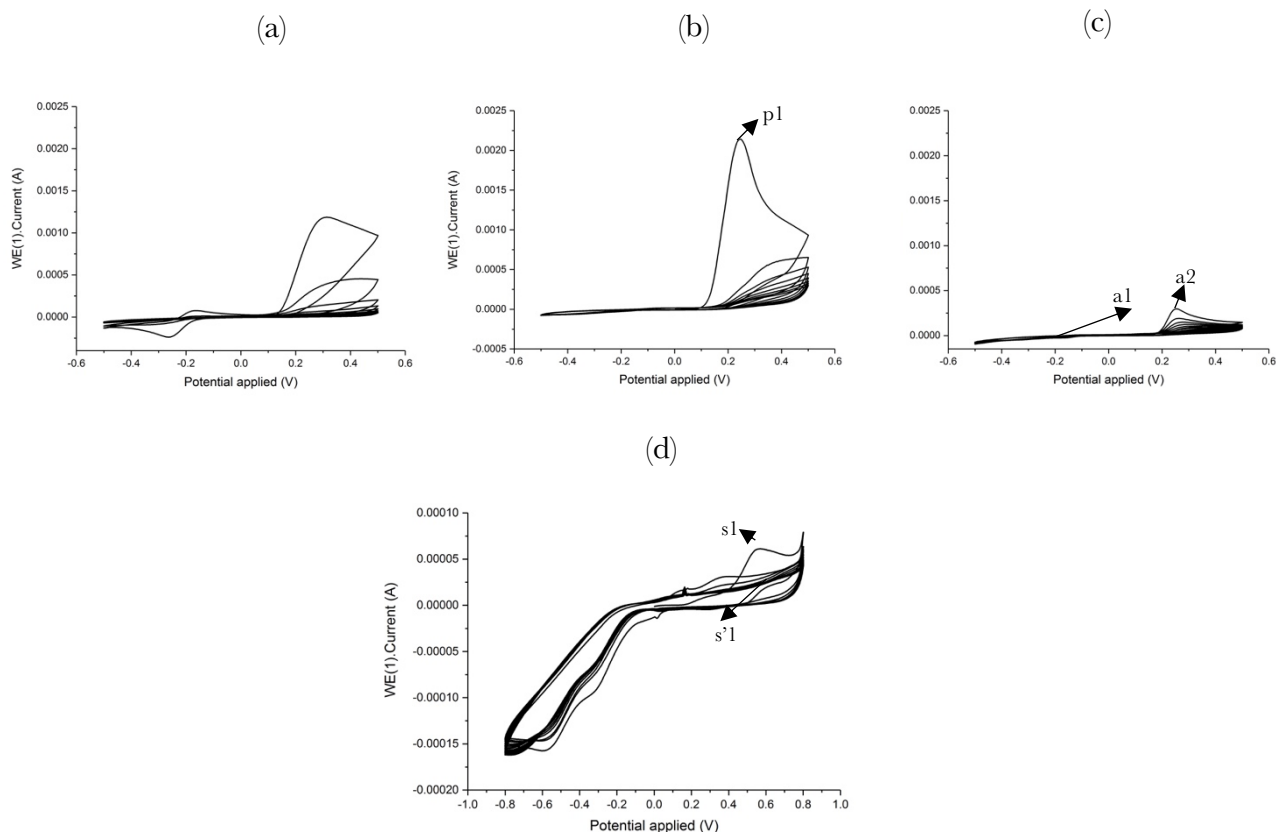
Figure 4.2 Cyclic voltammetry diagrams of synthesis of pure PDA (a) p-PDA (b) p-ALT (c)and p-Ser (d) by electropolymerization.

Figure 4.2 (b) and (c) show the cyclic voltammograms over 8 cycles for the electropolymerization of homopolymers p-PDA, and p-ALT respectively. A shift is observed in both the oxidation potential and current of the monomers in the first cycles of each; it is increased in the case of p-PDA as shown in Figure 4.2 (b) and decreased in the case of 3-amino-L-tyrosine as shown in Figure 4.2 (c). For p-PDA the decrease in current at the W.E. is similar to that of PDA indicating an insulating film formation on the substrate through polymerization, and despite their similar structure, polyaniline is conductive. Similar to the peaks reported in literature [71] with electropolymerization of polyaniline and p-PDA on Si/Pt substrates where an oxidation peak was observed at ~ +0.18 V, the first oxidation peak p1 is observed at ~ +0.2 V. The slight shift can be explained by the change of substrate used as Au as well as reaction conditions; the study used acidic electrolytes while here, the phosphate buffer used has a pH of nearly 7. Similar to the reported data for polyaniline on Si, the oxidation of p-PDA is also irreversible due to the absence of a reduction peak in the CV diagram. The SEM images of

pure p-PDA are shown in Figure 4.3 (a), (b). The image shows the presence of microneedles with interconnections in between comparable to those found in literature when p-phenylene diamine was synthesized in an acidic environment [21]. Other microstructures are also possible for synthesis however, examining this is beyond the scope of this thesis. Also visible are thicker cuboidal rod-like structures encapsulated by fibrous structures.

(a)   (b)
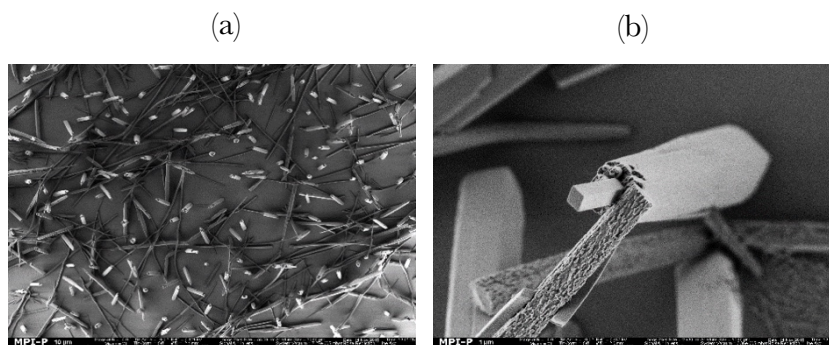
Figure 4.3 SEM images of pure p-PDA (a), (b)

The electropolymerization of pure p-phenylenediamine has been presented by B. Lakard et al. [72] using CV technique on Pt wire-electrode at pH 7.0 in phosphate buffer solution where a thin insulating film with microneedle structures on top was obtained. From their thermochemical calculations, it was confirmed that the mechanism is a linear one with carbocation formation in the first step and the products have the structure:

$$NH_2 - Ph^+ + NH_2 - Ph - NH_2 \rightarrow - Ph - NH_2^+ - Ph^- NH_2$$

Different types of working electrodes have been used in the electropolymerization of p-phenylenediamine including Pt, IrO_2, Ti, and graphite but the electropolymerization on Au has (to the best of knowledge) not been reported in literature. Comparable to observations made by Cataldo et al. [22], there is initial oxidation of the monomer seen by the purple/reddish colour of the solution formed on the electropolymerizer cell surface. However, unlike the conditions used by Cataldo and Lakard where the polymerized product simply dissolved, similar conditions used during experiments yielded adhesion of the polymerized product onto the Au substrate although no film was verified to be present underneath. Thus, the formation of these microneedles under these conditions without irradiation of UV light and supporting surfactant polyvinylpyrrole (PVP) as studied by Min et al. [21] is possible and is reported here on an Au substrate for the first time. The formation of p-PDA microneedles is related to intermolecular $\pi-\pi$ interactions and the electrostatic repulsion interactions [73]. It is suggested

that the monomer is oxidized directly (without intermediates) to a pernigraniline-like structure and thus the reaction does not involve radical cation (polarons) or carbocation formations and polymerized in a chain-growth process [23] by end-to-end polymerization with the final straight chain structure shown in Figure 4.4.
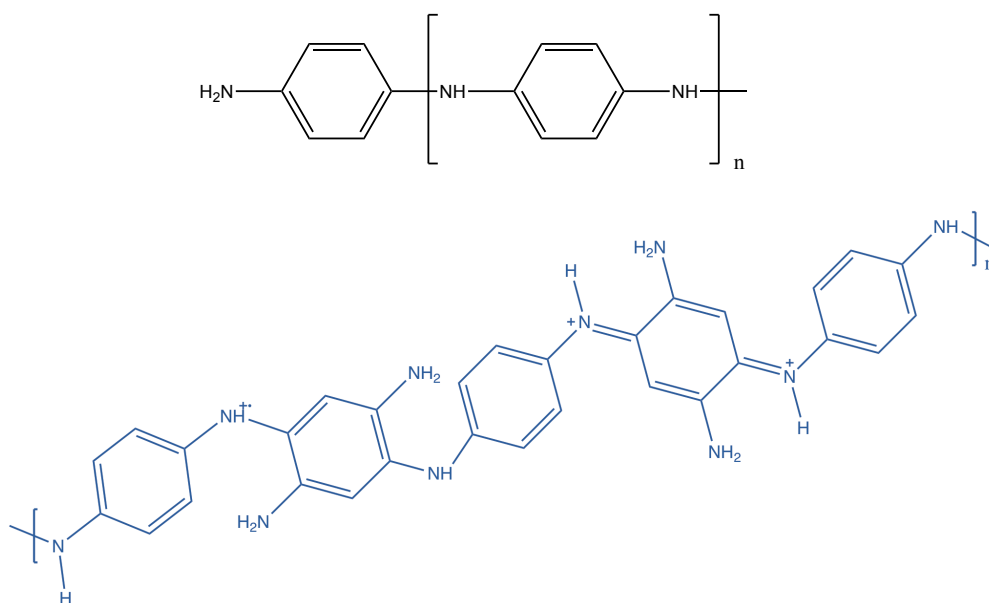
Figure 4.4 Repeating unit of polymerized p-PDA (top) and possible structure after polymerization (bottom; adapted from [23] [74]
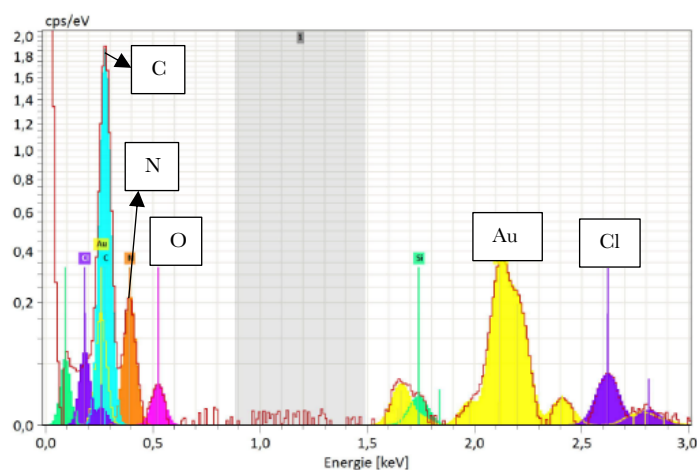
Figure 4.5 EDX spectrum of p-PDA samples showing an expected ratio of C:N

The EDX spectrum measured by Gunnar Glaser in Figure 4.5 shows the following peaks: a C:N ratio consistent with that expected for the structure of p-phenylenediamine and Au from the Au substrate used for electropolymerization. Peaks for O could arise from atmospheric oxygen and the presence of Cl could indicate chloride ions adhered to the structure from the use of 3 M KCl (Ag/AgCl bridge) R.E. for electropolymerization.

In contrast, from the CV diagram for the electropolymerization of p-ALT, a fall in the rate of current decrease at the W.E. over 8 consecutive cycles is observed; indicating that the polymer formed is not as readily insulating as PDA or p-PDA. This could also be because the number of cycles used do not reflect the maximum or the optimum number of cycles required by the system to come to equilibrium. Thus, one limitation of the study is that the number of cycles for the synthesis of p-ALT was not optimized based on non-zero slope differences between cycles. However, since too many variations in parameters during electropolymerization would cause complexity in data analysis, this could present scope for future work. The SEM image of pure ALT is shown in Figure 4.6.
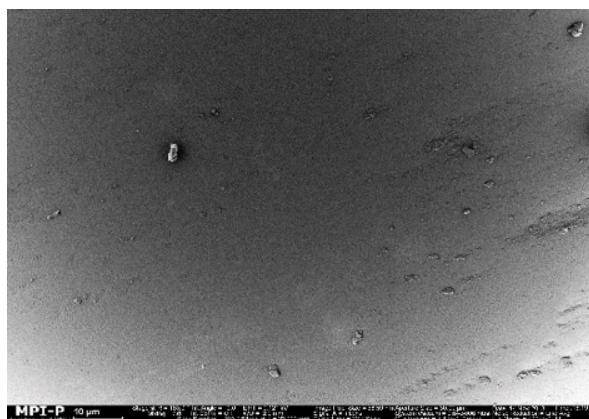
Figure 4.6 SEM image of pure p-ALT

A smooth thin film surface is visible with few particles on the surface, possibly from contaminants. Such a polymer film formed from an amino derivative of tyrosine by electropolymerization is examined and reported here for the first time (to the best of knowledge). In 2018, Lee et al. [31] conducted an analysis of the 3-amino-L-tyrosine monomer protein incorporated into biological proteins with linear sweep voltammetry. Though the polymerization or film formation of 3-amino-L-tyrosine was not attempted in the analysis by Lee et al., an explanation for the initiation process by a 2-electron oxidation-reduction reaction of the monomer which eventually leads to polymerization can be hypothesized from their work as shown in Figure 4.7. This could also explain the redox peaks a1 at ~ -0.2 V and a2 at ~ +0.3 V in the cyclic voltammogram. Though the final polymer is assumed to be linear, there is also a possibility for cross-linkage between the straight chains at the NH_2 groups. The possibility of this is further explored in Section 4.1.3.
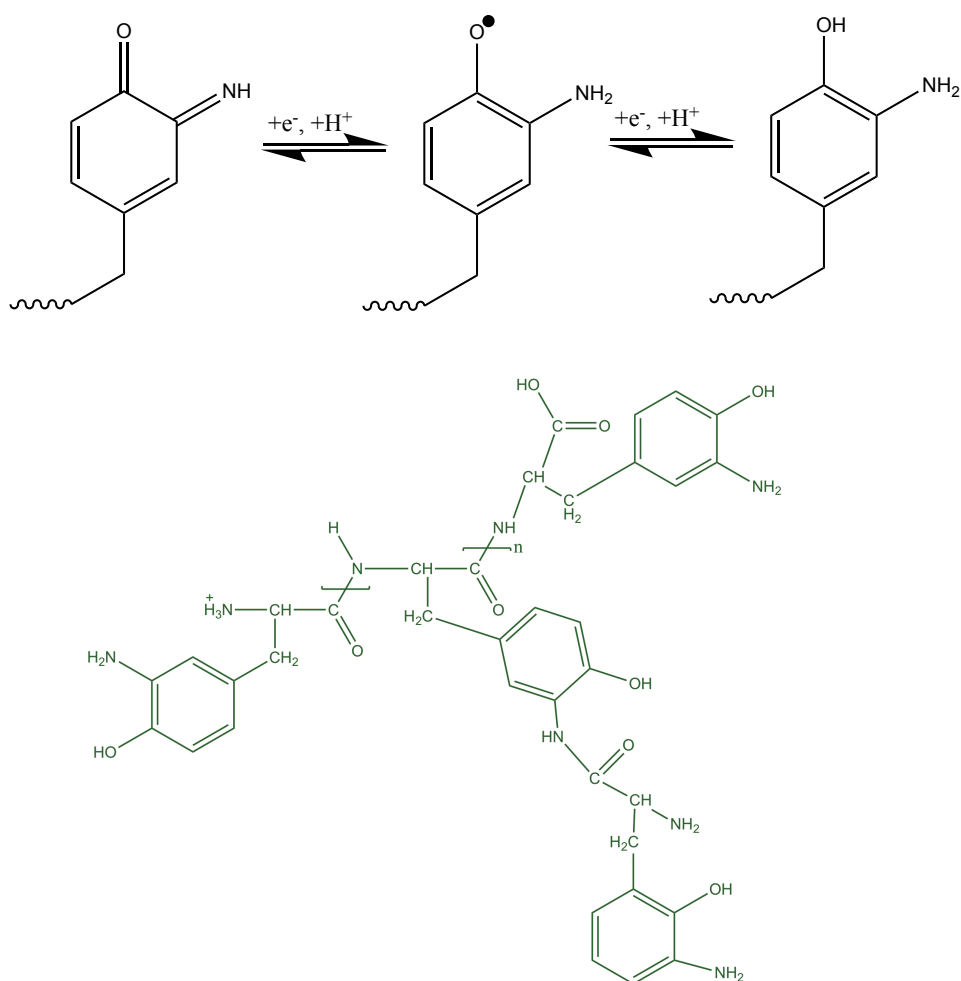
Figure 4.7 Two-electron oxidation-reduction reaction of 3-amino-L-tyrosine which initiates the polymerization process (top) and proposed structure of p-ALT (bottom); adapted from [31]

Figure 4.2 (d) shows the cyclic voltammograms over 8 cycles for the electropolymerization of homopolymer p-Ser. Note the difference in scale from the other CV diagrams. The CV diagram for the electropolymerization of pure serotonin is quite different from those of the other homopolymers due to the change in the buffer used (HEPES) and a difference in scan voltage limits also showing a varied deposition rate for p-Ser on Au which has lower adhesion properties in comparison with polydopamine. It was also verified that the film formation is only possible via electropolymerization by attempting dip coating of the Au substrate in the monomer solution overnight which did not yield any film on the surface of the gold plate. Several trials were conducted using HEPES buffer to optimize film formation by p-Ser (see Appendix 1 in Section 6.1) since the film formation was found to be absent in case of basic phosphate buffer. This is summarized in Figure 4.8.
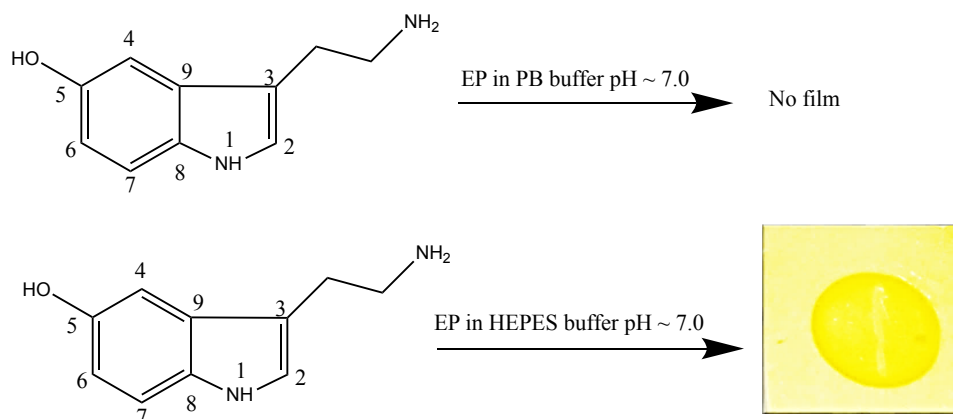
Figure 4.8 P-Ser film formed on Au by electropolymerization: comparison of results from two synthesis methods

P-Ser thin film formation has been studied earlier for the purpose of developing an enzyme-immobilization matrix for amperometric and biofuel cell (BFC)-based biosensing [67] where the possible polymerization sites for serotonin were discussed using the principles of Density Functional Theory (DFT) calculations and electrochemistry. This was done in 0.1 M phosphate buffer (pH 7.0) containing Serotonin in varying concentrations. For 20 μM Serotonin, a cathodic current ramp s'1 due to the irreversible reduction of the soluble oxygen was observed at ~ -0.3 V (0.1 V lesser than the value reported in literature, as expected due to the lower scan rate used − 0.01 V/s instead of 0.1 V/s), which is also observed in the CV diagram obtained in Figure 4.2 (d). This cathodic current ramp was also observed becoming notably smaller after nitrogen saturation of the solution (see Appendix 1 in Section 6.1). A small anodic shoulder peak s1 due to oxidation of 5-HT (defined earlier) was observed at ca. 0.3 V, which can be attributed to the oxidation of phenolic hydroxyl and indole groups which also reduces with decreasing serotonin content [75]. It was proposed that the reactive species adsorb irreversibly on the electrode surface resulting in fouling through the formation of an insoluble polymer-like by-product. This is visible during experiments where the Au C.E. turns dark as shown in Figure 4.9, and must be cleaned in Piranha solution before further use.
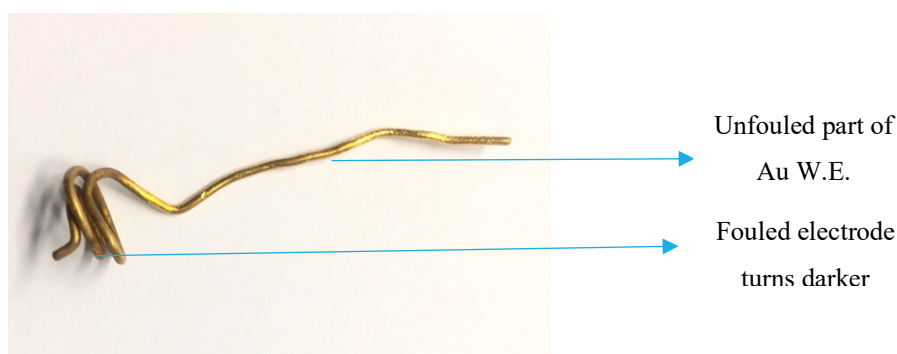
Figure 4.9 Fouling of electrode due to p-Ser deposition during electropolymerization

Huang et. al. inferred that oxidative polymerization of serotonin is a complex multi-step process where at very low concentrations (as was used in this thesis), oxidation of 5-HT may produce a dihydroxyindole derivative as the main product, and the chemical bonding between Serotonin molecules for chain propagation is very difficult due to the reduced probability of mutual collisions of 5-HT molecules. The oxidative polymerization mechanism of 5-HT is the indole-like polymerization through chain propagation mainly at sites 1, 2, 4, 6, and 7 as shown in Figure 4.10 (a) and (b) [66],[76]. Patel et. al [66] studied the film formation properties of serotonin by electropolymerization on a polycrystalline boron-doped diamond substrate using cyclic voltammetry and *in-situ* electrochemical AFM. In this study, an electrochemical cell was filled with a solution containing 0.5 mM 5-HT in 0.1 M NaCl with a 5 mM HEPES buffer. A chloridized Ag/AgCl (0.1 M Cl) wire electrode served as the reference and Pt gauze was used as the counter for electropolymerization at 0.1 V/s. The possible mechanisms of electropolymerization and film formation proposed can be extended to the electropolymerized p-Ser film in this work and are summarized in Figure 4.10 (b).
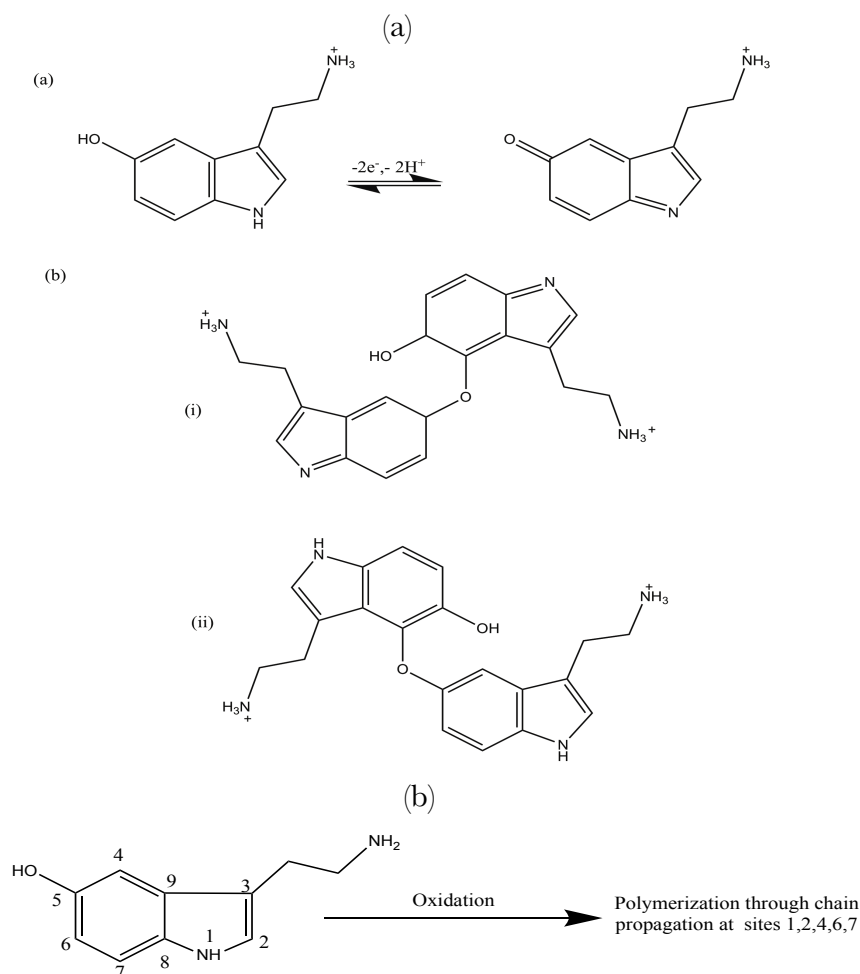
Figure 4.10 Proposed mechanism for the two-electron oxidation of Serotonin in steps (a) inset (a) and (b) in figure; leading to dihydroxyindole formation shown in structures (i) and (ii) and (b) polymerization sites of Serotonin (b); adapted from [66],[76]

Considering the dimer formation in Figure 4.10 (a) inset (b)-(ii) and chain propagation at site 4 depicted in Figure 4.10 (b), the formation of a trimer is possible as shown in the reaction in Figure 4.11. These structures are based on the proposed mechanisms of polymerization of serotonin given by Nakatsuka et al. [34] and Wrona et al. [77].
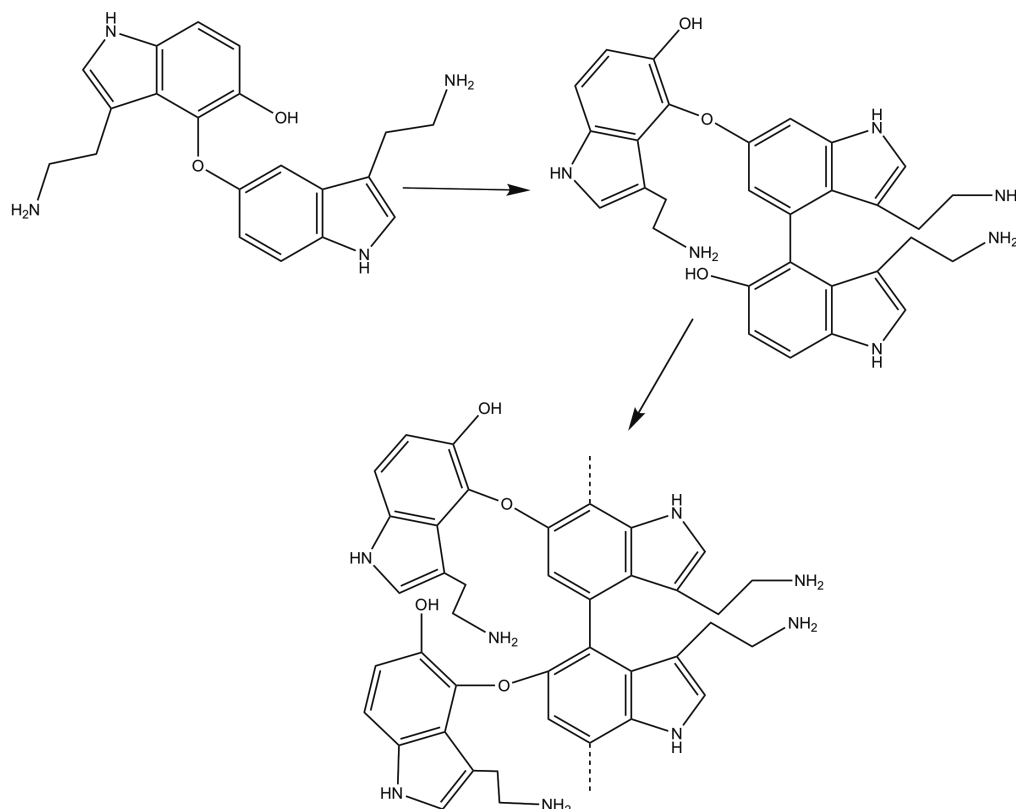
Figure 4.11 Proposed mechanism for the polymerization process for p-Ser formation up to trimer formation; own figure; adapted based on concepts from [34],[66],[76],[77]

Despite the available literature on the use of electrodes for 5-HT detection, information about film formation during 5-HT oxidation is limited. The film formation of p-Ser on an Au substrate using such low concentrations of the monomer is not yet reported in literature as Huang et al. [76] used high concentrations of 40 mM which is about 8 times the concentration used here and the scan rate was 0.1V/s which is 10 times the value used here and could result in increased electrode fouling. The presence of the various homopolymer films was tested using profilometry and AFM as shown in Figure 4.12 and Figure 4.13 respectively (not all profilometry data is shown).
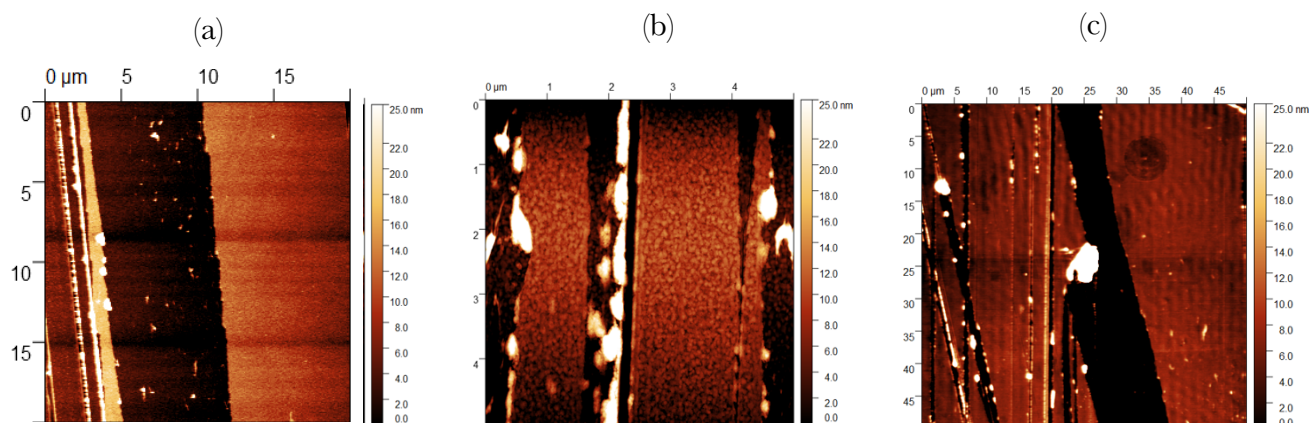
Figure 4.12 AFM micrographs of pure PDA (a) p-ALT (b) p-Ser (c)
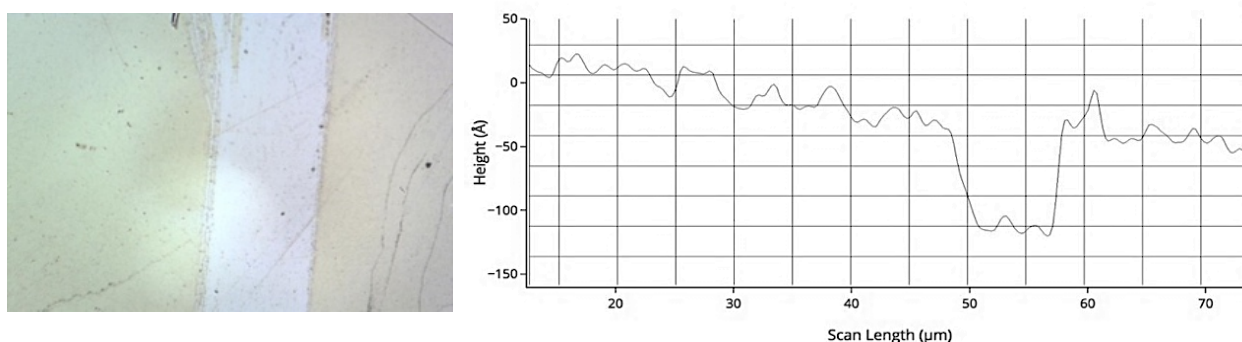
Figure 4.13 Profilometry image and profile of pure p-Ser across a ~ 80 μm scan length

4.1.2 Polydopamine-based copolymer films

Figure 4.14 (a)-(d) shows the cyclic voltammograms for the copolymer films made by electropolymerization of DA with p-phenylenediamine in different ratios. No significant shift is observed in the oxidation potential of the monomer mixtures from PDA in the first cycle, however, the current at the W.E. of the monomers in the first cycles decreases, and with increased incorporation of DA, the current in subsequent cycles decreases at a faster rate.

(a) (b) (c)

(d) (e)
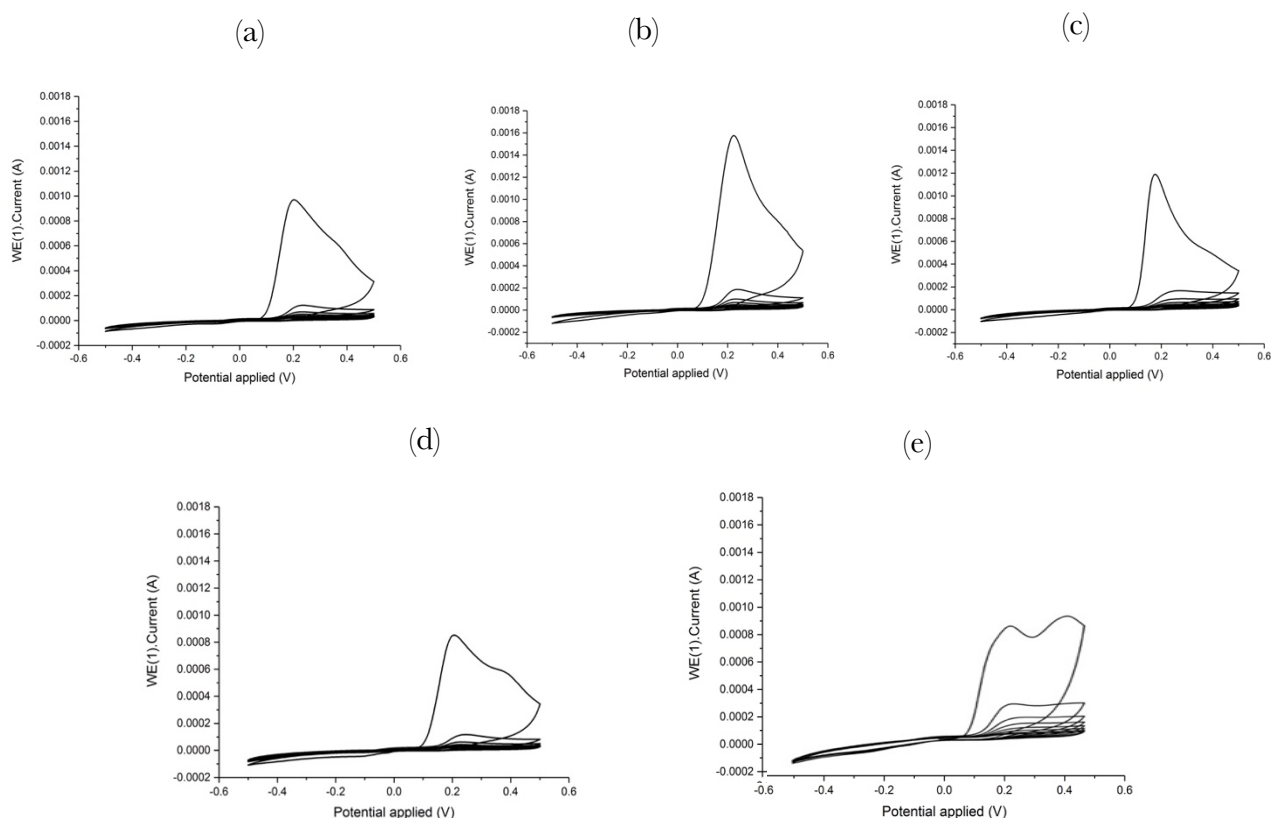
Figure 4.14 Cyclic voltammetry diagrams of synthesis of PDA + p-PDA copolymers by electropolymerization in the ratio 1:1 (a) 4:3 (b) 3:1 (c) 6:1 (d) 10:1 (e)

For the ratio 1:1, 3:1, and 4:3 the oxidation process appears irreversible as the CV diagram shows no reduction peak, while in the ratios 6:1 and 10:1 they are quasi-reversible. With increased incorporation of DA, the current in subsequent cycles does not show a specific trend

indicating that the monomer ratios or concentrations do not affect deposition capability. The current in the first cycle for the 10:1 film is significantly lower than that of the other ratios indicating greater insulating behaviour on the surface of the film formed. Figure 4.15 shows the characteristic colour expected when p-phenylenediamine is used in the monomer mixture and oxidized on exposure to air.
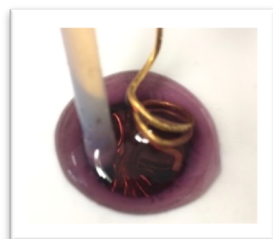
Figure 4.15 Darkening of the monomer mixture containing dopamine-HCl and p-phenylenediamine in phosphate buffer on exposure to air to reddish-purple

Figure 4.16 (a)-(d) shows the cyclic voltammograms for the copolymer films made by electropolymerization of DA with 3-amino-L-tryosine in different ratios. No significant shift is observed in the oxidation potential or the current at the W.E. of the monomers in the first cycles. For the ratio 1:1, 6:1 and 4:3 the oxidation process appears irreversible while in the ratios 3:1 and 10:1 they are pseudo-reversible. With increased incorporation of DA, the current in subsequent cycles decreases at a faster rate (showing increasing insulating behaviour). Thus, the ratio 10:1 implies greater film deposition due to the increasing insulation in subsequent cycles.

The optimum molar ratios for solubility and adhesion properties during copolymerization with DA by autooxidation of p-PDA and ALT given by Ambrico et al., were 1:1 and 3:1 respectively. However, synthesizing the same using electropolymerization for the production of thin copolymer films for the purpose of PWS is reported here for the first time (to the best of knowledge). Also, though capacitance-voltage characteristics were studied earlier, capabilities of tuning redox potentials or pH-based behaviour for catalytic functionality is focused on here for the first time (to the best of knowledge).
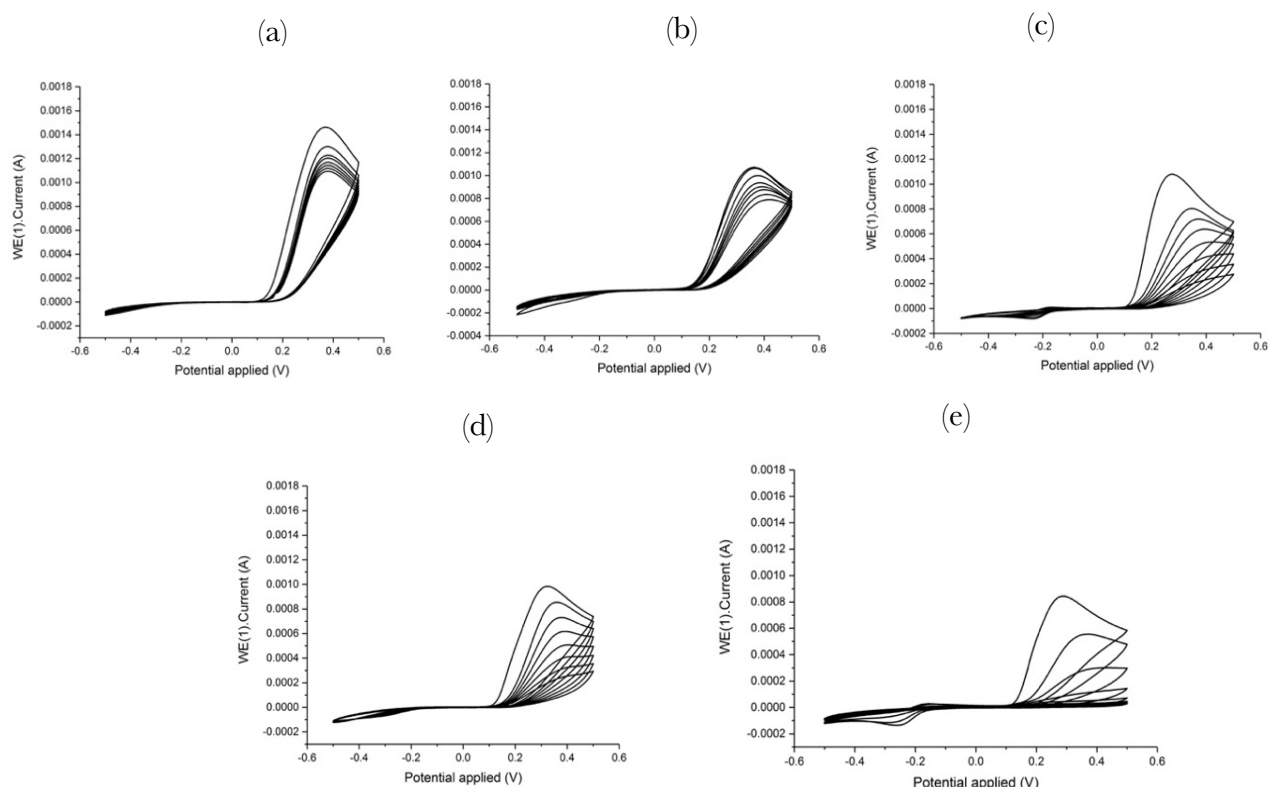
Figure 4.16 Cyclic voltammetry diagrams of synthesis of PDA + ALT copolymers by electropolymerization in the ratio 1:1 (a) 4:3 (b) 3:1 (c) 6:1 (d) 10:1 (e)

The ratio of the second comonomers were kept below that of DA to ensure that the polydopamine system is still the main matrix as otherwise, the catechol-quinone interplay could be lost. The presence of the films and their thickness were both verified using profilometry measurements as a second physical characterization method. The presence of the p-PDA fibers was absent in copolymer samples of p-PDA and PDA indicating that the presence of DA hinders the formation of these fibers as expected when copolymerizing polydopamine with its analogous structures/other comonomers [78]. In future work, the possibility of incorporating these fibers as one part of a polydopamine nanocomposite structure could be explored for its characteristics. The proposed mechanism of oxidative coupling of the comonomers leading up to polymerization is given in Figure 4.17 [65].
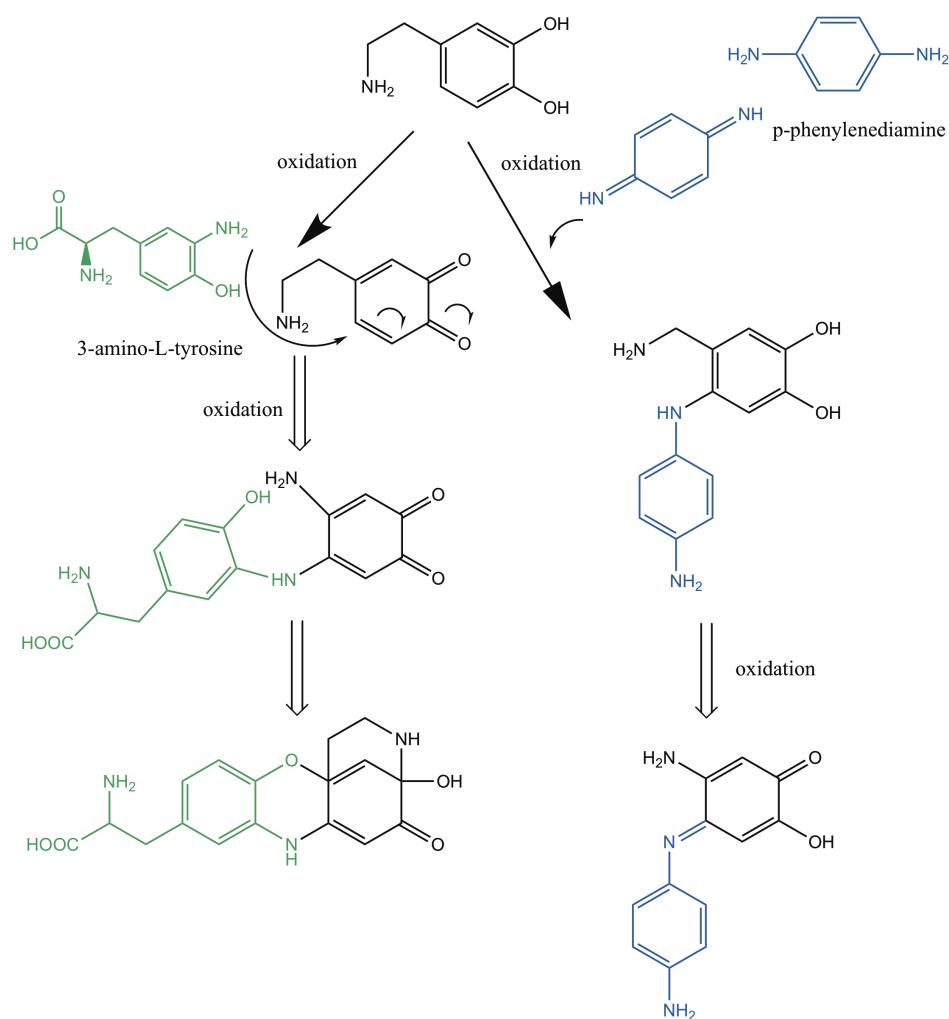
Figure 4.17 Proposed mechanism for the oxidative coupling of PDA with p-phenylenediamine and 3-amino-L-tyrosine; redrawn and adapted from [65]

Based on the oxidative coupling mechanisms of DA with p-phenylenediamine and 3-amino-L-tyrosine as shown in Figure 4.17 as well as the homopolymer structures of p-PDA and p-ALT proposed earlier, a hypothetical copolymerization mechanism can be proposed for PDA + p-PDA. This is further based on the mechanism proposed for PDA + polyethyleneglycol nanoparticles proposed by Harvey et al. The proposed copolymerization mechanism is shown in Figure 4.18.
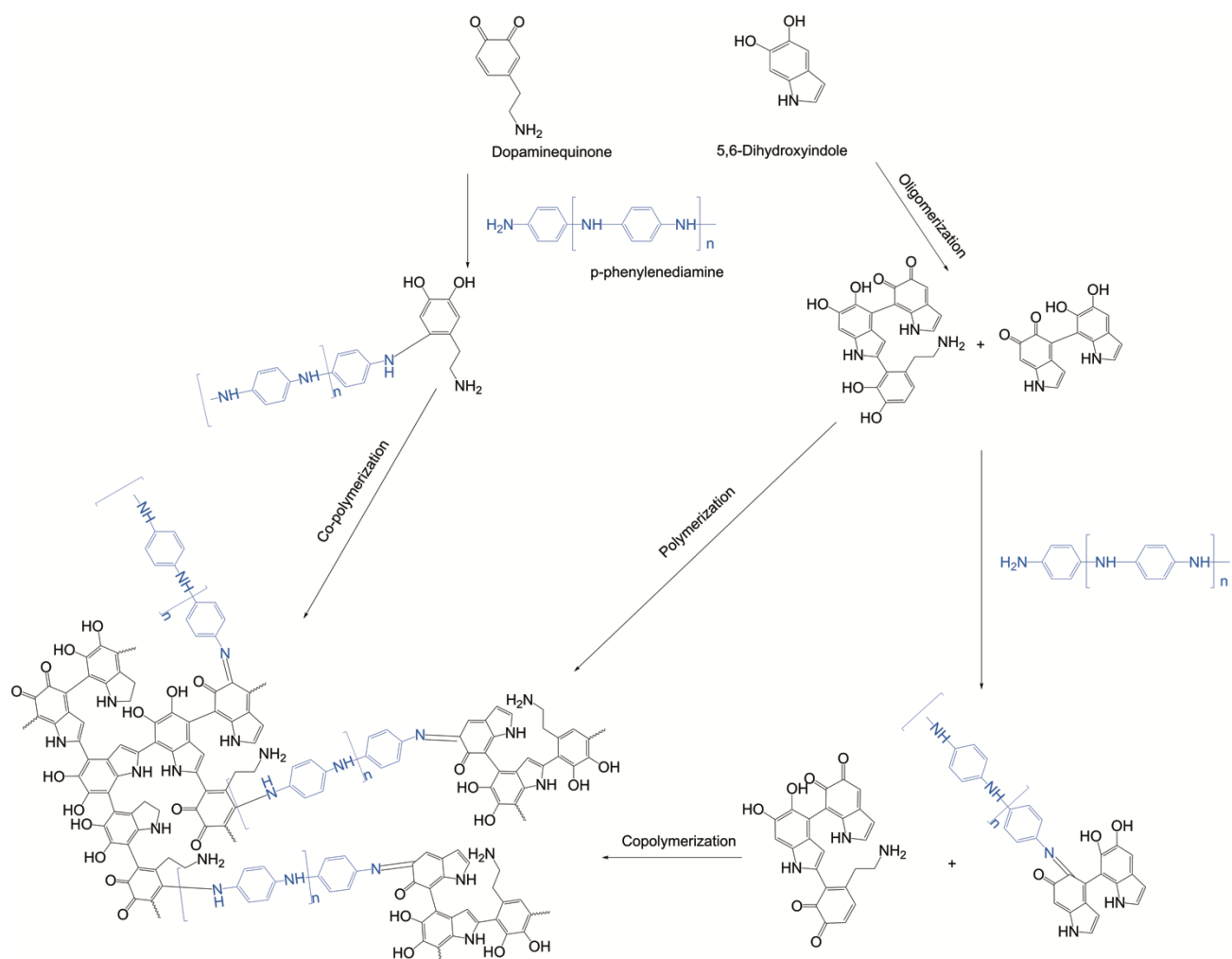
Figure 4.18 Proposed mechanism for the copolymerization of PDA p-PDA; own image, adapted based on concepts from [23],[65],[74],[79]

Similarly, a hypothetical mechanism can be proposed for the copolymerization of PDA + ALT based on the molecular structure formed by oxidative coupling of the quinone moiety of DA and 3-amino-L-tyrosine as shown in Figure 4.19. Though the proposed structures assume actual copolymer formation between the comonomers involved, it could also be possible that a blend is formed between the two constituents. The percentage of these constituents in the final structure is also a matter for further investigation.
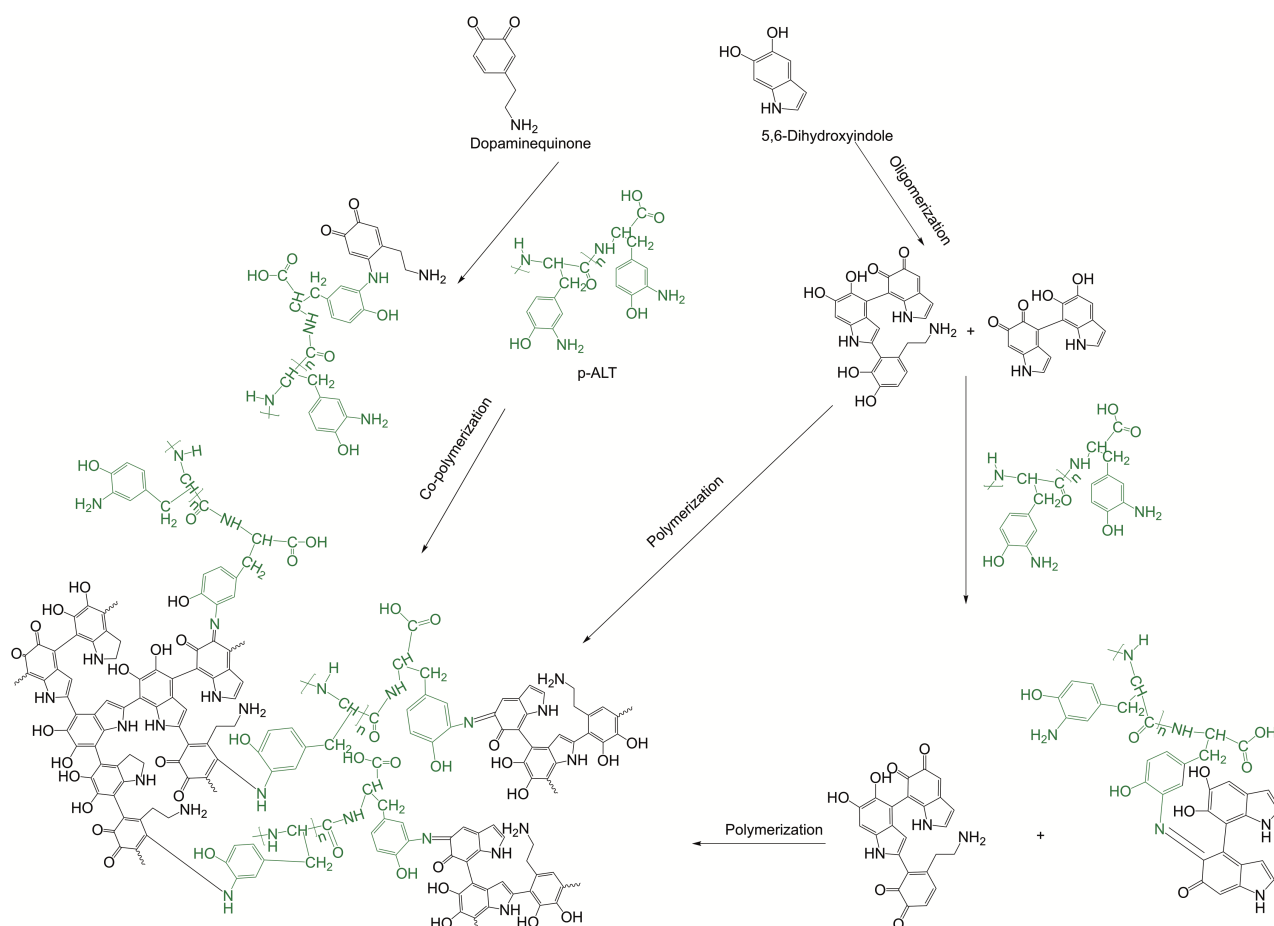
Figure 4.19 Proposed mechanism for the copolymerization of PDA + ALT; own image, adapted based on concepts from [65],[79]

The presence of a film in each copolymer sample was verified by AFM with the thickness and roughness analyzed as shown in Figure 4.20 and Figure 4.21. It is evident that some films are more homogenous across the area analysed. For example, the films formed from PDA + p-PDA in the ratios 1:1 and 3:1 are more homogenous than the 6:1 ratio.
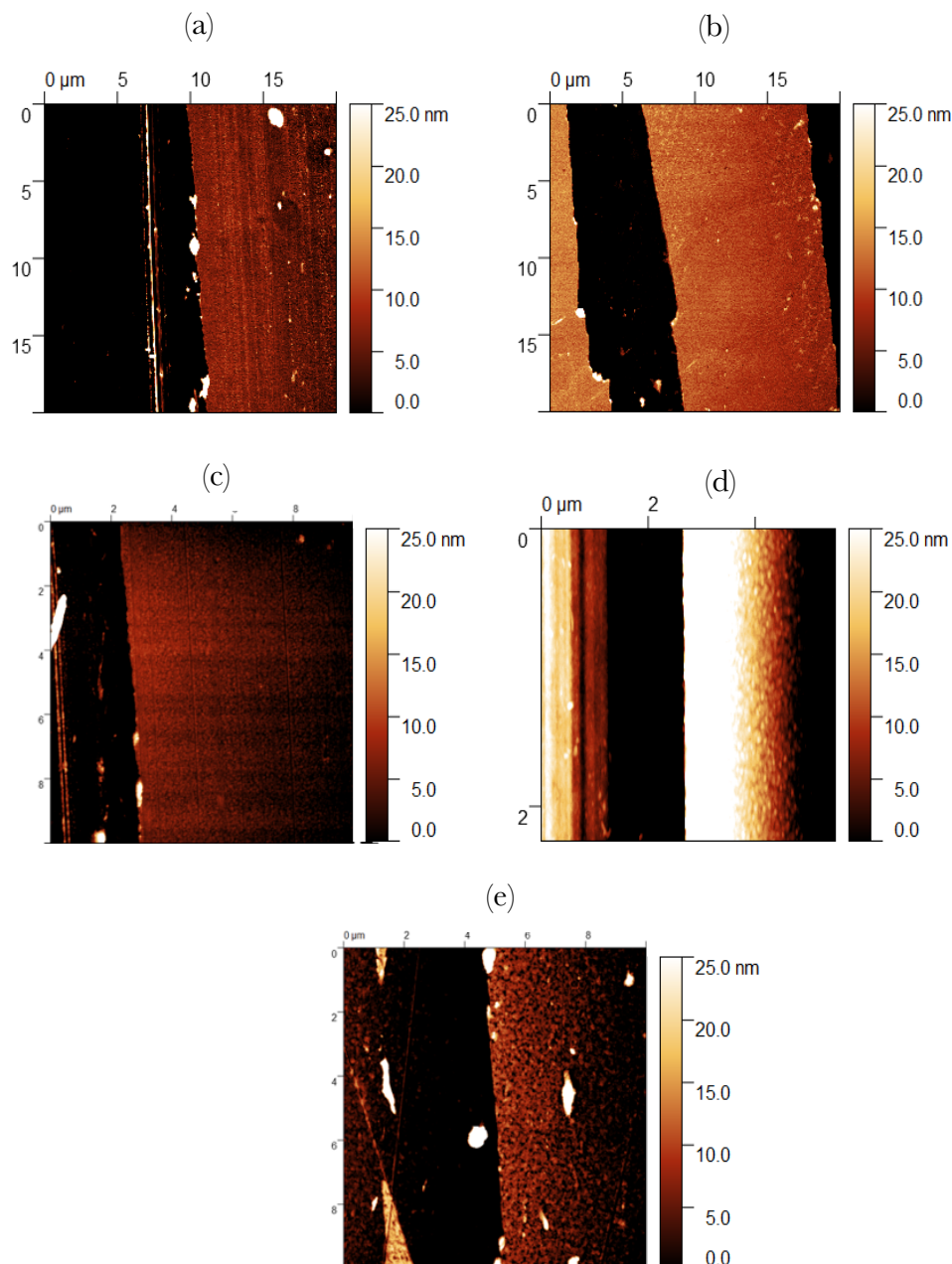
Figure 4.20 AFM micrographs of polydopamine-phenylenediamine copolymer films synthesized in the ratio 1:1 (a) 4:3 (b) 3:1 (c) 6:1 (d) 10:1 (e)

Similar to the AFM data for the PDA + p-PDA systems, it is visible that some films of PDA + ALT are more homogenous and reproducible than others. For example, the PDA + ALT films in the comonomer ratios 3:1 and 10:1 show fewer artefacts on the surface compared to the 4:3 or 6:1 ratios.
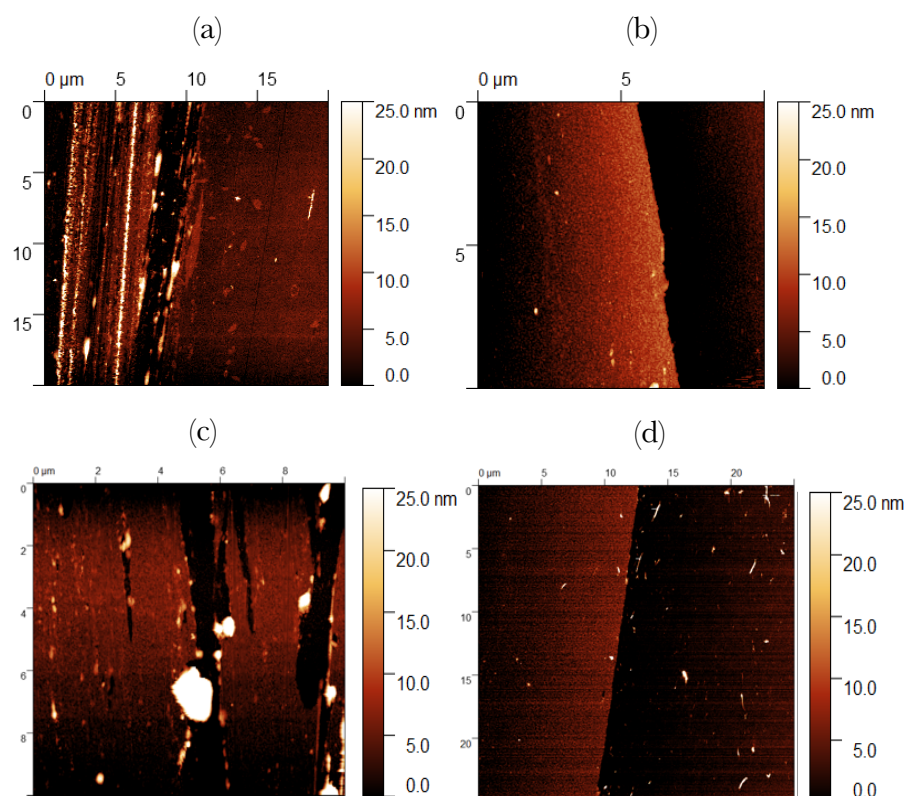
Figure 4.21 AFM micrographs of PDA + ALT copolymer films synthesized in the ratio 4:3 (a) 3:1 (b) 6:1 (c) 10:1 (d)

Figure 4.22 shows the cyclic voltammograms for the copolymer films made by electropolymerization of DA with serotonin in different ratios. No significant shift is observed in the oxidation potential or the current at the W.E. of the monomers in the first cycles. The films produced could not be homogenized due to the presence of several particles seen all over the surface and hence, these films will not be explored here for CV analysis. For the ratios 1:1 and 3:1 the oxidation process is irreversible as evident from the lack of a reduction peak, while in the ratios 2:1 and 10:1 they are pseudo-reversible. With increased incorporation of DA, the current in subsequent cycles decreases at a faster rate (showing increasing insulating behaviour). Thus, the ratio 10:1 implies greater film deposition due to increasing insulation in subsequent cycles.

(a)

(b)

(c)

(d)
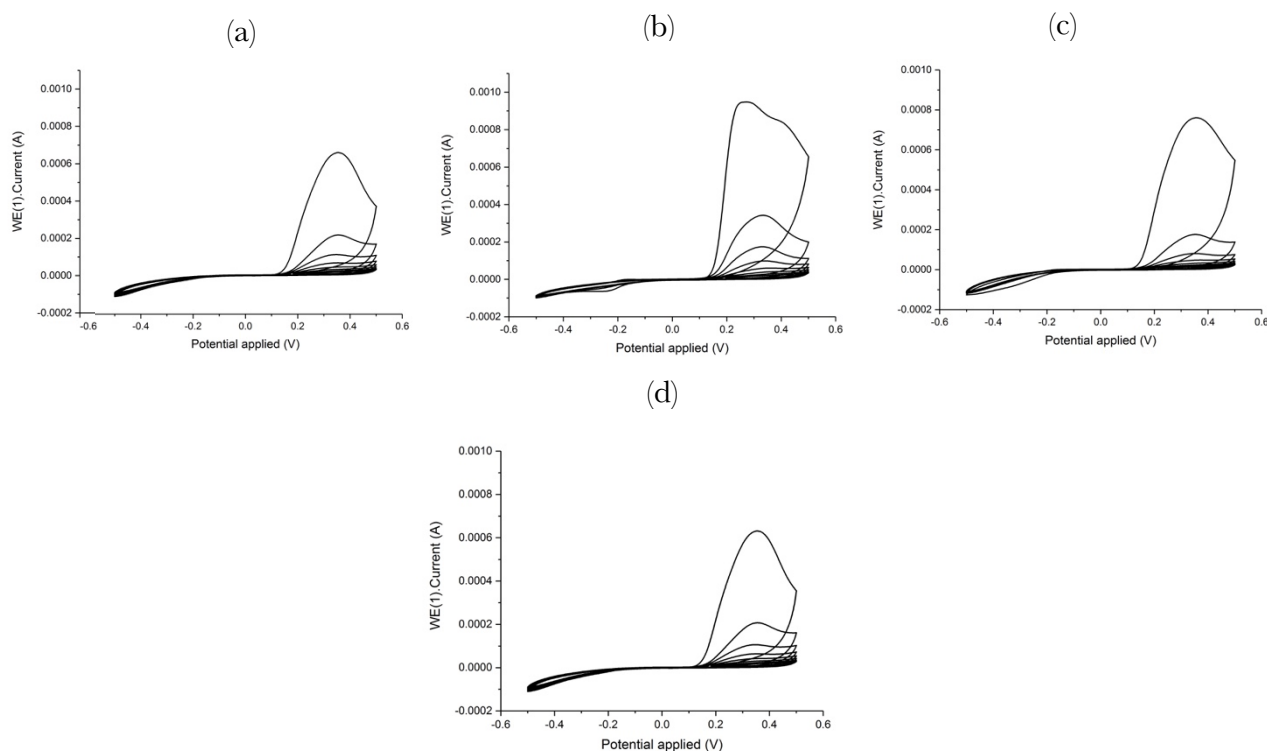
Figure 4.22 Cyclic voltammetry diagrams of synthesis of PDA + p-Ser copolymers by electropolymerization in the ratio 1:1 (a) 4:3 (b) 3:1 (c) 6:1 (d) 10:1 (e)

The presence of a film in each copolymer sample was verified by AFM and profilometry with the thickness and roughness analyzed as shown in Figure 4.23 and Figure 4.24. Several particles sporadically distributed are visible in both the profilometry images and AFM micrographs for the copolymer systems of p-Ser prepared at neutral pH using a phosphate buffer, while this is absent in the pure p-Ser films produced in HEPES buffer of acidic pH. This could be due to the increased polarity of the serotonin structure increasing the tendency to form aggregates. Unlike the copolymerization process for PDA + p-PDA and PDA + ALT, there was no supporting information available in literature for the copolymerization mechanisms involved in PDA + p-Ser synthesis in bulk. Due to difficulties in predicting copolymer structure, this system presents scope for further study before use in studying oxidation/reduction potentials, pH variation and other electrochemical properties and will not be covered in this thesis. The possible copolymerization of these two monomers is explored and reported here (to the best of the author's knowledge) for the first time. Despite the likelihood of blend formation in the PDA + p-PDA/PDA + ALT copolymers, the probability of blend vs. copolymer formation is greater for the PDA + p-Ser thin films due to the presence of particulate aggregates and breaks in the films. Hence a proposed structure for PDA + p-Ser is not given here.

(a)　　　　　　　　　　　(b)
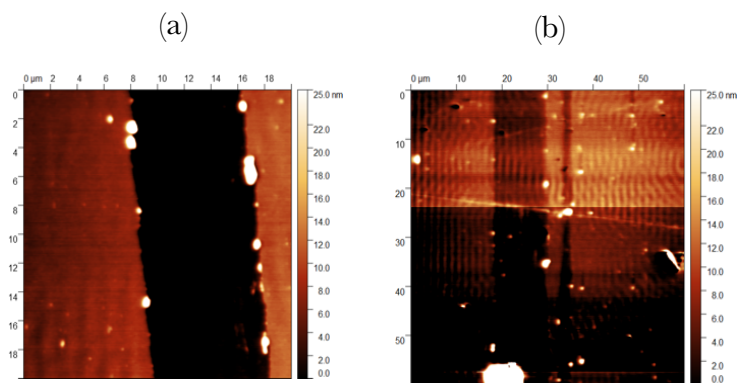
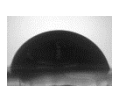*Figure 4.23 AFM micrographs of PDA + p-Ser (3:1) (a) PDA + p-Ser (10:1) (b)*
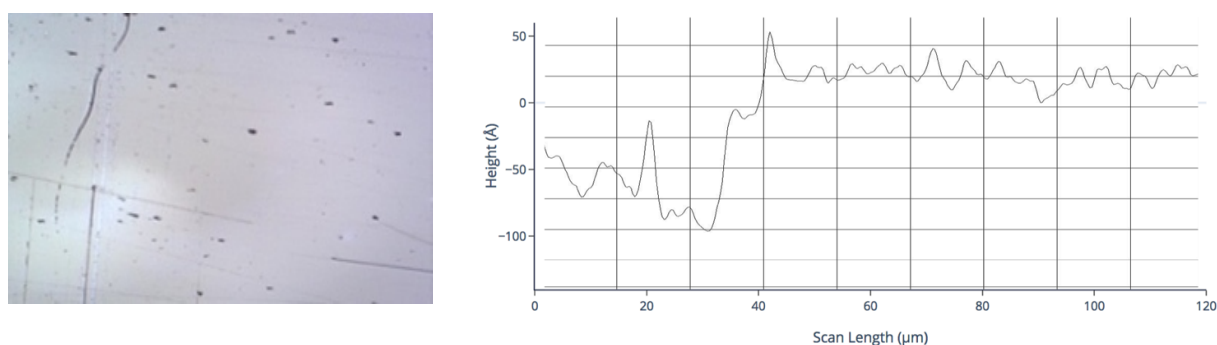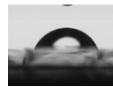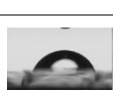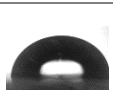
Figure 4.24 Profilometry image and profile of PDA + p-Ser (10:1) showing some particles on the surface dispersed sporadically over a thin film

4.1.3　Contact angle measurements

In order to confirm the incorporation of other comonomers on polymerization with DA the wettability was tested using contact angle measurements of water on the surface of the thin films. This was also done in order to further understand the results from the AFM for roughness and to further differentiate between the films, contact angle studies were performed. The films tested were selected based on earlier experiments and compared with contact angle measurements of polydopamine from literature as shown in Table 4.1-1. As seen, the wettability can be modified showing the incorporation of different monomers, even in case of low concentrations of ALT and p-Ser with PDA as the contact angles of the copolymer films vary from that of pure PDA. Thus, even though the presence of PDA suppresses the nucleation and growth of different self-assembling/shape-controlled structures, the second comonomers do get incorporated in the form of a film. As expected, the rough surface of the p-PDA due to the presence of the fibers/microneedles causes an increase in the hydrophobicity of the surface. The hydrophobicity of the pure p-Ser and p-ALT surfaces are also higher than the PDA films.

Table 4.1-1Summary of contact angle data for various low molar ratio films prepared by electropolymerization

Sample	Contact angle (degrees)	
PDA + p-PDA (3:1)	68 ± 2	
PDA + ALT (3:1)	35 ± 6.5	
PDA + p-PDA (10:1)	59.2 ± 1.5	
PDA + ALT (10:1)	69.3 ± 5.4	
PDA + p-Ser (10:1)	46.4 ± 2	
p-Ser	61.4 ± 4.4	
p-ALT	69.6 ± 5.2	
p-PDA	77.6 ± 3.1	
PDA	50-55 [80]	

The low contact angle of the PDA + ALT system in comparison to the other systems could indicate hydrophilicity caused by OH groups in the polymer structure as proposed earlier in Figure 4.11. It is also possible that despite the linear structure and solubility of p-ALT in water reported [77], the film formed undergoes cross-links and hence is not removed by washing with water after electropolymerization. Notably, the contact angle at the edges of the film where the morphology is thicker due to gradients in electropolymerization [39] shows a higher contact angle of about 65 ± 5º. Hence, it is unclear to what extent the structural features of the monomers (which translates into their polymeric structures) affects the contact angle results in comparison with the effects of the surface morphology of the films. It could be assumed that a combination of both contributes to the variation in the results.

4.1.4   Summary: thin film synthesis

Bruyne et al. gave three suggested mechanisms [81] of film formation during electropolymerization as shown in Figure 4.25 where initial oxidation of the monomer in solution and application of the first voltammetry cycle causes a decreased current compared to the bare electrode due to a) formation of an insulating film that partially blocks the electrode – as seen in the case of PDA, p-PDA and PDA + p-PDA copolymers or b) the insulating film can cover the electrode but is porous allowing film formation at the electrode interface (not depicted in this thesis but usually occurring for PDA film formation in basic pH) or c) full coverage of the electrode surface occurs but the film is partially conducting, allowing electropolymerization to take place at a reduced rate – this situation is comparable to the electropolymerization of 3-amino-L-tyrosine and its copolymers with PDA.
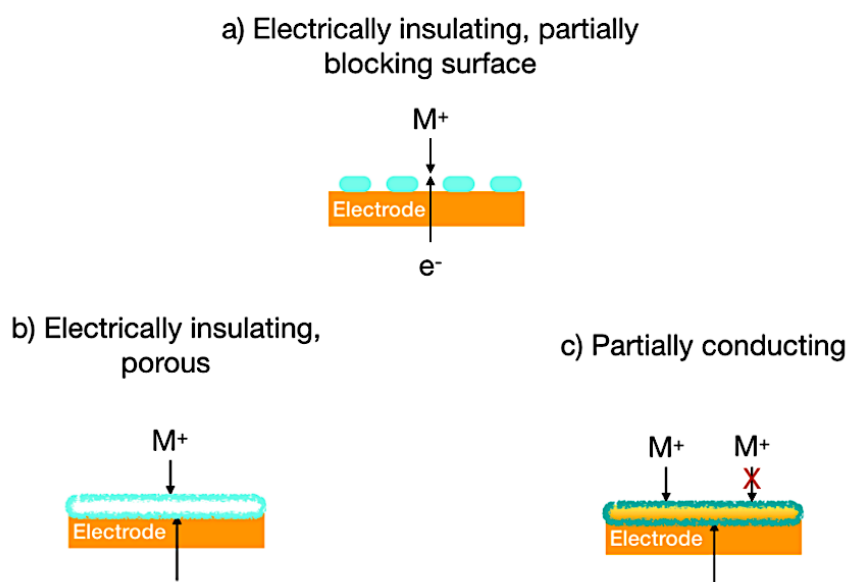
Figure 4.25 Proposed mechanisms for film formation using electropolymerization; own figure adapted from [81]

The data from AFM and profilometry shows that the thickness of the films increases with decreasing incorporation of ALT and the opposite occurs – decreasing thickness with decreasing p-PDA occurs as graphed in Figure 4.26. The thickness of the PDA + p-PDA films is higher than that of the PDA + ALT films in general. This could be due to the conducting nature of 3-amino-L-tyrosine films which hinders further deposition as an insulating thin film layer which is seen in the case of polydopamine formation during electropolymerization. Thus, the copolymerization process was optimized based on the thickness of the films and their

reproducibility. Table 4.1-2 and Table 4.1-3 summarize the results of the synthesis data from different types of thin films.

Table 4.1-2 Summary of data for various DA + p-phenylenediamine/DA + aminotyrosine copolymer films and homopolymer films prepared by electropolymerization

Sample	Polymer form	Thickness using AFM (nm)	Roughness (nm)	Thickness using Profilometry (nm)	Reproducible?
PDA ~ 5 mM	Film	12 ± 0.2	2 ± 0.2	12 ± 0.3	Yes
p-PDA ~ 2mM	Fibres/Needles	-	-	-	No film
ALT 0.7 mM	Film	5.2 ± 0.6	1.4 ± 0.1	5 ± 0.2	Yes
PDA + p-PDA (1:1)		15.3 ± 0.3	2.5 ± 0.4	17 ± 1	Yes
PDA + p-PDA (4:3)		13 ± 0.5	1.7 ± 0.1	13 ± 1	No
PDA + p-PDA (3:1)		10 ± 0.4	2 ± 0.3	11 ± 0.2	Yes
PDA + p-PDA (6:1)		12 ± 0.2	4 ± 0.6	13 ± 0.5	Yes
PDA + p-PDA (10:1)		18 ± 1.5	1.3 ± 0.2	15 ± 2	No
PDA + ALT (1:1)	No film	-	-	-	-
PDA + ALT (4:3)		5 ± 0.2	2 ± 0.3	5 ± 0.3	No
PDA + ALT (3:1)		9 ± 0.5	1 ± 0.1	9 ± 0.3	Yes
PDA + ALT (6:1)	Film	6.3 ± 0.6	1 ± 0.1	7 ± 0.2	Yes
PDA + ALT (10:1)		14 ± 0.3	1.8 ± 0.2	15 ± 0.2	Yes

As evident from the data above, some films were reproducible in terms of thickness and despite thickness variation existing across the sample (homogeneity) such as PDA + ALT 3:1 whereas some were not such as PDA + ALT 4:3. The former types of films were selected for use in later experiments. The data is based on analysis of the surface of two samples of each type of film. Since the thickness of the 3:1 films for both systems seem to match each other more closely than the other molar ratios (~ 10 nm), they can be used for further experiments in evaluation

and comparison of redox potentials in order to keep two parameters (molar ratio, dimensionality) constant while modifying others. The 1:1 ratio for PDA + p-PDA and 10:1 ratio for PDA + ALT will also be studied for comparison noting that these are also dimensionally similar (~15-17 nm), and the former ratio was reported by Ambrico et al. as the optimum concentration for mutual adhesion of PDA with p-PDA in copolymer formation with PDA.

Table 4.1-3 Summary of data for various dopamine + serotonin copolymer films prepared by electropolymerization

Sample	Nature	Thickness using profilometry (nm)	Thickness using AFM (nm)	Roughness using AFM (nm)
PDA + p-Ser (1:1)	No film	-	-	-
PDA + p-Ser (2:1)	No film	-	-	-
PDA + p-Ser (3:1)	Thin film	10 ± 0.96	10 ± 0.8	0.84± 0.70
PDA + p-Ser (10:1)	Thin film	10 ± 1	9 ± 1.3	1.72 ± 1.69
p-Ser by Method II 0.5 mM	Thin film	10 ± 1.03	12 ± 0.7	1.54 ± 0.72
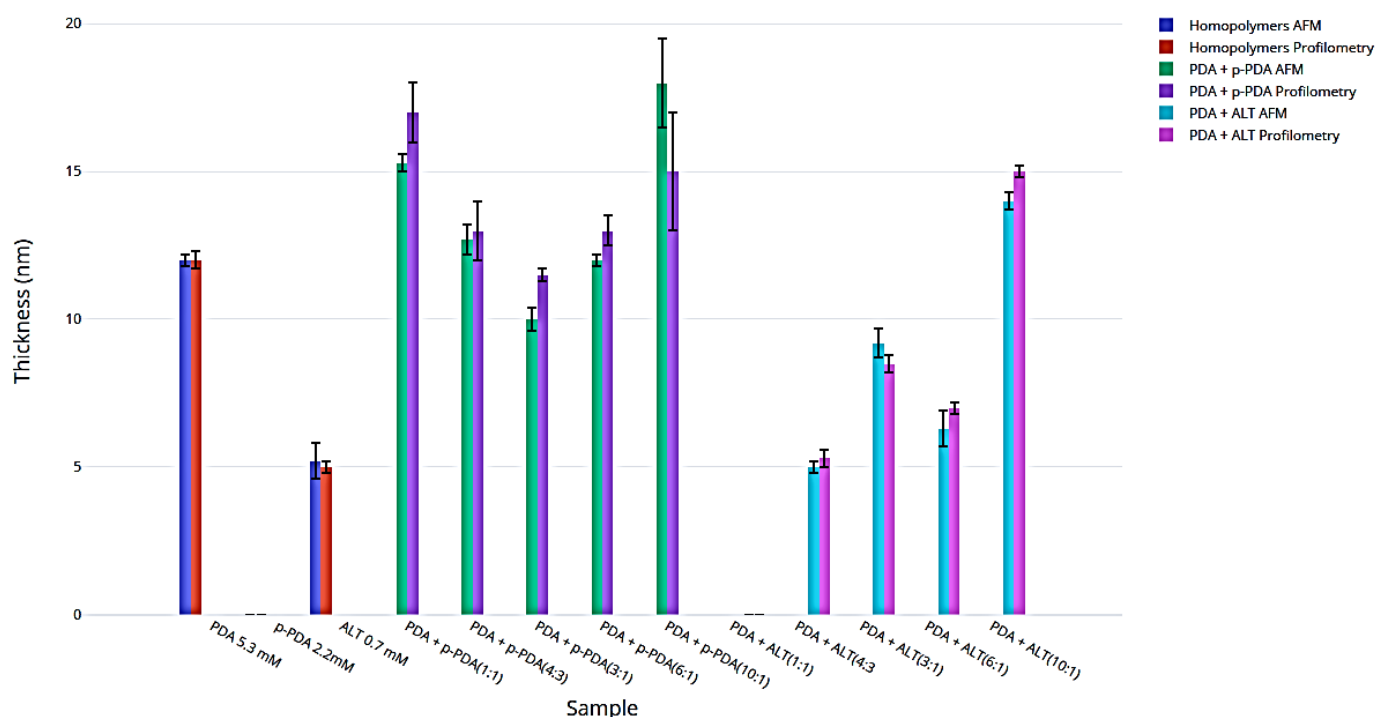
Figure 4.26 Thickness profile variation of different homopolymer/copolymer films with molar ratio of PDA – from two trials each

Figure 4.27 shows comparisons of the CV diagrams for different polymers - taken from the 4th cycles of each EP synthesis, 0.01 V/s scan rate and monomer concentrations as mentioned in Table 3.1-1.
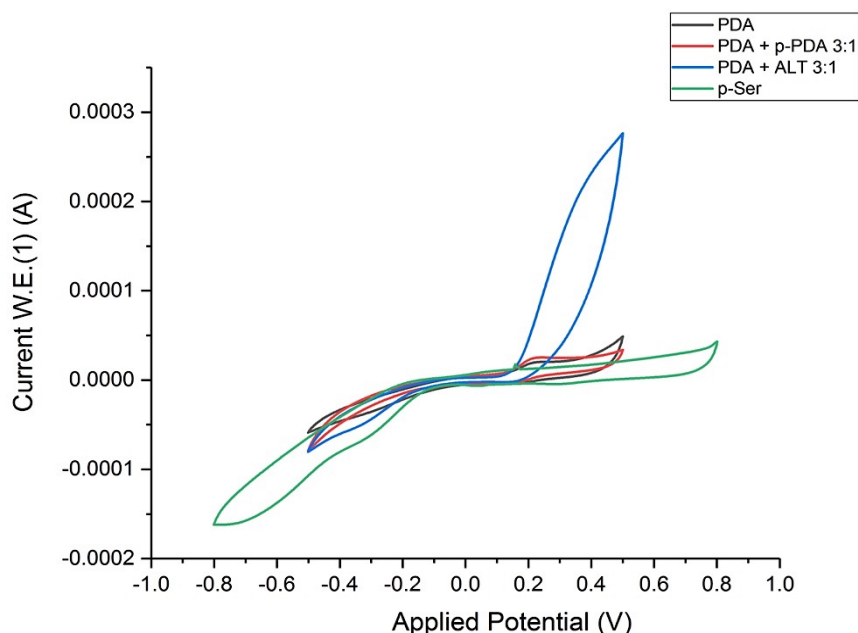
Figure 4.27 Comparisons of CV diagrams for different polymers - taken from 4th cycles of each synthesis, 0.01 V/s scan rate and monomer concentrations as mentioned in Table 3.1-1

Increasing the accuracy of AFM and Profilometry measurements and understanding sample reproducibility can be understood using Figure 4.28. The figure shows the Au substrate with the polymer thin film over it scratched so that the bottom part of the substrate (Au layer) is exposed. In order to ensure that the height is taken correctly, only regions that are scratched completely until the bottom of the electrode by the pipette tip are taken into consideration. When scratching off the film layer, it is possible that the displaced atoms pile up at the edge of the scratch and the profile can show a sharp peak increase in this region which must be omitted during thickness analyses. The AFM and Profilometry measurements were performed on separately synthesized samples (at least two for each measurement) and the thickness was averaged over at least two points on the sample surface from which the thickness data was extracted. The contact angle variations between low-comonomer concentrations of other monomers with dopamine in the ratio 10:1 were compared with pure homopolymer films and they were found to be increasingly hydrophobic in the following order: PDA + ALT 3:1 < PDA + p-Ser < PDA < PDA + p-PDA 10:1 ~ p-Ser < p-ALT ~ PDA + p-ALT 10:1 ~ PDA + p-PDA 3:1 < p-PDA.
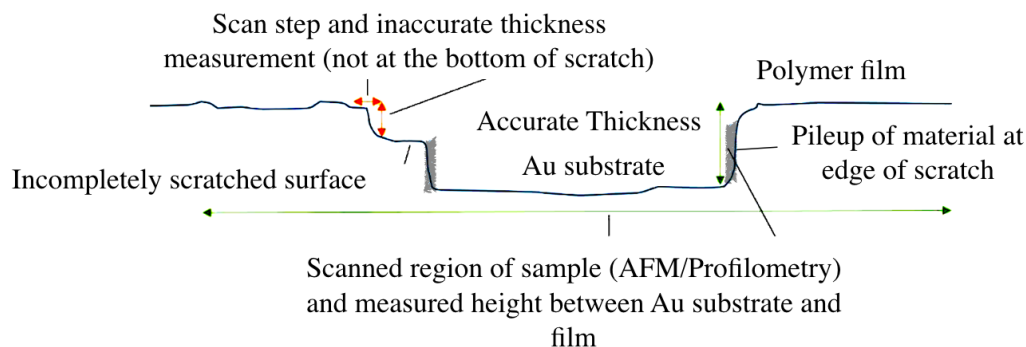
Figure 4.28 Simplified diagram of sample surface on which a scratch is made and thickness analysed; modified and adapted from [39]

Transmission Mode ATR-FTIR signals sometimes show very low intensities (see Appendix 3 in Section 6.3), and the spectra obtained do not give discernible information. ATR-FTIR results in transmission mode are inconclusive. In the reflection mode, the light to the detector is obtained due to reflection off the sample surface rather than transmitted light. This could potentially increase the information obtained from the surface of the film because in the latter case, the low available penetration depth due to the ultrathin nature of the films (nm range) leads to low-intensity signals that cannot be distinguished from the Au reference signal [47].

Table 4.1-4 Reference for FTIR peaks [39] [82]

Wavenumber (cm^{-1})	Group
3400	v (N-H), (O-H)
2860-2970	v (C-H)
1730	v (C=O)
1510-1630	v_{ring} (C=C), v (N-H)
1350	v (C-O-H, v (C-N-C)
1290	v (C-O)
1200-1210	C-OH stretch
820-890	∂ (=C-H)

The plots of the spectra for the films are shown in Figure 4.29. Various peaks are visible for PDA and the other samples as shown in the marked regions. The spectrum for PDA is comparable to previous studies and also comparable to the monomer form [83]. No differences are observed in the peaks for all other samples from PDA in the region between 820-890 cm^{-1} for ∂ (=C-H) as marked. At 1290 cm^{-1} for v (C=O) differences p-ALT shows broadening of the peak in comparison with PDA while the PDA copolymers both show reduced intensities of the peak. At 1350 cm^{-1} for v (C-O-H) and v (C-N-C), the peak for p-ALT and the copolymers a broadening of the peak is observed with a decrease in intensity. Between 1510-1630 cm^{-1} the

peaks for v_{ring} (C=C) of p-ALT and copolymers all appear different from PDA indicating differences in the structure. In the case of PDA + p-PDA 3:1 this could be due to stretching of the aromatic rings [84] which appears as a sharp peak increase in comparison with PDA at about 1600 cm^{-1}. Slight differences in intensity are seen for v (C-H) or v (N-H), (O-H). The intensity of transmission varies across all samples. The peaks obtained for PDA + p-PDA/ALT copolymers and are comparable to literature [65]. In addition to the peaks mentioned above, all spectra show an ammonium band at 1403 cm^{-1}. Despite differences in the peaks, no standout spectral feature of ALT was detectable in PDA + ALT, possibly to the low contribution to material composition except for the C-OH stretching peak for this sample visible in the range 1200-1210 cm^{-1}. The p-ALT FTIR spectrum has no reference in literature for comparison, however, the spectral differences between this new thin film synthesized and PDA are justified especially with a key spectral feature appearing near the C=O region.
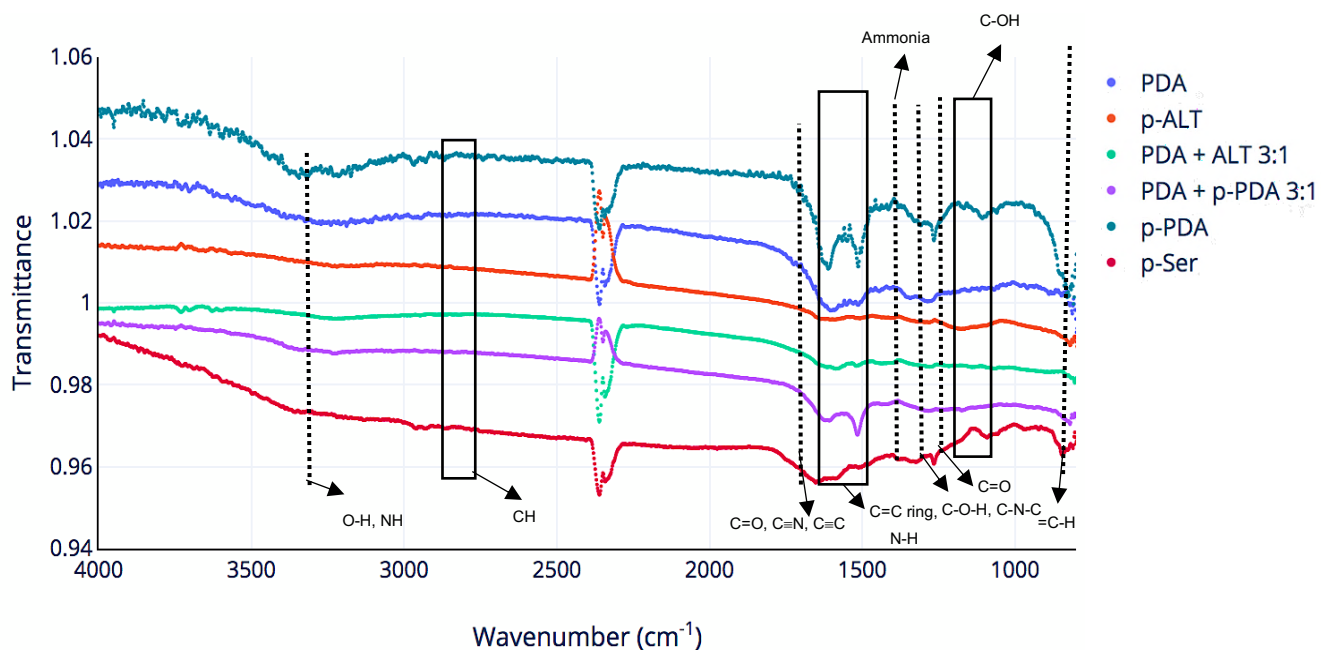
Figure 4.29 FTIR spectra for various films

The presence of p-PDA in the p-PDA + PDA 3:1 copolymer is verified by the C=C aromatic ring spectral feature of pure p-PDA between 1510-1630 cm^{-1} and comparable to that of the FTIR spectrum for the monomeric form [85]. The ∂ (=C-H) peak of p-PDA at ~ 890 cm^{-1} is markedly higher than that of the other samples. The absence of this peak in the copolymer with PDA could explain the suppression of the microneedle formation. The C=C aromatic ring structure of p-Ser is quite similar to PDA as expected, with a slight shift towards the left. Similar to p-ALT and expected from the monomer structure, a C-OH peak is visible at ~ 1200 cm^{-1}. From the FTIR data, it can be concluded that PDA+ALT and PDA+ p-PDA exhibit chemical

and spectral properties that indicate a PDA-like system that is modified by covalent interactions of 3-amino-L-tyrosine or p-phenylenediamine with DA as given by Ambrico et al. [65]. Such interactions, that have been enumerated from the spectral features marked, could lead to structural property changes and chemical disorder of the resulting copolymers compared to the PDA homopolymer. The incorporation of p-phenylenediamine and 3-amino-L-tyrosine comonomers can be supported by the peaks observed with similar features between pure homopolymers and copolymers with PDA. However, a more quantitative study of the incorporation of these different comonomers is not available.

4.2   Influence of Scan Rate

Examining the redox potentials of a polymer system using cyclic voltammetry would be incomplete without considering the scan rate used for measurement. It is already known that the scan rate of synthesis can affect the CV output [54]. However, the same is not often considered for analysis procedures. Figure 4.30 shows the summary of peak separation voltage values ΔE_{ps} for trials conducted in a PB of pH ~ 7.0. The differences in height of the anodic (oxidation) and cathodic (reduction) peaks and the increase of the reduction peak as the scan rate increases indicates the existence of a chemical step after the main oxidation process [86]. This is further supported by the ratio between the cathodic and anodic peak current that, in most cases, deviates from unity as evident from the plots of oxidation and reduction peak currents in Figure 4.1. In fact, the ratio nears ~ 0.5-0.7 for most cases.
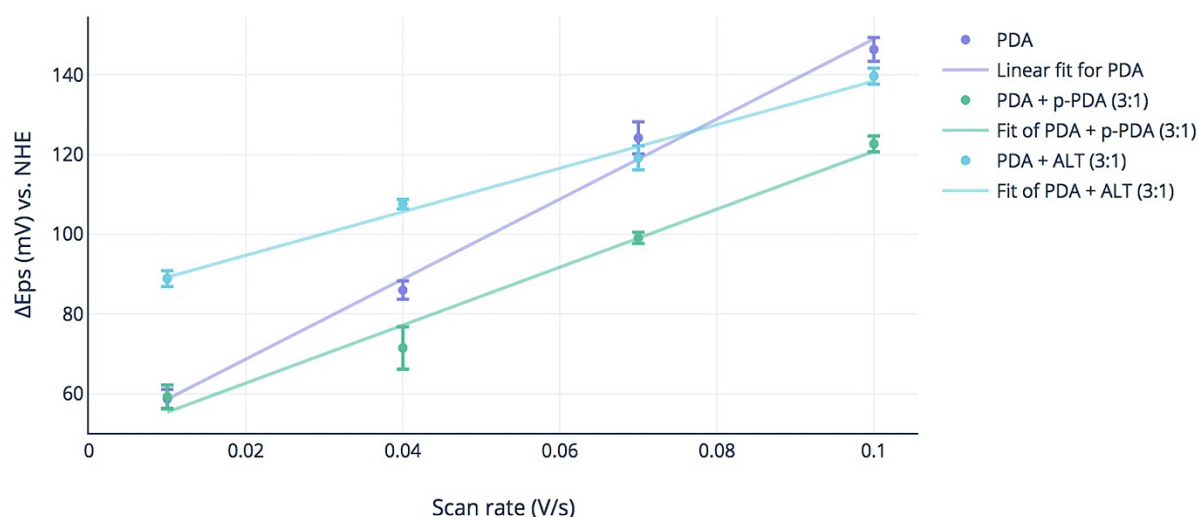
Figure 4.30 Variation of peak separation ΔE_{ps} with scan rate for (a) PDA (b) PDA + p-PDA (3:1) (c) PDA + ALT (3:1) reported vs. NHE

(a)

(b)
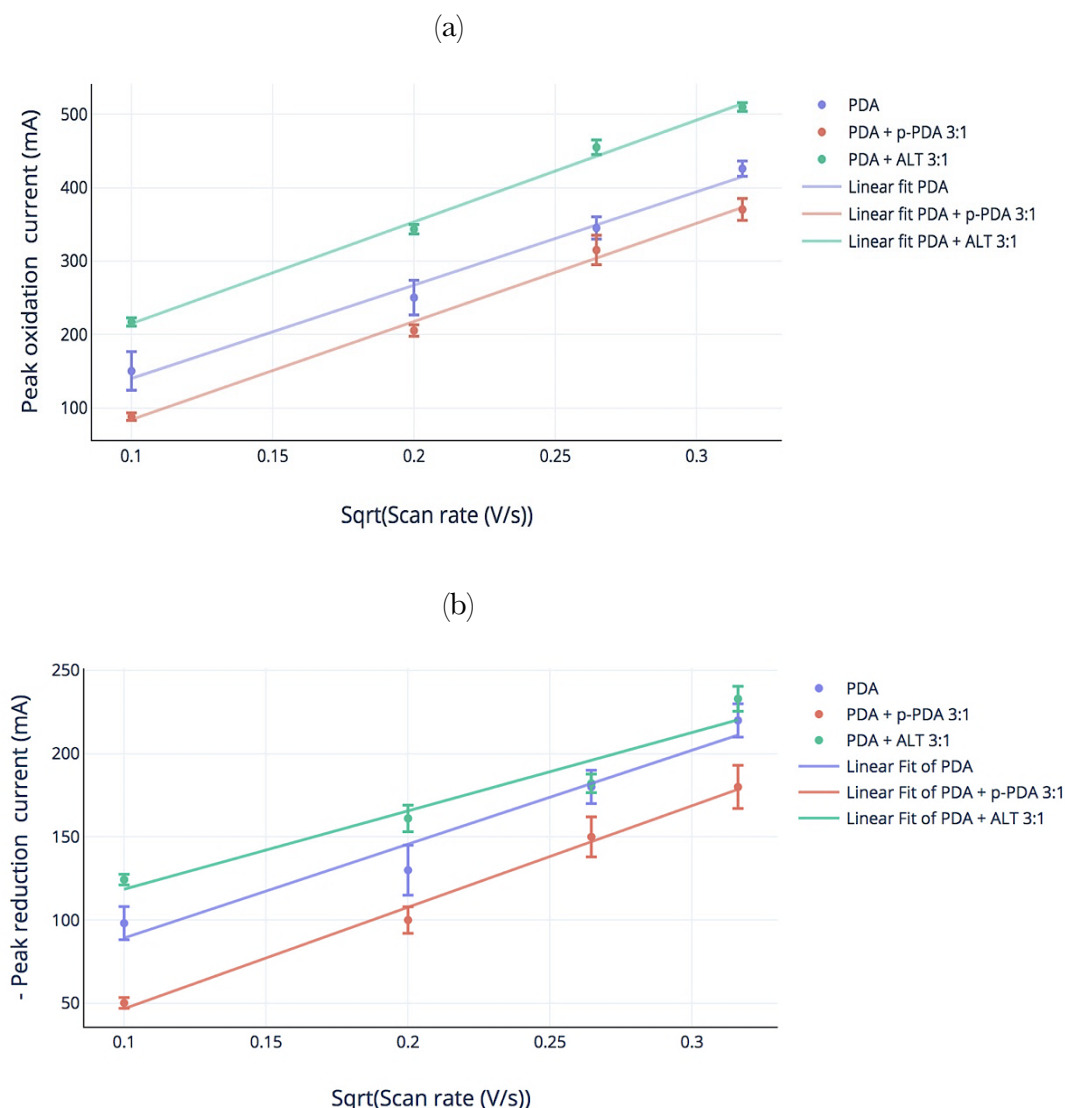
Figure 4.31 Variation of peak currents with scan rate for (a) PDA (b) PDA + p-PDA (3:1) (c) PDA + ALT (3:1) reported vs. NHE

The peak separation voltages ΔE_{ps} of PDA + ALT 3:1 are in general, higher than that for pure PDA and that of PDA + pPDA 3:1 are in general, lower. The correlation coefficients for the ΔE_{ps} with scan rate are: 0.98654 (PDA), 0.9937 (PDA + p-PDA 3:1) and 0.9764 (PDA + ALT 3:1). With all the systems studied, higher scan rates and lower pH values reduce the extent of fouling of the electrodes indicated by the higher oxidation potentials and lower peak separation voltages. The increased fouling of the electrode surface at higher scan rates could also contribute to the scatter in the data. The faster surface blocking at high pH indicates that the coupled chemical reactions occur to a greater extent under these experimental conditions. This is due to the higher amount of deprotonated species that favours hydroxylation among other

reasons. The peak oxidation and reduction currents increase with scan rate as expected from the Randles-Sevcik equation [40] which relates the peak current i_p with scan rate v as:

$$i_p \propto (v)^{1/2} \qquad\qquad \text{4-1}$$

Chumillas et. al [87] studied the variation of ΔE_{ps} with scan rate for polydopamine and the values of the peak separation with the scan rates obtained here are in the range expected from literature with changes expected since the study used a Pt W.E. while here an Au W.E. is used. This could be used a reference to compare the behaviour of the copolymers. They noted that low scan rates (<0.05 V) cause reduction peaks to disappear at pH values above 10. However, here this is not a concern since the analysis was done at pH ~ 7 using PB. Since the current is measured in mA and not A by the instruments any physical disturbances to the setup can cause current fluctuations and higher scatter in the data. Other sources of error include thermal noise also called Johnson-Nyquist noise [88] which is unavoidable at non-zero temperatures. It occurs due to random thermal motion of charge carriers inside an electrical conductor and does not depend on applied voltage. This explains the slightly lower correlation coefficient for the peak oxidation/anodic current i_{pa} of 0.9579 and i_{pc} of 0.9826 for PDA. The correlation coefficients for PDA + p-PDA 3:1 are 0.9937 for i_{pa}, 0.99729 for i_{pc} and that of PDA + ALT 3:1 are 0.9957 for i_{pa}, and 0.9666 for i_{pc}.
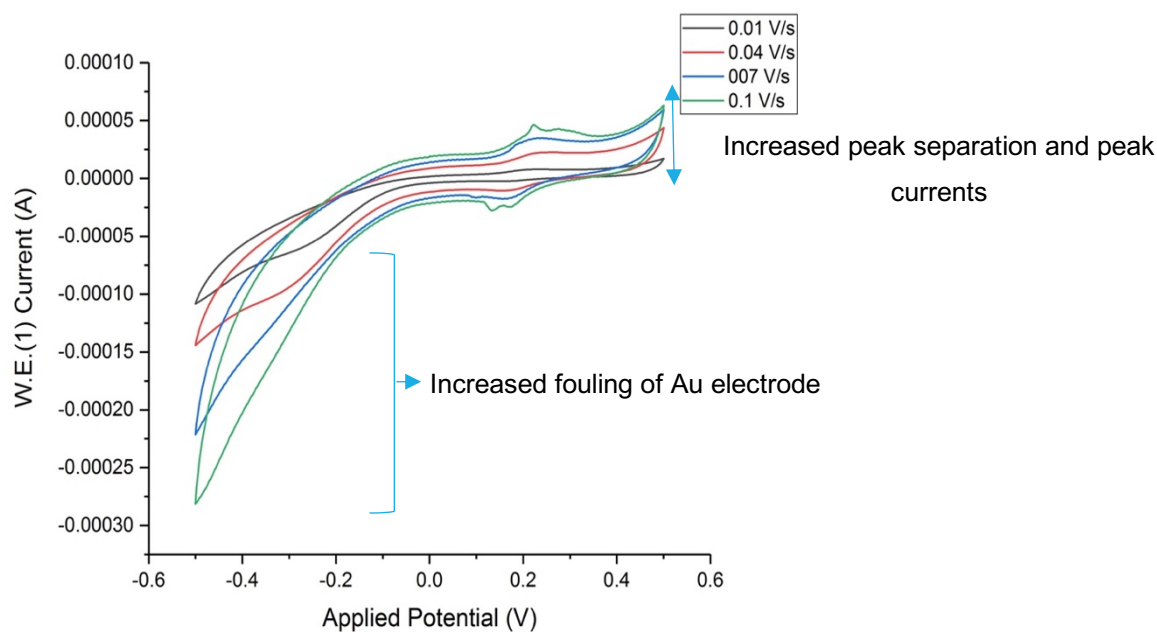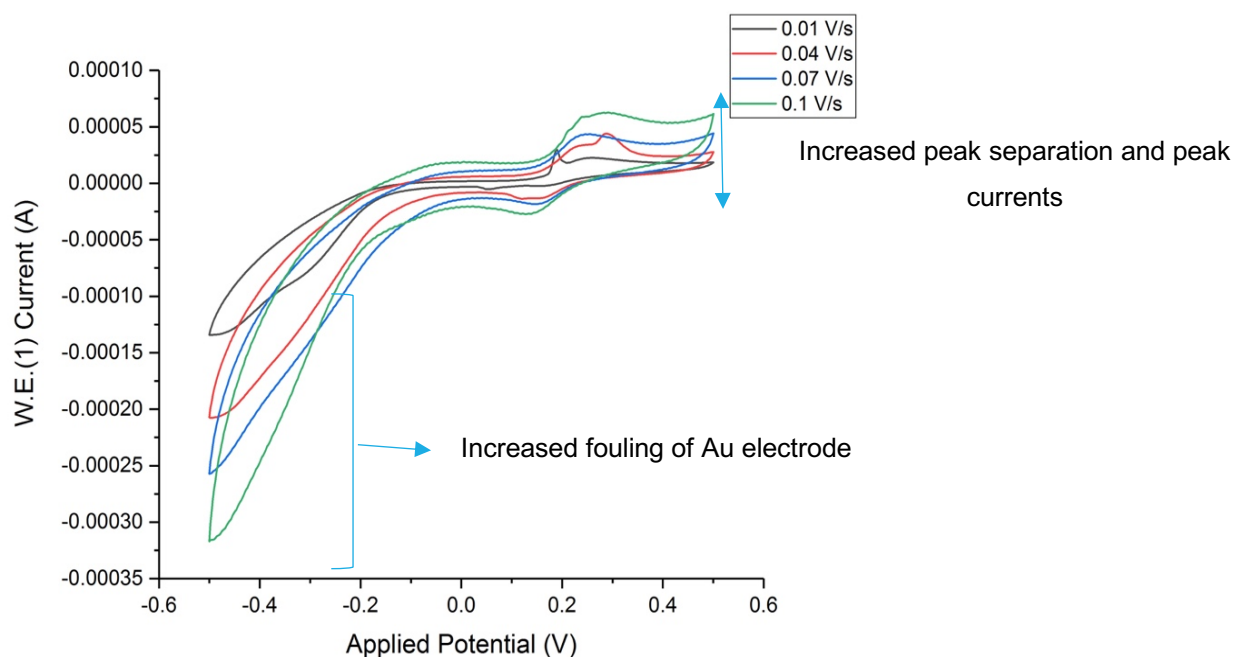

Figure 4.32 Variation of CV diagram of PDA with scan rate showing increased Au electrode fouling and increased peak separation

The currents measured using cyclic voltammetry depend on the concentration gradient that is established near the electrode called the Nernst diffusion layer during electrolysis. The relationship between the scan rate and the current peak height can be explained by considering the size of the diffusion layer and the time taken to record the voltammogram which increases as scan rate decreases [89]. At a slow scan rate, the diffusion layer will grow much further from the electrode as compared to a fast scan. This leads to a concentration gradient to the electrode surface that is much lower as compared to a fast scan. Electrode surface fouling has been recognized as a significant reason for lower accuracy in synthesis techniques and data acquisition in biosensing applications. It generally involves deposition of a fouling agent (in this case from monomer solutions) that forms an increasingly impermeable layer on the electrode and inhibits direct contact of the analyte or solution of interest with the electrode surface which consequently reduces electron transfer efficiency. Strategies proposed to combat the effects of electrode fouling include lowering scan rate (as evident from the CV studies). Since the monomer solutions and PB analytical buffer used are all aqueous it can be assumed that the fouling interactions are hydrophilic which is more reversible [90] than those occurring in hydrophobic mechanisms. Hanssen et al. [70] proposed that during DA formation on an electrode surface, fouling occurs due to melanin formation and that monomeric species can adsorb onto the W.E. surface in a more energetically favourable manner.
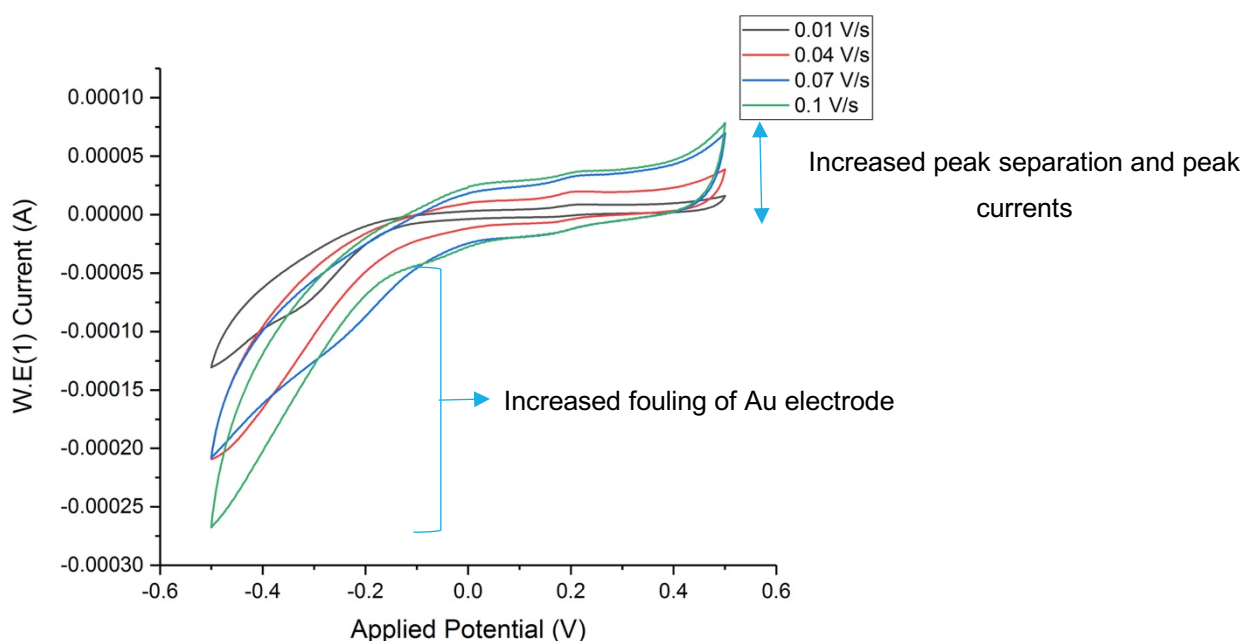
Figure 4.33 Variation of CV diagram of PDA + p-PDA 3:1 with scan rate showing increased Au electrode fouling and increased peak separation

It can be seen that, the values of peak oxidation and reduction currents for PDA + ALT 3:1 are higher than that of pure PDA in the order of ~ 100 mA while those of PDA + p-PDA 3:1 are lower in the order of ~ 50 mA. This indicates that the copolymerization of PDA with these monomers can indeed adapt the systems to give varying oxidation/reduction currents and peak separation voltages. Notably, the variation of peak separation with scan rate indicates that the oxidation and reduction potentials cannot be defined as absolute values for a given pH environment but are rather available in a range of values higher and lower than that of pure PDA.

Figure 4.34 Variation of CV diagram of PDA + ALT 3:1 with scan rate showing increased Au electrode fouling and increased peak separation

However, based on the data adapting PDA to different pH environments using different monomers for copolymerization has been made possible especially. Though the values of the oxidation and reduction potentials still lie in the given range for PDA between 0-1 V vs. NHE (Figure 2.3 (b)) the values of the potentials and currents are higher and lower than that of PDA even at a given pH and thus, extend its functionality. Such a trend using these specific copolymers has not been reported (to the best of knowledge) in literature.

4.3 Influence of pH

4.3.1 CV characterization of PDA + p-PDA 3:1 and PDA + ALT 3:1

The characterization of the various thin films using cyclic voltammetry has two purposes:

1) to judge the effect of incorporation of comonomers to the dopamine system and

2) to check the tunability of the oxidation/reduction potentials of the systems at the same pH based on π-electron mobility changes.
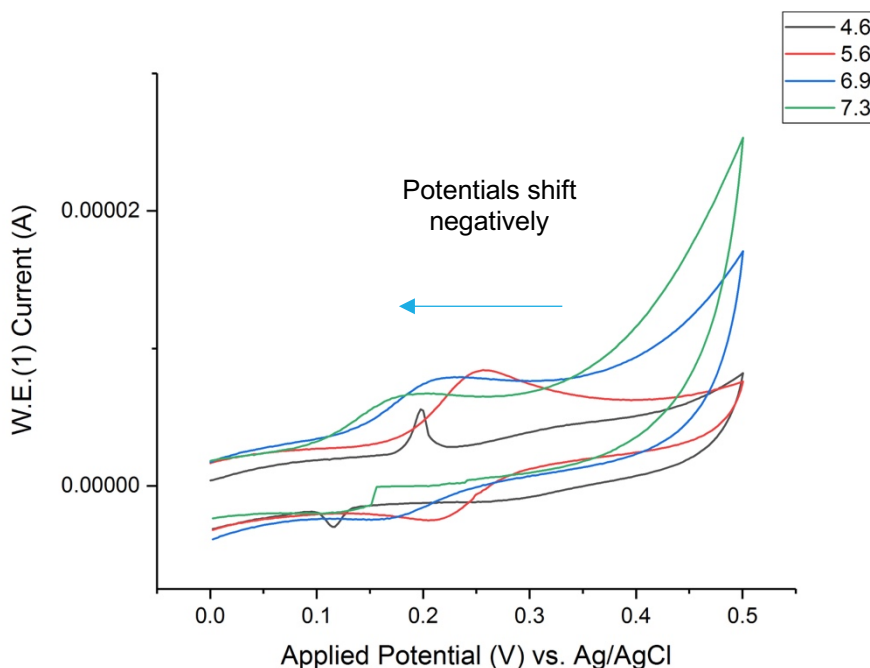
Figure 4.35 CV characterization of PDA homopolymer films under phosphate buffer of pH values 4.6, 5.6, 6.9, 7.3

The negative current portion of the CV diagram is excluded for the comparison since it only shows the characteristics of the Au substrate and not the polymer sample itself. Each monomer mixture solution was swirled 2-3 times to ensure homogeneity before use for film formation and during the recording of the cyclic voltammogram, the solution was not physically perturbed in any way to prevent errors. The electrodes were cleaned and blotted dry before changing the solutions in order to prevent sample contamination. The characterization of PDA using cyclic voltammetry in different pH environments is shown in Figure 4.35 with applied voltage reported vs. Ag/AgCl (3 M KCl bridge). The oxidation and reduction potentials were converted from V to mV to better resolve the data and are reported vs. NHE (Normal Hydrogen Electrode) in Figure 4.36 and Figure 4.37 instead of vs. Ag/AgCl (3.5 M KCl bridge) that was used for analysis. The decrease in potentials, obeys the following equations for PDA:

$$Epa\ (mV) = -56.40pH + 803.5;\ R = -0.9946 \qquad\qquad \text{4-2}$$

$$Epc\ (mV) = -55.75pH + 754.6;\ R = -0.9991 \qquad\qquad \text{4-3}$$
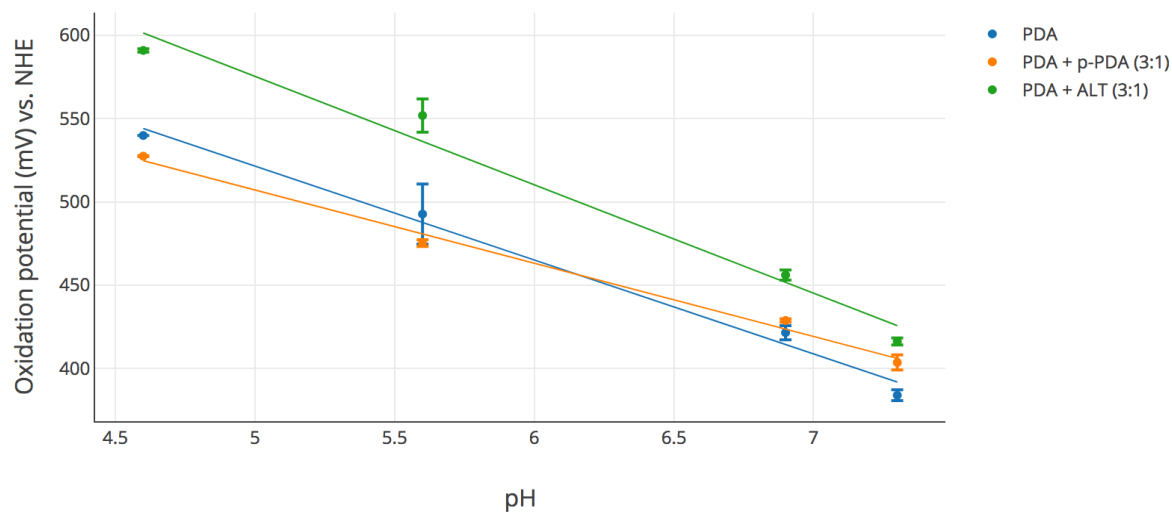
Figure 4.36 Comparison of oxidation potentials for the 3:1 copolymer systems and PDA with varying pH values: 4.6, 5.6, 6.9 and 7.3

The slope of the equations for PDA, 56.4 mV/pH and 55.75 mV/pH for the anodic and cathodic peak potentials respectively can be compared to the expected theoretical value of 59 mV/pH [41]; thus, suggesting that the number of electrons transferred is equal to the number of hydrogen ions participating in the electrode reaction. This is comparable to a study [62] by Kanyong et al. The range of oxidation voltages in mV vs. NHE reported here are in the range expected from previous studies by Medintz et al. [87] and Amiri et al. [61] and hence is a suitable reference for the values obtained for the copolymer systems.
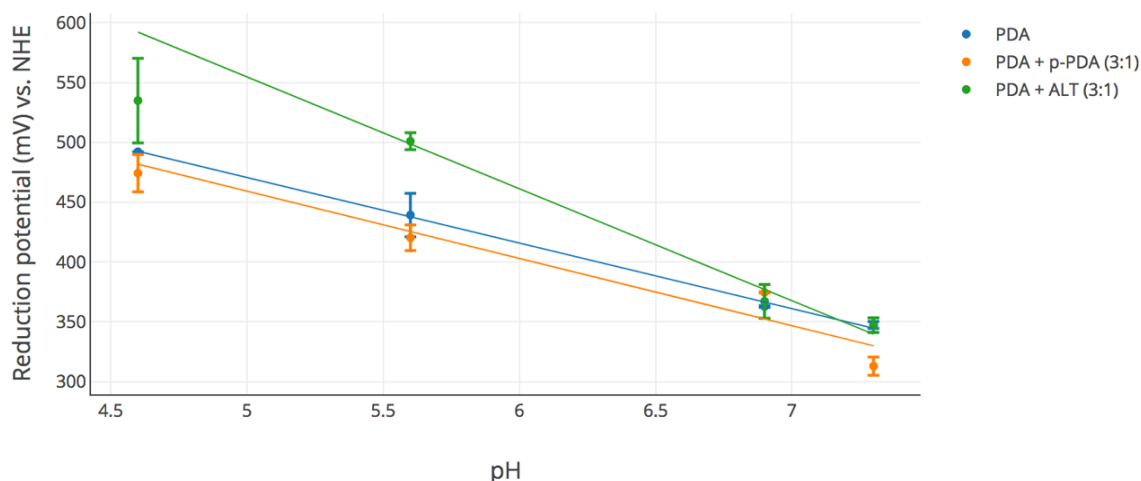
Figure 4.37 Comparison of reduction potentials for the 3:1 copolymer systems and PDA with varying pH values: 4.6, 5.6, 6.9 and 7.3

The decrease in potentials obeys the following equations for PDA + p-PDA (3:1), as also depicted in Figure 4.38:

$$Epa\ (mV) = -44.00pH + 727.2;\ R = -0.9961 \qquad \text{4-4}$$

$$Epc\ (mV) = -56.21pH + 740.3;\ R = -0.9704 \qquad \text{4-5}$$

It must be noted that Medintz et al. conducted the experiments using a glassy carbon electrode at a scan rate of 0.05 V/s and the data is for DA-labelled peptides, not pure polydopamine. Also, the studies performed by Amiri et al. used a glassy carbon electrode at a scan rate of 0.05 V/s and potentials are reported vs. SCE and cyclic voltammetric studies of PDA were used for pH sensing. They also reported that buffer composition does not affect measured voltage values on GCE however whether the same extends to an Au W.E. is not yet known.

The slope of the equations for PDA + p-PDA 3:1, 44 mV/pH and 56.2 mV/pH for the anodic and cathodic peak potentials respectively, are only close to the expected theoretical value of 59 mV/pH in the cathodic peak; thus, suggesting a quasi-reversible electrode reaction and a system with novel properties from a one-electron reversible system [42] as well as a lack of an Ohmic drop [43]. The electron transfer also occurs at the same rate as mass transport. The decrease in potentials obeys the following equations for PDA + ALT (3:1):

$$Epa\ (mV) = -65.09pH + 900.87;\ R = -0.988 \qquad \text{4-6}$$

$$Epc\ (mV) = -93.54pH + 1022.5;\ R = -0.9842 \qquad \text{4-7}$$
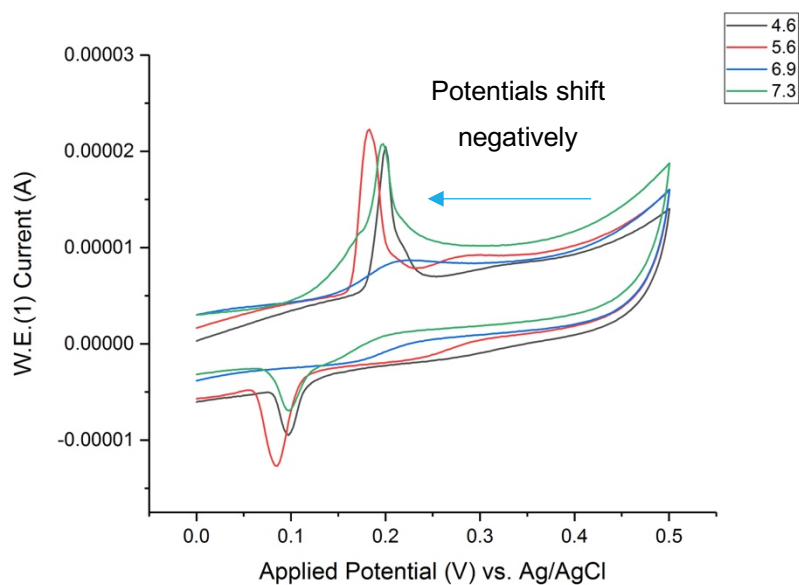
Figure 4.38 CV characterization of PDA+ p-PDA (3:1) films under phosphate buffer of pH values 4.6, 5.6, 6.9, 7.3

The slope of the equations for PDA + p-PDA 3:1, 65.1 mV/pH and 93.5 mV/pH for the anodic and cathodic peak potentials respectively, are greater than the expected theoretical value of 59 mV/pH; thus, suggesting a quasi-reversible electrode reaction and a system with novel properties from a one-electron reversible system. The decrease in potentials o for PDA + ALT (3:1) is also depicted in Figure 4.39.
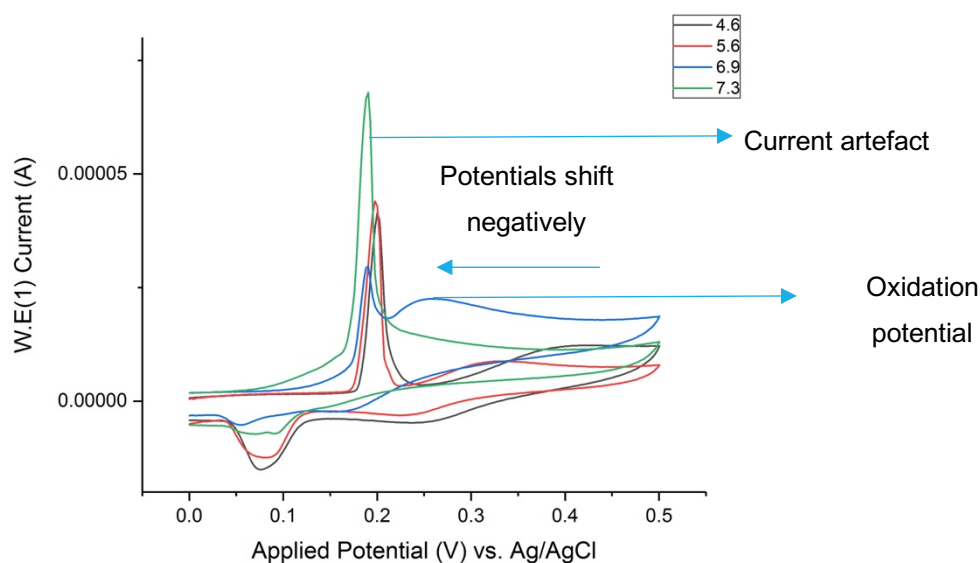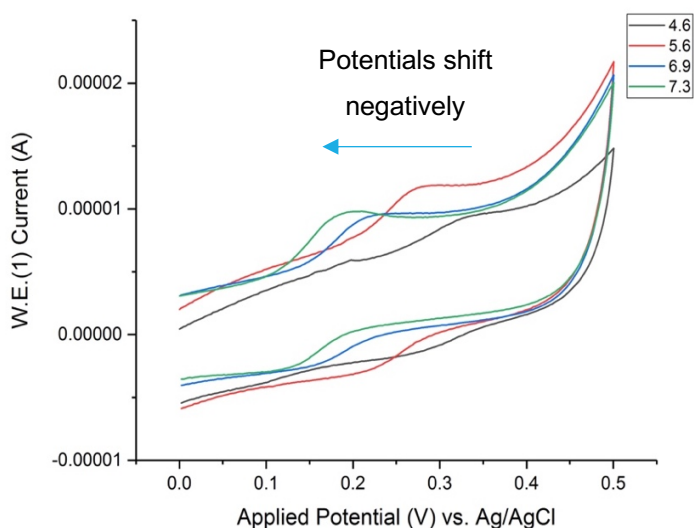

Figure 4.39 CV characterization of PDA+ ALT (3:1) films under phosphate buffer of pH values 4.6, 5.6, 6.9, 7.3

An increase in oxidation and reduction potentials for the PDA + ALT (3:1) in the order of ~100 mV was observed whereas that of the PDA + p-PDA (3:1) system did not vary so greatly (~20 mV). The pH dependence on the redox potential of polydopamine has been studied earlier [61] and the electropolymerization of DA in itself is a widely studied topic. However, an analysis of the redox potentials for such copolymer systems is given here for the first time. The decrease in the oxidation peaks is indicative of the oxidation process being followed by either a water nucleophilic attack that generates hydroxylated species or by dimerization or polymerization reactions [91]. Thus, electrode reaction can be affected by the pH of the medium and the solution pH influenced both the anodic and cathodic peak potentials considerably. However, there was no significant change in peak current. The potentials of these systems show a decreasing trend with the band gaps of the PDA + ALT (3:1) system being slightly greater than the PDA + p-PDA (3:1) system. Though, as expected, there is no fixed trend for the change in peak separation voltage ΔE_{ps} the value of ΔE_{ps} is highest around neutral pH for PDA. For PDA at pH 6.9 the ΔE_{ps} value of 58.7 mV is higher than all other reported values. This was explained by Laviron et al. [89] and Deakin et al. [92] where they state that at very acidic pH, the first electron transfer $QH_2 \rightarrow QH_2^+ + e^-$ (Q = Quinone) leads the deprotonation step, while at neutral solutions the electron transfer occurs on an already deprotonated species (QH^-), resulting in a neutral radical species. This neutral radical can cause a second deprotonation step, leading up to a second electron transfer. Under basic pH conditions, a second deprotonation could lead up to the first electron transfer, resulting in a Q^{2-} charged species. acidic or alkaline conditions. The band diagrams for redox potentials (reported in mV vs. NHE after conversion) are shown in Figure 4.40.
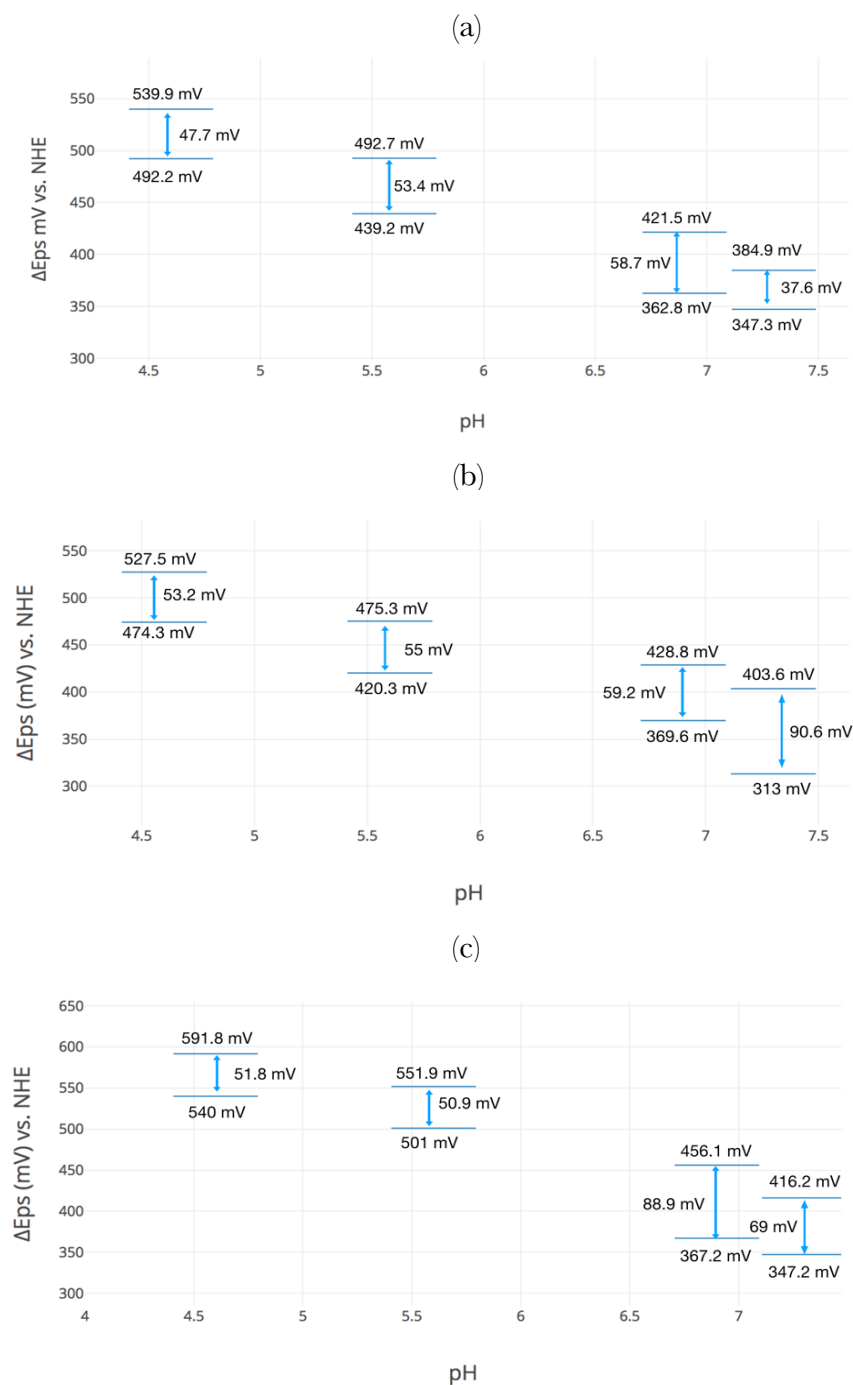
Figure 4.40 Variation of peak separation ΔE$_{ps}$ with varying pH for PDA (a) PDA + p-PDA (3:1) (b) and PDA + ALT (3:1) (c) reported vs. NHE

For PDA + p-PDA 3:1 the highest peak voltage appears at pH 7.3 instead of neutral pH indicating possible changes to the quinone structure made during copolymerization, thus affecting the electron transfer reactions. For PDA + ALT 3:1, the highest peak separation voltage $ΔE_{ps}$ value of ~ 89 mV is seen at pH 6.9. The trends for even higher pH values are not reported here due to time constraints on experimental work. However, they can be inferred using extrapolation from the existing data. It must also be noted that the data can only be

obtained up to pH 10 or lower for PDA and PDA-based films as very basic pH environments can delaminate the films.

4.3.2 CV characterization of PDA + p-PDA 1:1 and PDA + ALT 10:1

In order to judge whether the relative concentrations of the monomers could affect the oxidation and reduction potentials, a comparison was made using CV characterization with PDA + p-PDA (1:1) and PDA + ALT (10:1) systems. The monomer ratios of the systems were chosen in terms of their reproducible film formation properties and similarity in dimension. The PDA + p-PDA (1:1) ratio was chosen for comparison because it is the ideal ratio reported in literature for adhesion and solubility of the comonomers in bulk solutions. PDA + ALT (10:1) represents a copolymer with low concentration of 3-amino-L-tyrosine which could affirm that incorporation of ALT actually results in a change as shown previously.

Figure 4.41 CV characterization of PDA+ p-PDA (1:1) films under phosphate buffer of pH values 4.6, 5.6, 6.9, 7.3

The decrease in potentials as taken from Figure 4.42 and depicted in Figure 4.41 obeys the following equations for PDA + p-PDA (1:1):

$$Epa\ (mV) = -47.66pH + 757.4;\ R = -0.9978 \qquad \text{4-8}$$
$$Epc\ (mV) = -55.31pH + 734.7;\ R = -0.9947 \qquad \text{4-9}$$

The decrease in potentials as taken from Figure 4.39 and depicted in Figure 4.43 obeys the following equations for PDA + ALT (10:1):

$$Epa\ (mV) = -47.48pH + 745.2;\ R = -0.9866 \qquad \text{4-10}$$

$$Epc\ (mV) = -55.75pH + 754.6;\ R = -0.9997 \qquad \text{4-11}$$

(a)

(b)
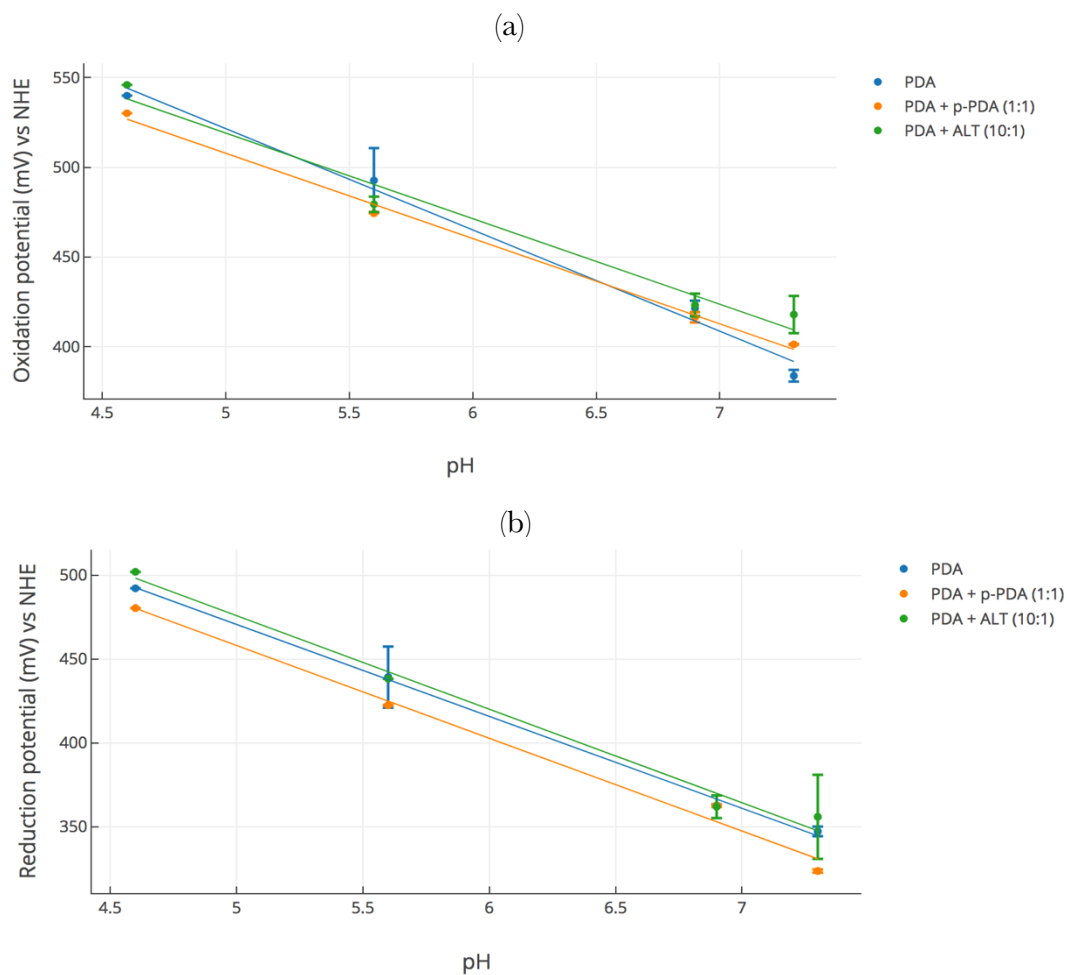
Figure 4.42 Comparison of (a) oxidation and (b) reduction potentials for the three systems with varying pH values: 4.6, 5.6, 6.9 and 7.3
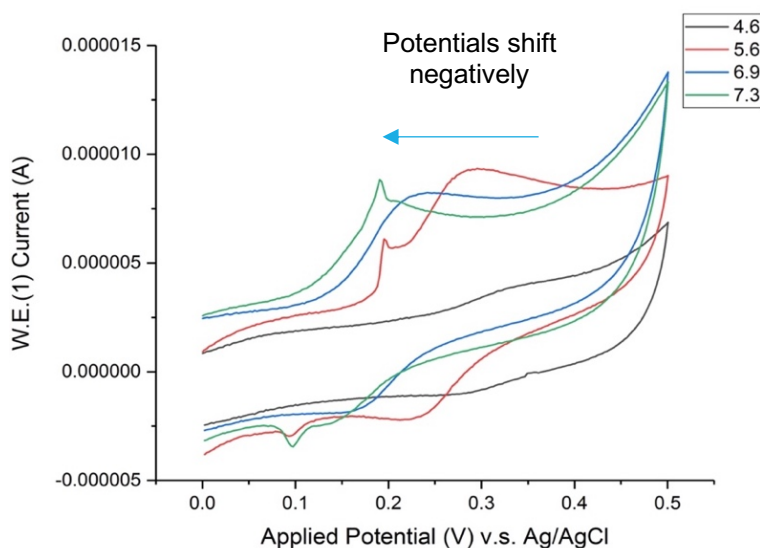
Figure 4.43 CV characterization of PDA+ ALT (10:1) films under phosphate buffer of pH values 4.6, 5.6, 6.9, 7.3

The slope of the equations for PDA + p-PDA (1:1) 55.31 mV/pH for the cathodic peak potential and that for PDA + ALT (10:1) 55.75 respectively, are close to the expected theoretical value of 59 mV/pH like PDA. In fact, the latter value exactly matches that of pure PDA. The only difference arises in the anodic peak caused by a slight shift in the oxidation potentials. In case of the PDA + ALT 10:1 system, the oxidation and reduction potentials assume values closer to that of PDA with a slight increase in the order of ~ 10 mV.

Notably, when comparing the shifts in the oxidation and reduction potentials of the PDA + p-PDA 1:1 copolymer the values are lower than that of PDA by an order of ~ 20 mV which is almost the same as that of the PDA + p-PDA 3:1 system. Thus, monomer concentration of DA and p-phenylenediamine does not seem to play a role in altering oxidation or reduction potentials with pH. Similar to the trends for peak separation voltages ΔE_{ps} reported for the PDA + p-PDA 3:1 copolymer systems, PDA + p-PDA 1:1 shows the highest peak separation voltage (within the measured range) at pH 7.3 with a value of ~ 78 mV. This is much lower than the ΔE_{ps} reported for the PDA + p-PDA 3:1 system indicating that though oxidation and reduction potentials do not vary much from PDA across different pH environments, at slightly basic pH, the peak separation is affected by the molar concentration of the comonomers DA and p-phenylenediamine. This could be explained by the peak separation values obtained from the slope of the pH-activity analysis, indicative of a one-electron system unlike PDA + p-PDA 3:1, similar to the assumption made for PDA.

PDA + ALT 10:1 shows the highest ΔE_{ps} value (see Figure 4.44) of 62 mV at 7.3 which is higher than that of pure PDA by about 4 mV and indicates that even a small amount of ALT incorporated could lead to proportional changes in ΔE_{ps}. However, this is still lower than the ΔE_{ps} value for the PDA + ALT 3:1 system by ~ 30 mV, indicating that comonomer concentration is important in the pH and redox activity PDA + ALT system.
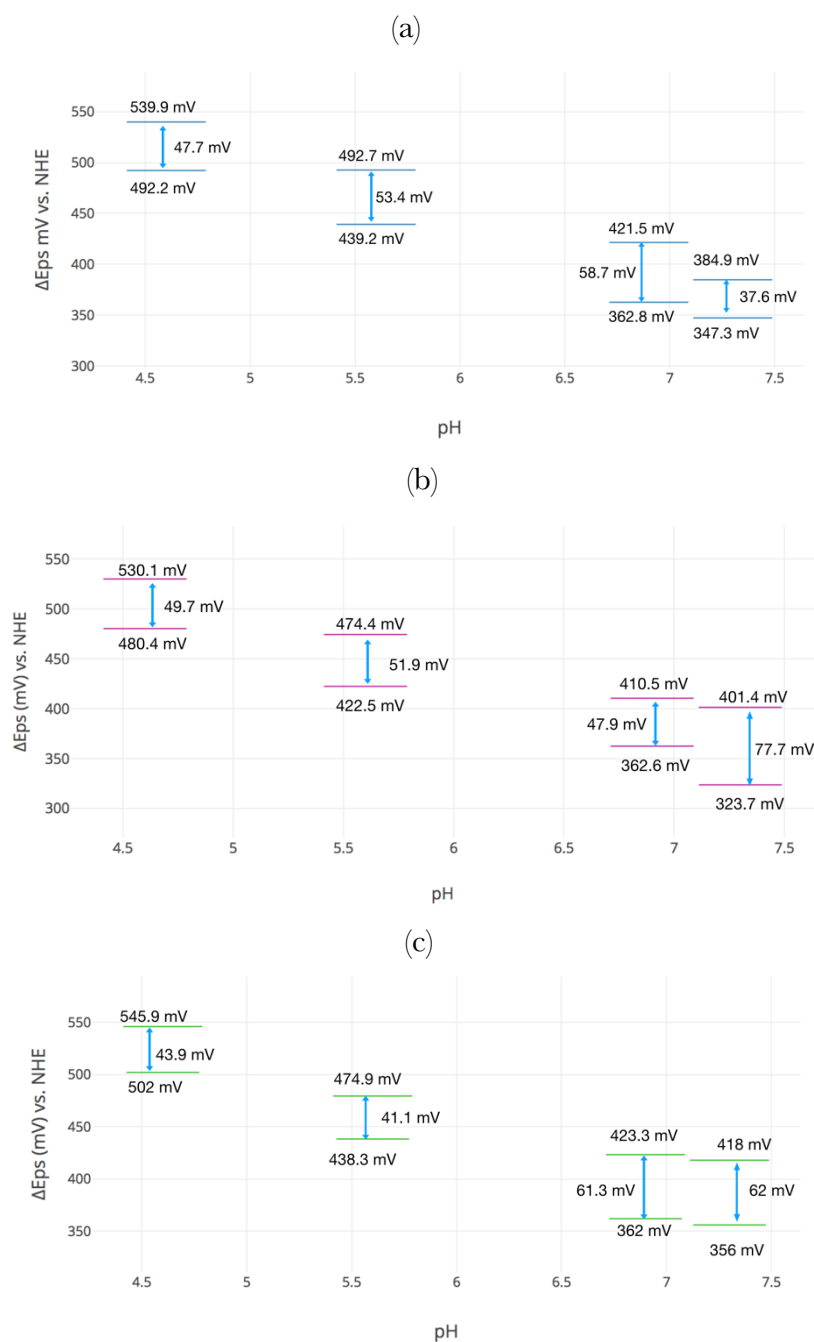
Figure 4.44 Variation of peak separation ΔE_{ps} with pH for (a) PDA (b) PDA + p-PDA (1:1) (c) PDA + ALT (10:1) reported vs. NHE

In comparison with the PDA + ALT 3:1 system, the values of the oxidation/reduction potentials vary by about ~ 40 mV which indicates that the concentration of the 3-amino-L-tyrosine comonomer with DA could play a role in its pH and redox activity.

4.3.3   CV characterization of p-Ser

The summarized peak separation diagram of p-Ser analyzed by cyclic voltammetry showing oxidation and reduction potentials at three different pH values are shown in Figure 4.45 with applied voltage reported vs. NHE. Unlike the copolymer systems, the pure p-Ser systems analyzed using cyclic voltammetry did not show variations in the oxidation and reduction potentials with 3 different pH values (Note: the trials were conducted only once). Also, similar to PDA, the film delaminates at higher pH suggesting that a test of pH dependence of redox potentials is not possible above its pKa value of 10. Slight variations in peak separation voltage ΔE_{ps} are seen. However, these values are too low and almost indicative of a conducting material thus indicating diffusion of charged species through the film onto the Au substrate. Hence, the measurements are not reliable.
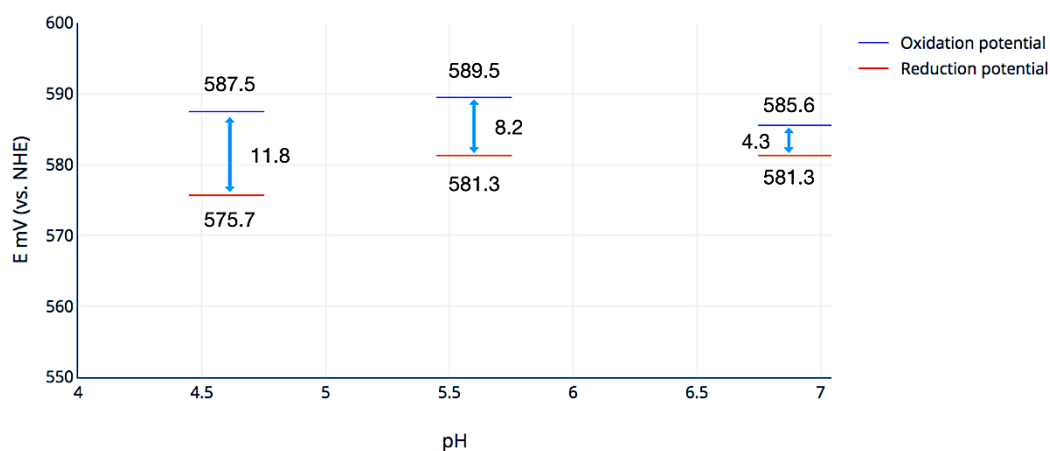
Figure 4.45 Variation of peak separation ΔE_{ps} and oxidation/reduction potentials with pH for p-Ser

It was assumed that since the pKa value of serotonin is quite high (9.3) [67] that this could extend to p-Ser as well and influence changes in behavior with pH. Hence a trial was made to check the pH dependence of oxidation and reduction potential at a pH of ~ 10. However, similar to the data reported for PDA (S. Harvey, T. Marchesi unpublished), the film delaminates under highly alkaline conditions. The redox activity of the films could also be modified by the use of HEPES buffer for synthesis which is reported to affect the activity of the Au substrate [93],[94].

Table 4.3-1 Summary of oxidation and reduction potential variations with pH for two different PDA + p-PDA and PDA + ALT systems. The standard deviation (S.D) for all values is less than 10%

	Oxidation Potentials (mV vs. NHE)				
pH	PDA	PDA + p-PDA 3:1	PDA + ALT 3:1	PDA + p-PDA 1:1	PDA + ALT 10:1
4.6	540 ± 0	528 ± 0.3	591 ± 1	530 ± 0	546 ± 0
5.6	493 ± 18	475 ± 2	552 ± 10	474 ± 0	479 ± 4.3
6.9	422 ± 4	429 ± 1	456 ± 3	417 ± 3	423 ± 6.4
7.3	384 ± 3	404 ± 4.5	416 ± 2.1	401 ± 0.3	418 ± 10.4
-R	0.994686982	0.996057781	0.988353399	0.99787078	0.986663128

	Reduction Potentials (mV vs. NHE)				
pH	PDA	PDA + p-PDA 3:1	PDA + ALT 3:1	PDA + p-PDA 1:1	PDA + ALT 10:1
4.6	492 ± 0	474 ± 11	540 ± 30	480 ± 0	502 ± 0
5.6	439 ± 18	420 ± 7.6	501 ± 5	422 ± 0.25	438 ± 0.1
6.9	363 ± 0.7	375 ± 0.3	367 ± 10	363 ± 0.7	362 ± 6.7
7.3	347 ± 3	313 ± 5.4	347 ± 4.3	324 ± 1	356 ± 25.1
-R	0.999142101	0.970416142	0.984213783	0.994709324	0.994269855

Table 4.3-2 Summary of peak separation and peak current variation with scan rate for two different PDA + p-PDA and PDA + ALT systems. The standard deviation (S.D) for all values is less than 10%

	Peak separation ΔE_{ps} and peak currents						
	PDA						
Scan Rate V/s	$\sqrt{v}$	ΔE_{ps} (mV vs. NHE)	S.D.	i_{pa} (mA)	S.D.	i_{pc} (mA)	S.D.
0.01	0.1	58.7	2.4	59.2	3	88.9	2
0.04	0.2	86	2.3	71.5	5.3	107.6	1.2
0.07	0.264575131	124.2	4	99.1	1.4	119.2	3
0.1	0.316227766	146.4	3	122.7	2	139.7	2
R		0.9864	0.9731	0.9579		0.9826	0.9655
	PDA + p-PDA 3:1						
Scan Rate V/s	$\sqrt{v}$	ΔE_{ps} (mV vs. NHE)	S.D.	i_{pa} (mA)	S.D.	i_{pc} (mA)	S.D.
0.01	0.1	150.2	26.2	88.1	5.2	217.1	5.6
0.04	0.2	250.2	23.5	205.4	7.8	343.5	6.3
0.07	0.264575131	345.1	15.2	315	20	455	10
0.1	0.316227766	425.9	10.3	370.3	15	509.8	5.9
R		0.9937		0.9968		0.9973	
	PDA + ALT 3:1						
Scan Rate V/s	$\sqrt{v}$	ΔE_{ps} (mV vs. NHE)	S.D.	i_{pa} (mA)	S.D.	i_{pc} (mA)	S.D.
0.01	0.1	98.1	10	50.2	3.2	124.3	3.2
0.04	0.2	130	15	100	8	161.1	8
0.07	0.264575131	180	10	150	12	182.2	5.6
0.1	0.316227766	220	10	180	13	233	7.5
R		0.9764		0.9957		0.9666	

4.4 Critical parameters and sources of error

The relative importance of various operating parameters involved in an electropolymerization process decreases in the following order [36]: monomer concentration > solution pH > operating temperature and variations in these are potential sources of error or sources to explore for optimization of film formation in experiments. These parameters have thus been evaluated for their importance by the results given in previous sections. Polymerization rate increases with monomer concentration but results in low molecular weight polymers with low solubility and hence lower rates of solidification. Keeping this in mind, the concentrations of monomers in the case of p-ALT and p-Ser homopolymer and copolymer films were kept relatively low to increase chances of film formation. Very low or ambient pH can cause rapid decrease in current to be observed in the voltammograms indicating film formation and yet not lead to actual film formation or scattered deposits, possibly due to H_2 evolution. In contrast, high ambient pH leads to poor quality films also due to possible H_2 evolution and a large number of free radicals being generated on the surface. This explains the need for the phosphate buffers used for synthesis as well as the near-neutral ambient pH under which the various films were synthesized. Polymerization rate increases with ambient temperature thus resulting in thicker films until about 40°C. However, the temperature in laboratory conditions are more or less stable and major fluctuations in temperature are not a concern for experiments. As often indicated in literature, the role of atmospheric/dissolved oxygen in driving oxidative polymerization processes could be both that of an initiator or inhibitor [95],[89]. Therefore, the rate of the initiation reaction often depends on the applied electrode potential or the electrolysis current passing through the cell. In the case of the PDA + p-PDA/PDA + ALT copolymers, oxygen takes the role of an initiator since the mechanism of copolymerization is oxidative coupling. Hence, the lack of a vacuum or use of the horizontal electropolymerization setup helps rather than hinders the film formation process in both cases by increasing dissolved oxygen. A note on the use of phosphate buffers [93],[94]: the buffer of choice for synthesizing all polymer films (except p-Ser) and characterizing them was a sodium phosphate buffer because the use of Tris-HCl, MOPS, or HEPES buffers can suppress the activity of a polymer film on the Au/Pt C.E. However, the same does not occur while using phosphate buffers despite some adsorption onto the electrode surface being possible. Another reason that a phosphate buffer is a suitable candidate is that, the redox peaks measured in phosphate buffer indicate that the oxidation and reduction occur in a reversible manner, whereas in the case of the organic buffers, adsorption of the buffer's ions on the surface can block electron transfer

processes. One limitation of this buffer is due to low diffusion rates, thus lower scan rates (< 0.002 V/s) are ideal for better redox peak accuracy. However, this scan rate could not be used during analysis/synthesis during this thesis due to instrumental limitations, longer duration of measurement and lowered peak separation with slower scan rates. Notably, since the analyses performed at pH 4.6 were done with no significant time gap between trials, the data shows almost no scatter in the potentials measured between repeat trials. This could possibly be due to the high pH sensitivity of the system (since the oxidation/reduction potentials also show differences between pH 6.9 and 7.3), slight variations in the pH of the phosphate buffers over a span of days (though overall, their pH remained stable with only variations in the order of ± 0.1) and continuously reusing Au slides which can lead to film formation with holes. Thus, to minimize errors it is recommended that new Au slides be used whenever possible for each trial and for each repeat trial when using acidic pH environments for measurements. The samples analyzed by CV at a particular pH can be reused at the same pH for a repeat CV measurement without washing or degassing and will yield the same CV curve but not when the pH is switched (see Appendix 4 in Section 6.4). In this work, a new film was used for each analysis which could change the system and increase errors. It is recommended that the Pt and Au C.E.s be cleaned with Piranha solution, rinsed with MilliQ water and dried before each subsequent experiment to prevent using fouled electrodes. Due to time constraints on experiments, the analysis of pH dependence on pure p-PDA and p-ALT systems are beyond the scope of this thesis. However, this could present a scope for future work. Since the p-PDA fibers/microneedles are also found to be absent in the copolymer they could be incorporated via nanocomposite formation with PDA and tested for various functional properties.

4.5   Further characterization - XPS

Qualitative analysis of several thin films was performed using X-ray Photoelectron Spectroscopy (XPS). This provides only supporting information as XPS results are difficult to use to predict quantitative changes in chemical structure between samples.

Table 4.5-1 List of samples analyzed by XPS

Sample content
Pure ALT homopolymer
Pure p-PDA homopolymer
Pure p-Ser homopolymer
Pure PDA homopolymer
PDA + ALT (3:1) copolymer
PDA + p-PDA (3:1) copolymer
PDA + p-Ser (3:1) copolymer

Notably, the samples were analyzed about one month after submission and hence aging effects that have not been studied yet could affect the accuracy of the results provided here. The data was compared for the different systems based on the intensity of the peaks obtained for various chemical structural features. The spectra obtained were fitted using Origin (Peak Fitting Pro) to draw conclusions about the difference between the various films. The C1s region are fitted with four components: C-C / C-NH (2 284.8 eV), CO / CN (286.2 eV ± 0.1 eV), C = O / C = N (287.4 eV ± 0.1 eV), and π-π * (289.7 eV ± 0.2 eV). The π-π * - Satellite corresponds to the energy loss of aromatic carbon species. The N1s region consists of three parts: primary amines (R-NH$_2$, 400.9 eV ± 0.3 eV), secondary amines, (R$_2$-NH, 399.9 eV ± 0.1 eV) and aromatic amines/ imines (= NR, 398.3 eV ± 0.1 eV). Primary amines include DA, secondary amines and aromatic intermediates and polydopamine assigned to the [96] tautomers of 5,6 Dihydroxyindole and 5,6-indolequinone. The spectrum for O1s (Figure 4.48, below) was divided into three signals: quinone - (O = C) at about 531.1 eV ± 0.1 eV and catechol signal (OC) at 532.7 eV ± 0.1 eV as well as an additional peak of Na-KLL (sodium Auger) at about 534.7 ± 0.3 eV eV. The Na- KLL signal comes from Na of the phosphate buffer, which is incorporated in the structure of PDA.
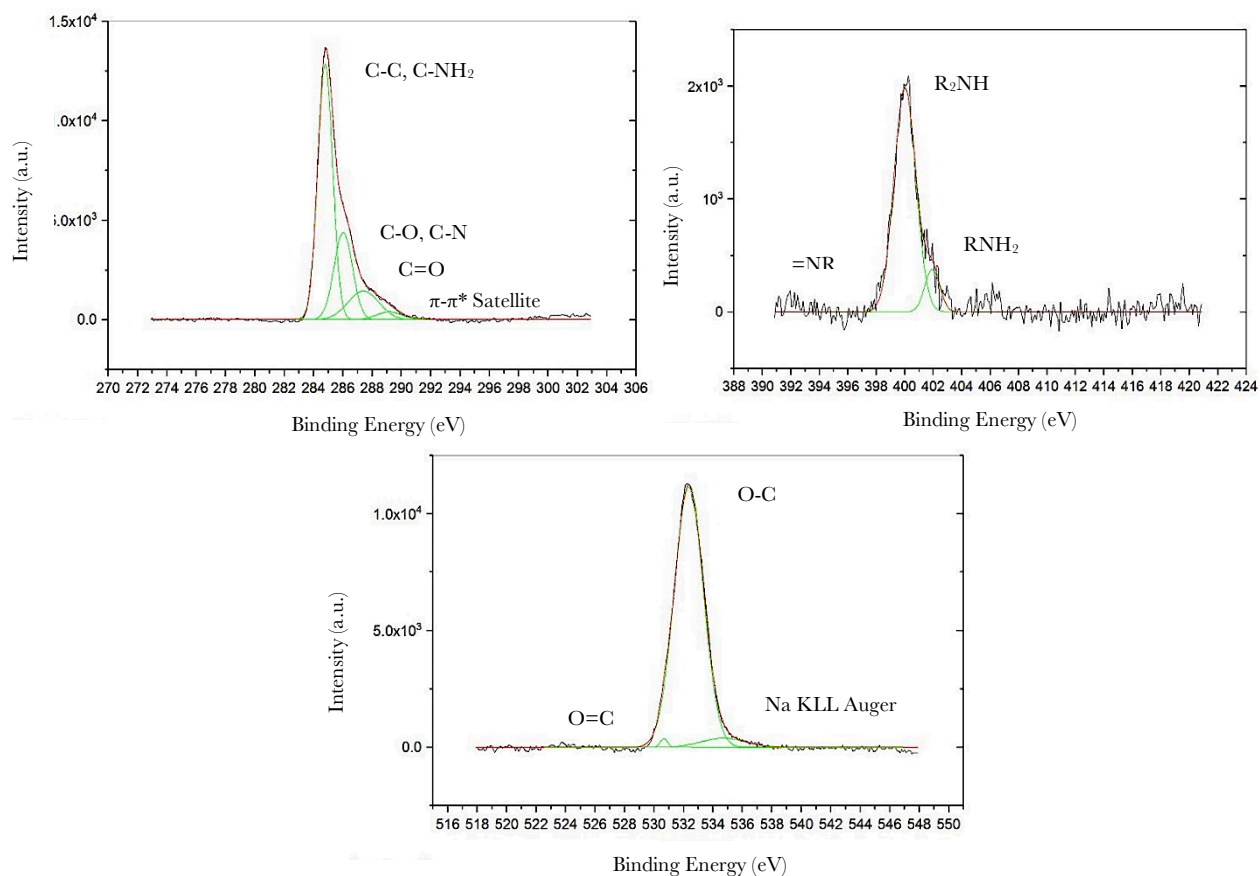
Figure 4.46 XPS data for PDA
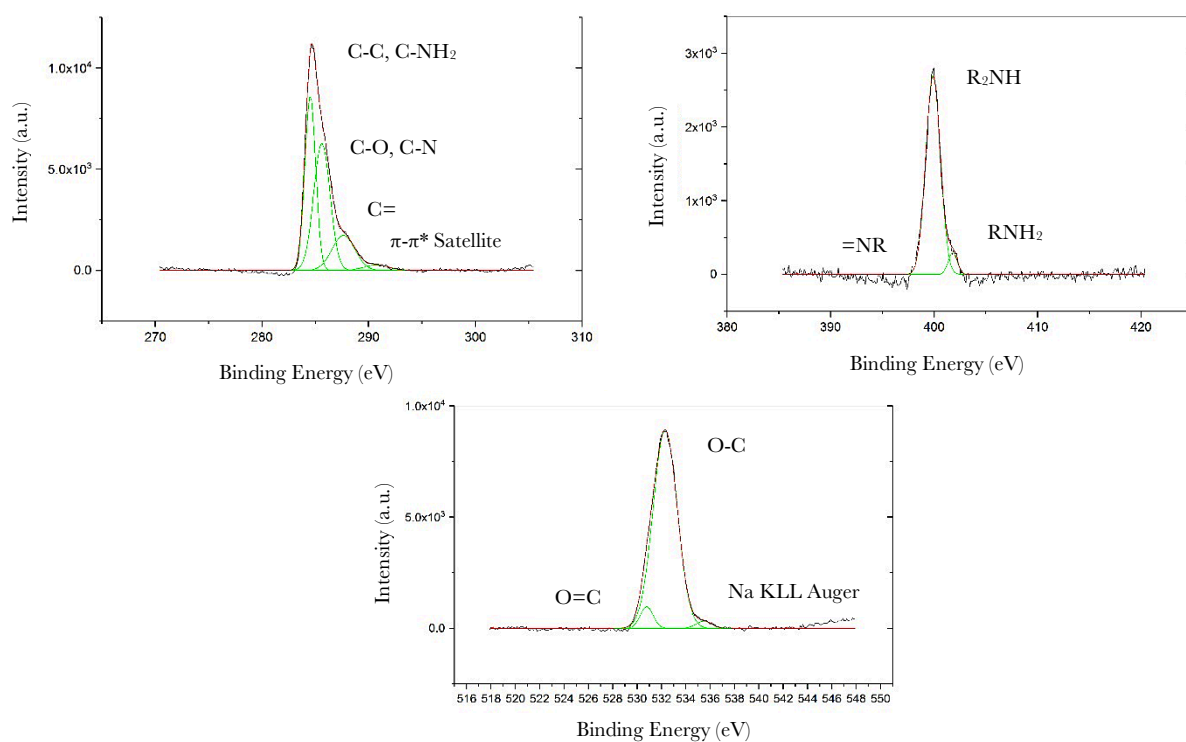
Figure 4.47 XPS data for p-Ser
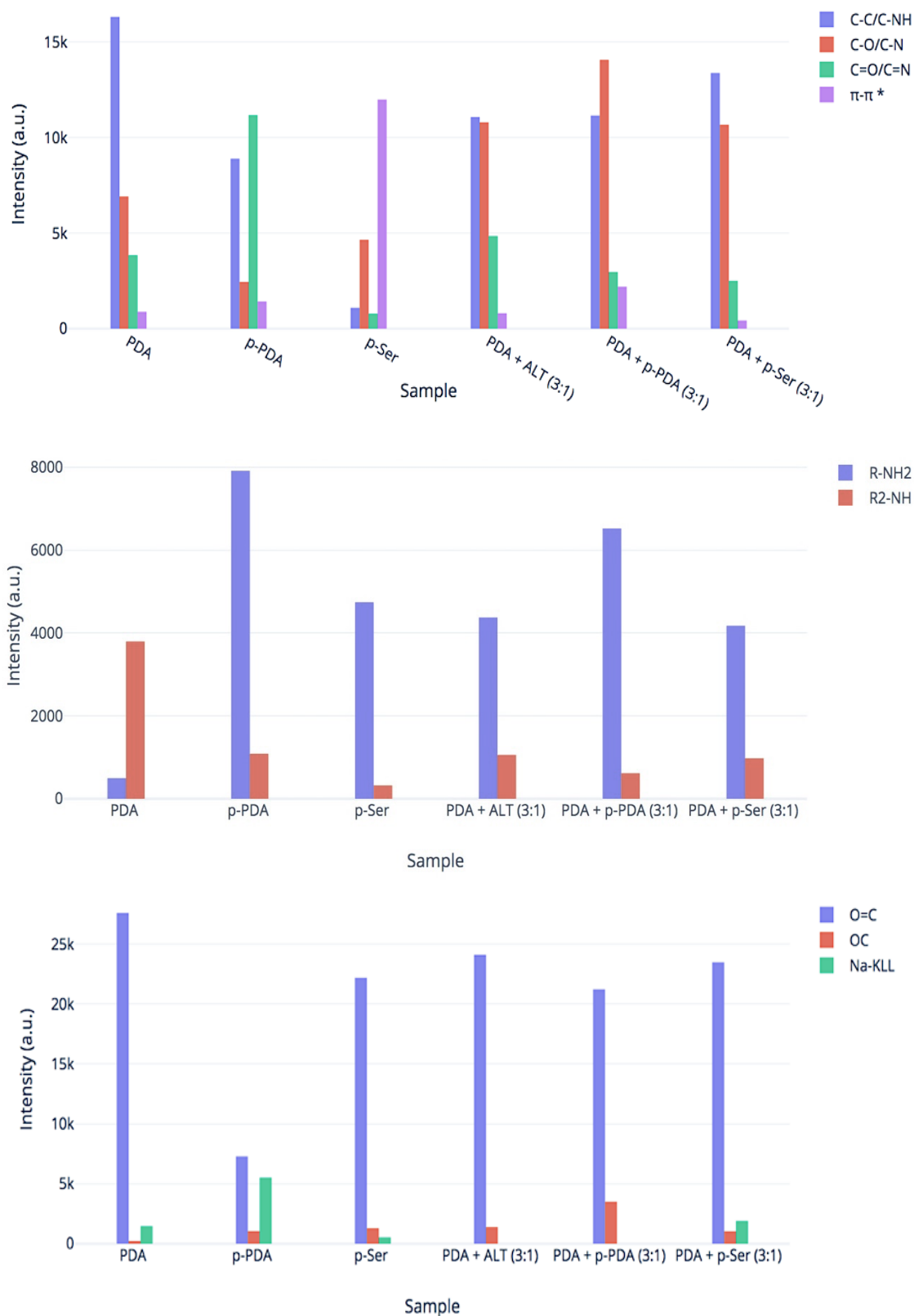
Figure 4.48 Comparison of peaks for C1s (top), N1s (middle) and O1s (bottom) of various samples using XPS

The main difference between PDA and PDA + p-Ser is the increase in the R-NH interaction. Apart from this no major differences between the homopolymer and copolymer were observed. The Na-KLL Auger peak is also still visible. Hence, it is not clear whether serotonin incorporates well into a dopamine copolymer. A distinct feature of p-Ser that differentiates it from PDA is the increase in π-π interactions observed as well as a decrease in the R_2NH peak. The various spectra for p-Ser are comparable to that found in literature for p-Ser nanoparticles [34] analysed by Nakatsuka et al. who also compare the XPS results with that of the serotonin monomer. They also recorded possible increases in π-π interaction. The qualitative differences in the data support the structural differences between PDA, P-Ser and the PDA copolymers. For example, in the copolymer samples PDA + p-PDA and PDA + ALT the Na-KLL Auger peak visible in the PDA sample due to the incorporation of Na from the phosphate buffer (possibly by complex formation) is absent. This indicates that the covalent bonding interactions between PDA and the second monomers hinder the incorporation of Na^+ into the structures. Also notable are the increases in OC peaks and R-NH interactions of both copolymers PDA+ p-PDA and PDA + ALT in comparison with PDA which is expected from their copolymerized structure, also indicating that the monomers were incorporated with DA unlike the case with serotonin.
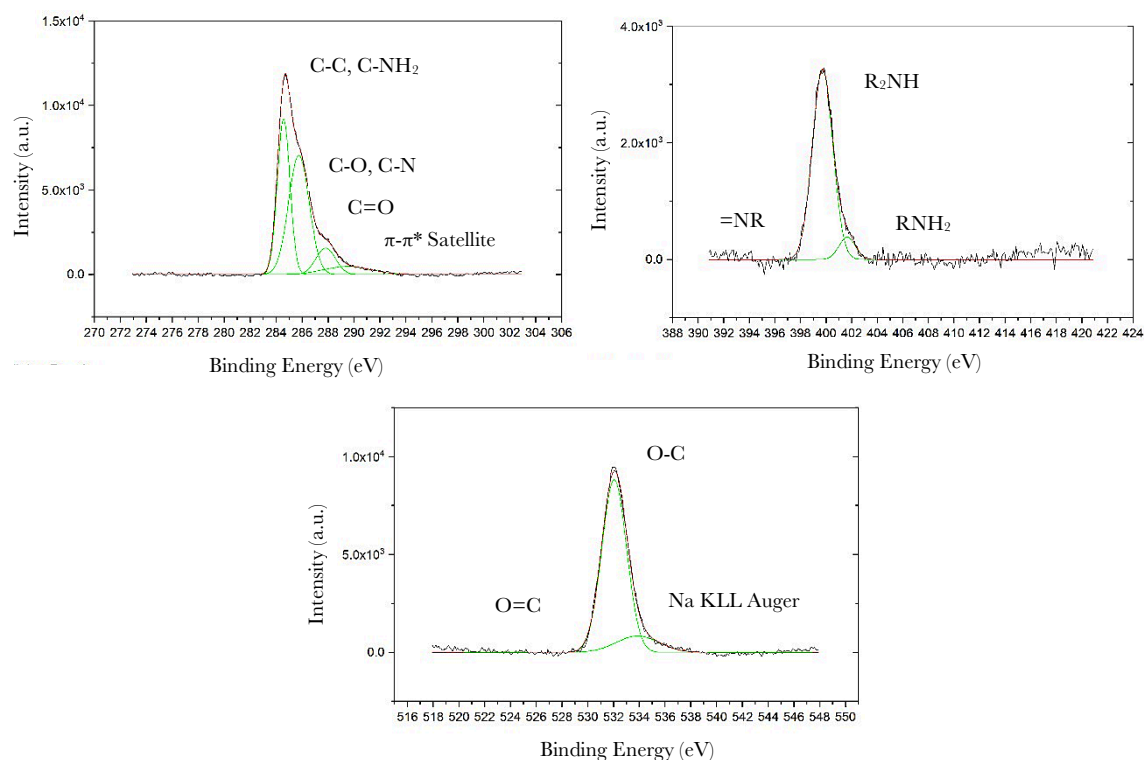
Figure 4.49 XPS data for PDA + p-PDA 3:1

A distinct decrease in the intensity of the C=O (the non-zero peak could arise from atmospheric oxygen) as well as an intense increase in the R-NH peaks of p-PDA as expected from its structure in comparison with PDA is a notable feature. The data for p-ALT is not available as part of this thesis as further investigation was needed to refine the XPS spectra. A drawback of using the XPS method is the duration needed for sample analysis and high sensitivity in fitting the spectra to reference values.

4.6   Executive Summary

The most relevant data obtained in the results and discussion section is summarized in Table 4.6-1. The XPS data was considered as supporting information and is not included as a part of the summary unless no other data is available. All samples were prepared in a PB of pH ~ 7.0 and CV parameters of -0.5 V to + 0.5 V scan voltage, 8 scan cycles and 0.01 V/s scan rate unless mentioned otherwise. All samples were prepared on Au substrates, Ag/AgCl R.E. and an Au C.E. When available, CV data was obtained using a Pt C.E. in PB of varying pH values between ~ 4.6-7.3. All other measurements were performed as mentioned in Section 3: Experimental Section.

Table 4.6-1 Executive summary of results

Sample	EP synthesis /CV characterization data	Spectral features	AFM/SEM/Profilometry/ Contact angle
PDA (reference material) ~ 5 mM monomer concentration	Reproducible film formed by EP, CV data for pH variation in the range expected for similar studies in literature [62]	Comparable to previous studies [39]	12 nm thickness, roughness of ~ 2nm. Contact angle of 50-55° [80]
p-PDA ~ 2 mM monomer concentration	– No film formation possible – No CV data for redox activity available. – Possible chain-growth polymerization mechanism	EDX: reasonable C:N ratios. FTIR: 890 cm^{-1} for v (=CH) and aromatic ring stretch from 1510-1630 cm^{-1}	No AFM/profilometry data. SEM shows microneedle/ microfiber formation. Contact angle higher than all other samples at 78°
p-ALT ~ 0.7 mM monomer concentration	– Reproducible film formed by EP – Possible two-electron oxidation mechanism – Known to be redox active [31], no pH-based CV data available	FTIR: 1290 cm^{-1} broadening of v (C=O) peak, lowered intensity of the C=C aromatic ring peak from 1510-1630 cm^{-1}	5 nm thickness, roughness of ~ 1 nm. Contact angle of 70°

Sample	EP synthesis /CV characterization data	Spectral features	AFM/SEM/Profilometry/ Contact angle
p-Ser 0.5 mM monomer concentration	– Reproducible film formed using EP in HEPES buffer pH ~ 5.5 – Not redox active or pH active – Film formed at 10 x lower monomer concentration than literature and of 1 cm diameter (scaled up. 8 x lower	The C=C aromatic ring peak of p-Ser is quite similar to PDA as expected, with a slight shift towards the left in the range 1510-1630 cm^{-1} C-OH peak is visible at ~ 1200 cm^{-1}	~ 10 nm thickness but formed with 15 EP cycles instead of 8 in other samples and higher scan voltages (± 0.8 V instead of ± 0.5 V). Roughness ~ 1.5 nm. Contact angle of 61°
PDA + p-PDA	– Reproducible films formed for 3:1 and 1:1 systems – CV data shows pH-dependent redox-active films with lower oxidation and reduction potentials than PDA. – ΔE_{ps} highest at pH ~ 7 – Concentration of p-phenylenediamine comonomer does not affect redox activity – v of CV analysis increases peak separation voltage – Oxidative copolymerization mechanism	Marked difference in C=C aromatic ring spectral feature similar to p-PDA between 1510-1630 cm^{-1}, possibly due to stretching of the aromatic rings [84]	Thickness of 3:1 system ~ 11 nm and roughness ~ 2 nm. Thickness of 1:1 system (ideal ratio for bulk copolymer formation from literature [65]) ~ 15 nm and roughness ~ 2.5 nm. Contact angle of 59° for 10:1 system.
PDA + ALT	– Reproducible films formed for 3:1 and 10:1 systems – CV data shows pH-dependent redox-active films with higher oxidation and reduction potentials than PDA – ΔE_{ps} highest at pH ~ 7 – Concentration of 3-amino-L-tyrosine comonomer increases oxidation/reduction potentials – v of CV analysis increases peak separation voltage – Oxidative copolymerization mechanism	No standout spectral feature of ALT detectable in PDA + ALT, possibly to the low contribution to material composition except for the C-OH stretching peak for this sample visible in the range 1200-1210 cm^{-1}	Thickness of 3:1 system (ideal ratio for bulk copolymer formation from literature [65]) ~ 9 nm and roughness ~ 1 nm. Thickness of 10:1 system ~ 14 nm and roughness ~ 2 nm. Contact angle of 69 for 10:1 system.
PDA + p-Ser	– No reproducible, homogenous film formation possible with EP – No CV data or pH-based data available	No spectral data available. XPS data shows an increase in the R-NH interaction compared to PDA	Thickness when films exist, ~ 10 nm and roughness of ~ 1.5 nm on average. Contact angle of 46 for 10:1 system, lower than all other systems.

Thus, it was possible to tune the oxidation/reduction voltages of PDA using PDA+ p-PDA and PDA + ALT 3:1 copolymers between 90-500 mV (anodic potential) and 50-220 mV (cathodic potential). The scan rate of measurement was also accounted for when taking CV data. FTIR spectra allow qualitative differentiation between structural differences of various polymer thin films. AFM, profilometry and contact angle studies provide morphological data about the thickness, roughness and surface wettability of the different thin films.

5   CONCLUSION AND OUTLOOK

In this thesis, the widely studied parameters and conditions used for polydopamine thin film synthesis by electropolymerization were extended to other homopolymer films synthesized from different monomers that incorporate aromatic amino groups including 3-amino-L-tyrosine, p-phenylenediamine and serotonin. The electropolymerization of 3-amino-L-tyrosine yielded a p-ALT thin film of ultrathin dimensions ($\sim$ 5 nm) which shows potential for biofunctionalization applications and photocatalytic applications as substituted tyrosines are known for being redox active [31]. Thin film formation was not possible using p-phenylenediamine but the presence of microneedles and fibers in the range of a few microns were visible using SEM for p-PDA. The microneedles are speculated to be conducting from literature [21]. There are possibilities for using these microneedles as composites with PDA to test the effects for further applications since the incorporation of p-PDA in copolymer form with PDA suppresses its morphological characteristics. It was possible to synthesize a p-Ser film of circular diameter $\sim$ 1 cm which is a 100 times scaled-up version of the diameter of films ($\sim$1 mm) electropolymerized earlier on boron-doped diamond substrates [67]. The p-Ser films had a thickness of $\sim$ 12 nm on an Au substrate and could be synthesized with a monomer concentration 8 times lower than that used in literature, and also with a scan rate 10 times lower which can reduce electrode fouling effects. The thickness of the films was almost twice that presented on the boron-doped diamond substrate. Possibilities exist to explore functionalizing p-Ser with dyes and also for biosensing applications.

The optimization and reproducibility of PDA-based copolymers: PDA + ALT, PDA + p-PDA and PDA + p-Ser in varying molar ratios and thickness was studied using electropolymerization, AFM and profilometry. Cyclic voltammetry studies with PDA + ALT (3:1) and PDA + p-PDA (3:1) films which had similar dimensions ($\sim$9-11 nm thickness) showed that the oxidation and reduction potentials made the electrochemical response of PDA adaptable to varying pH environments (in the range 4.6-7.3) and that the peak separation values depend on the scan rate at which they are analyzed with lower scan rates being ideal to prevent electrode fouling. The peak potentials of the PDA + ALT systems which range from $\sim$200-500 mV for anodic peaks and $\sim 120 - 220$ mV for cathodic peaks are in general higher than PDA. For PDA the anodic peaks range between $\sim$150 $- 420$ mV and cathodic peaks ranging between $\sim 90 - 210$ mV which is higher than that of PDA + p-PDA which shows anodic peaks ranging between $90 - 360$ mV and cathodic peaks ranging from $\sim 50 - 170$ mV.

This indicates a certain amount of tunability in both directions by copolymerization with the potentials generally varying in the following manner: PDA + p-PDA < PDA < PDA + ALT while still remaining comparable to that of the oxidation/reduction potentials of water and the band gap of the CdSe@CdS nanostructures. The results from these systems were juxtaposed with PDA + ALT (10:1) and PDA + p-PDA (1:1) systems which showed that the comonomer concentration affects the oxidation and reduction potentials in the former system (~ 40 mV) but not greatly in the latter. Thus, the cyclic voltammetry analysis thus played a dual role in the analysis of the systems by allowing an understanding of the adaptability of PDA copolymers to varying pH environments and also to qualitatively differentiate between the assumed one-electron system of PDA with the quasi-reversible, novel electron systems of the copolymers. Thus, PDA and PDA + p-PDA/ALT copolymers were found to be pH-active in the range 4.6-7.3. This presents scope for further studies on the pH activity of these systems at higher pH values as well as a promising feature for pH-sensing applications in the range 4.6-7.3.

The p-Ser system did not show any changes in its oxidation/reduction potentials with pH and the peak separation voltages did not yield sensible values as they were too low for an expectedly insulating system. The removal of the p-Ser film using the method for PDA was attempted but not satisfactorily possible in the time frame available, and hence can be studied further. Since ALT is known to be redox active [31], p-ALT could also be a candidate for further studies relating to PWS. The p-PDA homopolymer was not probed for its CV characteristics since no film was detectable (so far) under the fibers. Despite the likelihood of blend formation in the PDA + p-PDA/PDA + ALT copolymers, the probability of blend vs. copolymer formation is greater for the PDA + p-Ser thin films due to the presence of particulate aggregates and breaks in the films. Thus, redox-activity studies for this system was not performed and presents scope for further study. The chemical structural differences between the various films were analyzed using FTIR in the reflection mode, XPS and contact angle studies; indicating the incorporation of new homopolymer and possible copolymer structures. The contact angle variations between low-comonomer concentrations of other monomers with dopamine were compared with pure homopolymer films and they were found to be increasingly hydrophobic in the following order: PDA + ALT 3:1 < PDA + p-Ser < PDA < PDA + p-PDA 10:1 ~ p-Ser < p-ALT ~ PDA + p-ALT 10:1 ~ PDA + p-PDA 3:1 < p-PDA. The p-Ser film showed significantly greater π-π interactions from XPS and the copolymerization of p-PDA and ALT with PDA caused the Na-KLL Auger peaks to disappear indicating copolymer formation due to inavailbility of sites for Na^+ to form complexes.

Embedding co-catalysts into the PDA and copolymer films, such as Co-complexes, Mo-complexes, Pt etc. is also a possibility for further work. Data is not yet available in this work for the embedding of the CdSe@CdS sensitizers and will be explored further in collaboration with the group of Dr. Wächtler in Jena, after selection of optimal films. Electrochemical impedance spectroscopy could a useful tool to understand the impedance characteristics of the system but requires further studies before the characterization method can give conclusive data (see Appendix 2 in Section 6.2). The overall/actual effect of replacing PDA with the copolymers in the hybrid PWS system could be explored further. The removal and transfer of these films onto other substrates is also not yet possible and lower adhesion properties of p-Ser pose both an advantage and disadvantage.

Due to the wide array of monomers available in nature, the possibilities for combining these with dopamine for adapting its characteristics are nearly endless. Possible selection criteria for these monomers include light stability and the presence of electron donating groups such as the aromatic amines used in this study. The use of metallic nanoparticle dopants could also be explored to impart conducting properties to the PDA/PDA copolymer thin films for use in memristive biosensors. The copolymer systems PDA + p-PDA and PDA + ALT (3:1) present promising features for use in PWS including tunability of potentials and adaptability to varying pH environments. These properties could also be extended to applications such as pH sensing [62]. Dye-sensitization of the thin films for PWS could also be explored. The novel electron systems understood from CV analysis present possibilities for tuning the electron transfer characteristics, electron delocalization and electron recombination time in the sacrificial layer of the hybrid systems. This property can be extended for use of these copolymers in conjunction with Organic Field Effect Transistors, or for creating devices with lithographic techniques for biosensing or biointerfaces [97].

6   APPENDIX AND SUPPORTING INFORMATION

6.1   Appendix 1: Synthesis of polyserotonin films

Serotonin films were electropolymerized using 0.5 mM Serotonin in 0.1 M NaCl and 5mM HEPES using the following parameters: Lower Vertex: - 0.8 V; Upper Vertex: 0.8 V; Number of scans: 15; Scan rate: 0.01 V/s; Step: 0.00244 V. The solution was not bubbled under nitrogen. The number of scans and scanning voltage limits were increased in comparison with previous experiments to increase the chances of film formation. Profilometry measurements for pure Serotonin films made by Method 2 and PDA + p-Ser (1:1, 3:1 and 10:1) were performed to check film formation and obtain thickness. Figure 6.1 shows the CV for pure polyserotonin made attempted in a PB solution of pH 6.9 which did not yield any films and the trial using a HEPES buffer.

| (a) | (b) |
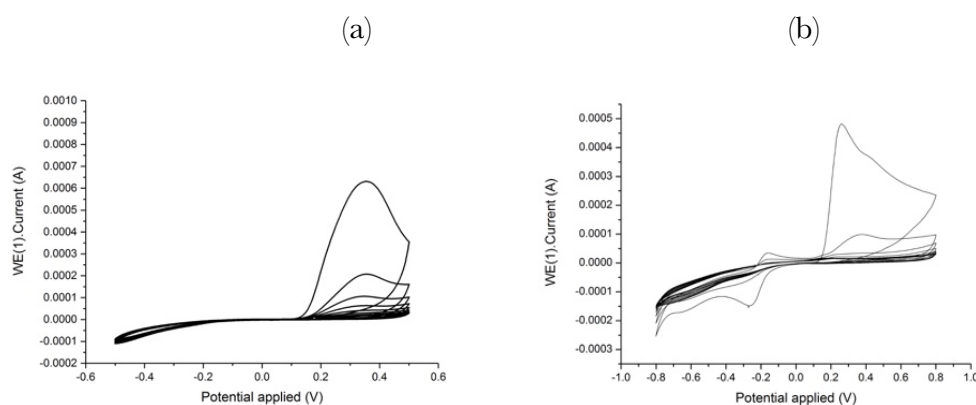
Figure 6.1 CV for EP of serotonin under (a) Phosphate buffer (b) HEPES buffer − Trial 1 − electrode contaminated by dopamine solution leading to dopamine-like cyclic voltammetry characteristics

The thickness of the film was found to be 25.5 ± 0.85 nm using profilometry and 22 ± 1.01 using AFM. Its roughness using AFM was found to be 0.56 ± 0.44 nm. Figure 6.2 (a) and (b) show the CV diagrams for testing the reproducibility of p-Ser pure films. It was later found that the instrument failed due to a loose wire and so these diagrams are not accurate and the results, unrepresentative. Figure 6.2 (c) shows the CV diagram of the electropolymerization of p-Ser film. However, this was conducted with an old solution (2 days old) and since serotonin is known to be unstable in solution, this trial cannot be considered an accurate attempt at reproducing a p-Ser film.
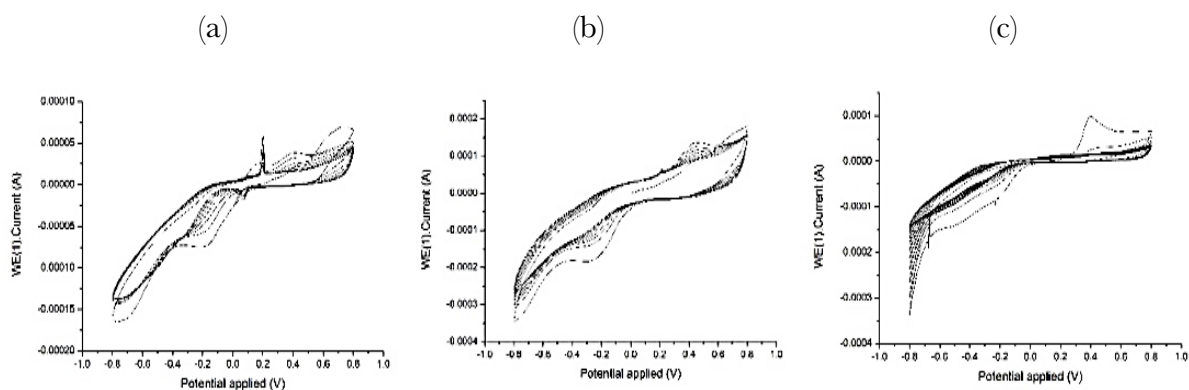
Figure 6.2 CV for reproducibility trials for pure p-Ser films (a) (b) while EP setup was damaged (c) using old Serotonin solution with HEPES buffer

Since the first trial for the synthesis of polyserotonin gave a homogenous film of good thickness (~25 nm) and was performed without nitrogen bubbling, an attempt was made at checking the reproducibility of Serotonin homopolymer films using electropolymerization with and without nitrogen bubbling by electropolymerization and analyzing thickness and homogeneity differences by AFM and profilometry. Serotonin thin films were electropolymerized using 0.5 mM Serotonin in 0.1 M NaCl and 5mM HEPES using the following parameters to test for reproducibility: Lower Vertex: - 0.8 V; Upper Vertex: 0.8 V; Number of scans: 15; Scan rate: 0.01 V/s; Step: 0.00244 V Au C.E., Au W.E. and Ag/AgCl (3 M KCl) R.E. In Trial 1, the electropolymerization was performed with N_2 bubbling of the sample for 10 mins and in Trial 2 it was performed directly after the solution was prepared. Both trials were repeated once. In both Trial 1 and 2, thin films of polyserotonin were obtained. The CV diagrams for electropolymerization are depicted in Figure 6.3. The CV curves differ in that Trial 1 shows an oxidation peak at ~ 0.2 V whereas this peak is much smaller in comparison in the CV curves from Trial 2. There is also a broadening of the curve in the negative part of the cycles observed in Trial 2. The variation between the curves in Trial 1 is somewhat greater possibly due to increased oxygen in solution in the absence of N_2 bubbling.
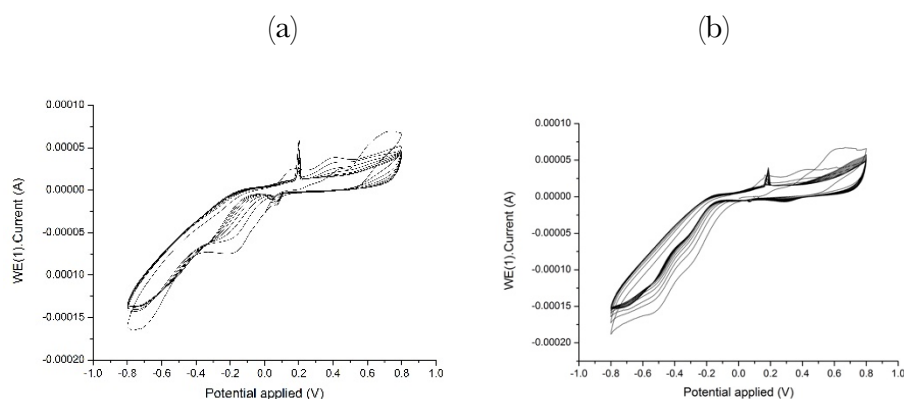
Figure 6.3 CV diagrams for synthesis of polyserotonin copolymer film (a) Trial 1 - with N₂ bubbling of the sample for 10 mins and (b) Trial 2 − without N₂ bubbling

Figure 6.4 shows the profilometry images of one set of samples from Trial 1 and Trial 2. It is apparent that oxidation produces dark spots on the surface of the sample in Trial 1 which are absent in the surface of the sample in Trial 2. Figure 6.5 shows the AFM micrographs of the same samples.
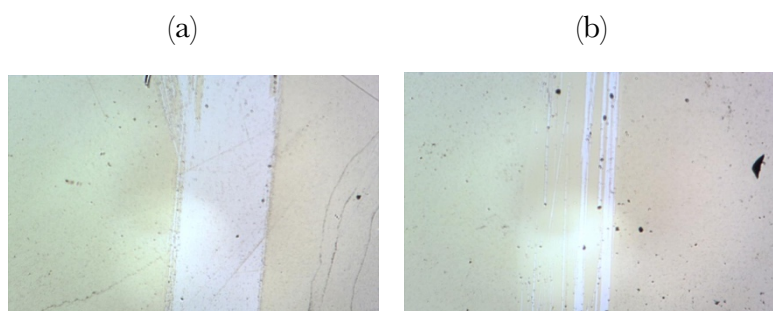
Figure 6.4 Profilometry images of reproducibility trials for pure p-Ser films (a) Trial 1 - with N₂ bubbling of the sample for 10 mins and (b) Trial 2 − without N₂ bubbling
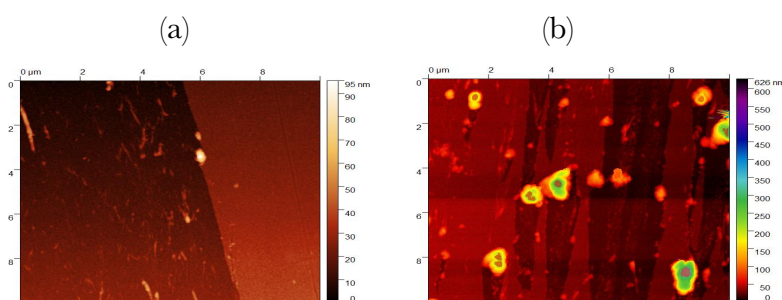
Figure 6.5 AFM micrographs of reproducibility trials for pure p-Ser films (a) Trial 1 - with N₂ bubbling of the sample for 10 mins and (b) Trial 2 − without N₂ bubbling

The AFM and profilometry data is summarized in Table 6.1-1.

Table 6.1-1 Summary of data using electropolymerization, profilometry, and AFM

Sample	Nature	Thickness using profilometry (nm)	Thickness using AFM (nm)	Roughness using AFM (nm)
p-Ser with N2 bubbling	Thin film	10.05 ± 1.03	12.13 ± 0.69	1.54 ± 0.72
p-Ser without N2 bubbling	Thin film	13.5 ± 2.2	8.51 ± 2.71	2.73 ± 2.42

The film produced in Trial 1 shows uneven thickness and is thus not very homogenous. Its roughness is also approximately twice that of the films produced in Trial 2. Thus, though the results from the first trial were irreproducible, a reproducible film without spots produced by oxidation of the sample could be synthesized as seen in Trial 2. The cause for the differences in the electropolymerization curves was found to be contamination by dopamine solution from previous trials. Hence, the C.E was cleaned thereafter by basic Piranha solution after each experiment.

6.2   Appendix 2: Electrochemical Impedance Spectroscopy trials

Figure 6.6 shows the Nyquist and Bode plots for pure PDA on an Au substrate synthesized for 8 cycles (Lower Vertex: - 0.5 V; Upper Vertex: 0.5 V; Number of scans: 8; Scan rate: 0.01 V/s; Step: 0.00244 V) from frequencies 1E+6 to 0.001. Though the Nyquist curve fits the semicircular plot until the mid-frequency range, it does not decrease after this point. The impedance value is also extremely high (order of 1E+5).
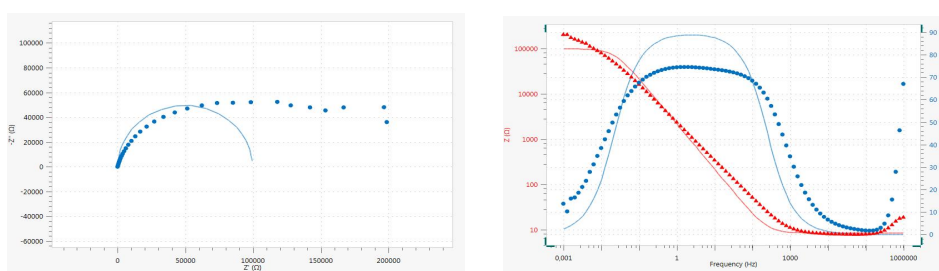
Figure 6.6 Nyquist plot left) and Bode plot (right) for pure PDA synthesized using EP with 8 cycles

 Figure 6.7 shows the Nyquist and Bode plots for pure PDA on an Au substrate synthesized for 3 cycles (Lower Vertex: - 0.5 V; Upper Vertex: 0.5 V; Number of scans: 5; Scan rate: 0.01 V/s; Step: 0.00244 V) from frequencies 1E+4 to 0.001. Though the Nyquist curve fits the semicircular plot until the mid-frequency range, it once again does not decrease after this point but rather increases. The impedance value is lower than the previous trial possibly due to the fewer cycles used to prepare the film but still quite high. Other trials were conducted using

PDA synthesized over 5 cycles and in different frequency ranges for impedance analysis such as 1E+4 to 0.01 and 1E+6 to 0.001 (plots not shown) but this still did not yield results that could give reasonable information about the system. Though the Nyquist curve fits the semicircular plot until the mid-frequency range, the values scatter in the low-frequency region as seen for pure PDA. The impedance value is lower than that of pure PDA as expected from the copolymer's CV deposition curves. The trial was only conducted once and not yet tested for reproducible results.
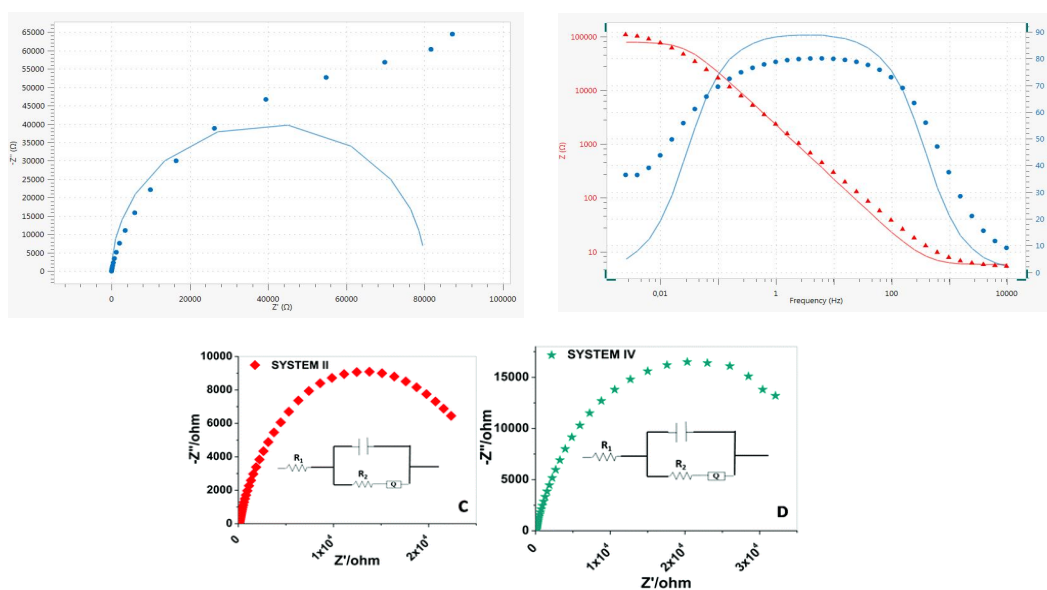
Figure 6.7 Nyquist plot (left) and Bode plot (right) for pure PDA synthesized using EP with 5 cycles and comparison with literature [98]
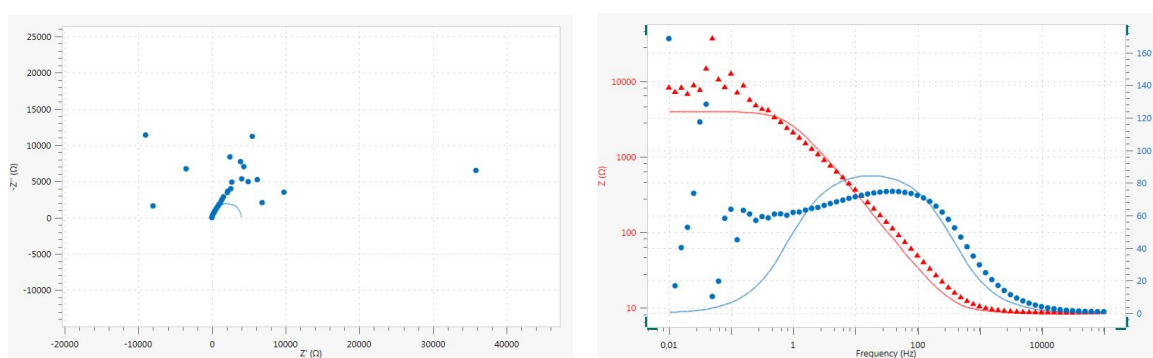
Figure 6.8 Nyquist plot (left) and Bode plot (right) for pure Au

6.3   Appendix 3: FTIR results

The copolymers of the three systems only show an intensity shift in comparison with their pure polymer counterparts as shown in Figure 6.8. In the case of pure p-PDA no signal was

detectable from the sample. No distinct spectral features of the films could be analysed using ATR-FTIR in transmission mode as seen in Figure 6.9. Thus, the characterization was performed using reflection mode as shown previously.
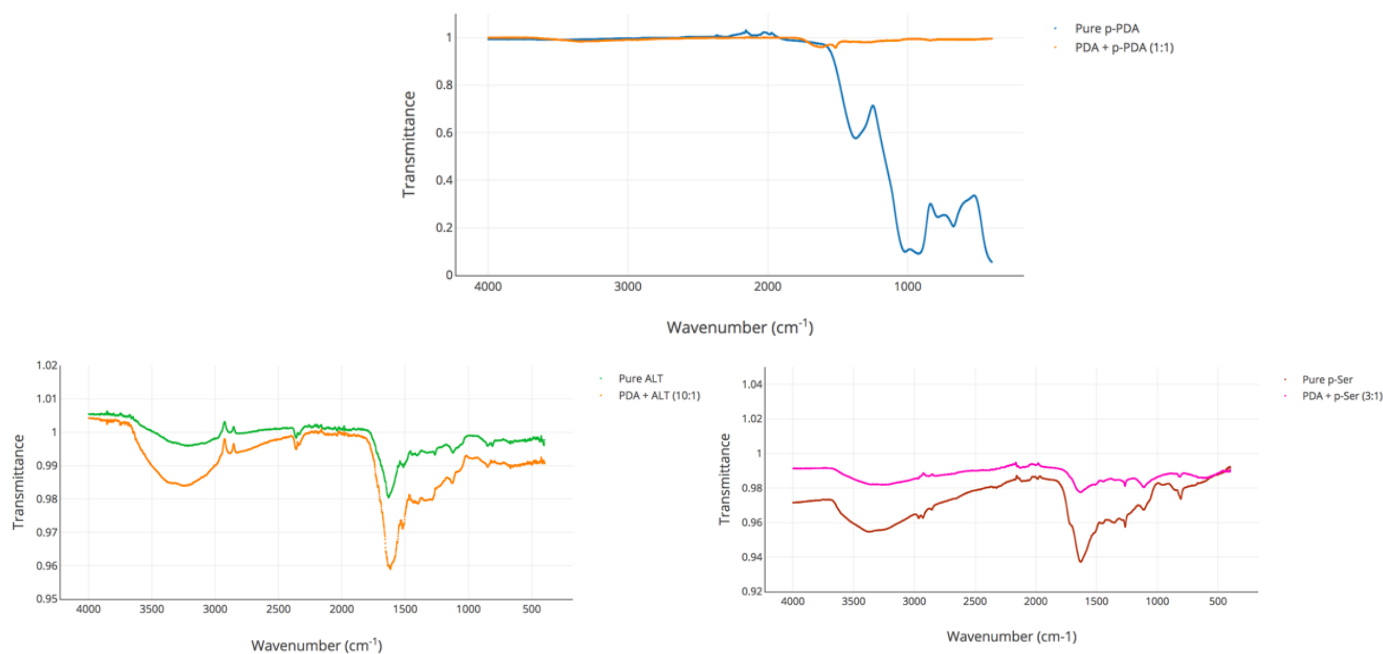
Figure 6.9 FTIR spectra (inconclusive) for various thin films Pure p-PDA and PDA + p-PDA (1:1) (top) Pure ALT and PDA + ALT (10:1) (bottom left) Pure p-Ser and PDA + p-Ser (3:1) (bottom right)

6.4   Appendix 4: Reusability of the films for analysis

Experiment 1: 10 mg of Dopamine HCl was dissolved in 10 mL in PB pH 7.0, bubbled under N_2 gas for 10 minutes and electropolymerized using a horizontal cell with the following parameters: Lower Vertex: - 0.5 V; Upper Vertex: 0.5 V; Number of scans: 8; Scan rate: 0.01 V/s; Step: 0.00244 V (Au C.E.). Then, a CV analysis using a PB of pH ~ 5.3 was performed with the following parameters: Lower Vertex: - 0.5 V; Upper Vertex: 0.5 V; Number of scans: 4; Scan rate: 0.01 V/s; Step: 0.00244 V (Pt C.E.). The same CV analysis was repeated on the sample without changing the PB solution. Experiment 2: 10 mg of Dopamine HCl was dissolved in 10 mL in PB pH 7.0, bubbled under N_2 gas for 10 minutes and electropolymerized using a horizontal cell with the following parameters: Lower Vertex: - 0.5 V; Upper Vertex: 0.5 V; Number of scans: 8; Scan rate: 0.01 V/s; Step: 0.00244 V (Au C.E.). Then, a CV analysis using a PB of pH ~ 5.3 was performed with the following parameters: Lower Vertex: - 0.5 V; Upper Vertex: 0.5 V; Number of scans: 4; Scan rate: 0.01 V/s; Step: 0.00244 V (Pt C.E.). The PB solution was rinsed off the sample using MilliQ water and then the same CV analysis was repeated with a PB of pH ~ 6.9. Note: Trials were conducted only once for each experiment.

The fourth cycles from each of the CV analyses were compared to test the reusability of the samples. Figure 6.10 shows the CV diagrams from Experiment 1. It is evident that the V-I values overlap. However, there is a small effect of electrode fouling in the part of the curve characteristic for the Au substrate (negative applied voltage regime) seen as a slight shift in the current to more positive values. This means that the samples are reusable when analyzing them at the same pH. Though the current artefact at ~ 0.2 V increases during the repeat trial with the reused sample, this does not affect the results for the CV analysis.
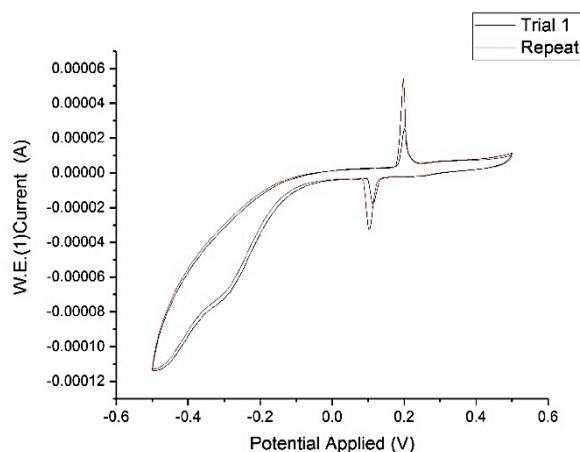
Figure 6.10 CV analysis of PDA on an Au substrate showing the fourth cycle for two trials
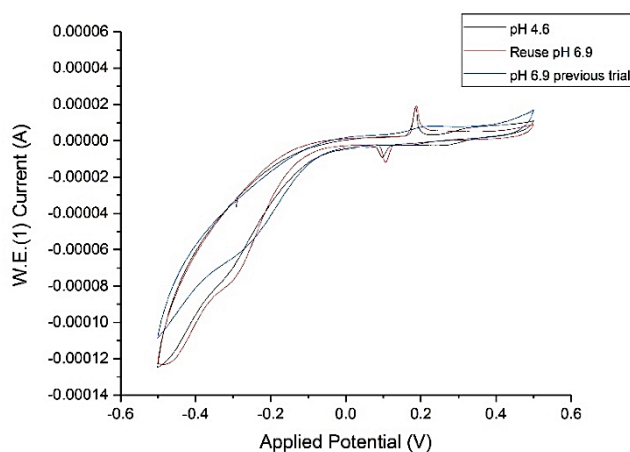
Figure 6.11 CV analysis of PDA on an Au substrate showing the fourth cycle for two trials at different pH and reference from a previous trial

It is evident from the CV diagram in Figure 6.11 that analyzing the PDA film under an acidic pH of 4.6 modifies the electrochemical properties of the film at the surface. This can be seen by the shift in the CV curves from the repeat trial at pH ~ 6.9 vs. the data obtained from a

previous trial at the same pH on a freshly prepared PDA film. Thus, reanalyzing the PDA film at the same pH (near-neutral) does not show a change in the CV characteristics. However, reusing the film after analyzing the PDA film at a non-neutral pH modifies the system so that the CV characteristics at near-neutral pH are not maintained.

7 REFERENCES

[1] S.J. Moniz, S.A. Shevlin, D.J. Martin, Z.-X. Guo, J. Tang, Visible-light driven heterojunction photocatalysts for water splitting–a critical review, Energy Environmental Science, 8 (2015) 731-759.

[2] W.J. Youngblood, S.-H.A. Lee, K. Maeda, T.E. Mallouk, Visible light water splitting using dye-sensitized oxide semiconductors, Accounts of chemical research, 42 (2009) 1966-1973.

[3] C. Department of Applied Chemistry, Photocatalytic water splitting reaction

[4] M.I. Litter, Heterogeneous photocatalysis: transition metal ions in photocatalytic systems, Applied catalysis B: environmental, 23 (1999) 89-114.

[5] M.A. Fox, Fundamentals in the design of molecular electronic devices: long-range charge carrier transport and electronic coupling, Accounts of chemical research, 32 (1999) 201-207.

[6] J. Oudenhoven, F. Scheijen, M. Wollfs, Fundamental of photocatalytic water splitting by visible light, Chemistry of Catalytic System 2: Photocatalysis, (2004) 1-22.

[7] M. Ni, M.K. Leung, D.Y. Leung, K. Sumathy, A review and recent developments in photocatalytic water-splitting using TiO2 for hydrogen production, Renewable Sustainable Energy Reviews, 11 (2007) 401-425.

[8] H. Yan, J. Yang, G. Ma, G. Wu, X. Zong, Z. Lei, J. Shi, C. Li, Visible-light-driven hydrogen production with extremely high quantum efficiency on Pt–PdS/CdS photocatalyst, Journal of Catalysis, 266 (2009) 165-168.

[9] H. Liu, J. Yuan, W. Shangguan, Photochemical reduction and oxidation of water including sacrificial reagents and Pt/TiO2 catalyst, Energy fuels, 20 (2006) 2289-2292.

[10] H. Lee, S.M. Dellatore, W.M. Miller, P.B. Messersmith, Mussel-inspired surface chemistry for multifunctional coatings, Science, 318 (2007) 426-430.

[11] J.r. Liebscher, R. Mrówczyński, H.A. Scheidt, C. Filip, N.D. Hădade, R. Turcu, A. Bende, S. Beck, Structure of polydopamine: a never-ending story?, Langmuir, 29 (2013) 10539-10548.

[12] Y. Liu, K. Ai, L. Lu, Polydopamine and its derivative materials: synthesis and promising applications in energy, environmental, and biomedical fields, Chemical reviews, 114 (2014) 5057-5115.

[13] F. Yu, S. Chen, Y. Chen, H. Li, L. Yang, Y. Chen, Y. Yin, Experimental and theoretical analysis of polymerization reaction process on the polydopamine membranes and its corrosion protection properties for 304 Stainless Steel, Journal of Molecular Structure, 982 (2010) 152-161.

[14] V. Ball, D. Del Frari, V. Toniazzo, D. Ruch, Kinetics of polydopamine film deposition as a function of pH and dopamine concentration: Insights in the polydopamine deposition mechanism, Journal of colloid interface science, 386 (2012) 366-372.

[15] J. Yang, L. Niu, Z. Zhang, J. Zhao, L. Chou, Electrochemical behavior of a polydopamine nanofilm, Analytical Letters, 48 (2015) 2031-2039.

[16] Y. Ding, L.-T. Weng, M. Yang, Z. Yang, X. Lu, N. Huang, Y. Leng, Insights into the aggregation/deposition and structure of a polydopamine film, Langmuir, 30 (2014) 12258-12269.

[17] H.W. Kim, B.D. McCloskey, T.H. Choi, C. Lee, M.-J. Kim, B.D. Freeman, H.B. Park, Oxygen concentration control of dopamine-induced high uniformity surface coating chemistry, ACS applied materials and interfaces, 5 (2013) 233-238.

[18] M.E. Lynge, R. van der Westen, A. Postma, B. Städler, Polydopamine—a nature-inspired polymer coating for biomedical science, Nanoscale, 3 (2011) 4916-4928.

[19] R. Luo, L. Tang, J. Wang, Y. Zhao, Q. Tu, Y. Weng, R. Shen, N. Huang, Improved immobilization of biomolecules to quinone-rich polydopamine for efficient surface functionalization, Colloids Surfaces B: Biointerfaces, 106 (2013) 66-73.

[20] N.C.f.B. Information, PubChem Compound Database; CID=7814,.

[21] Y.-L. Min, T. Wang, Y.-G. Zhang, Y.-C. Chen, The synthesis of poly (p-phenylenediamine) microstructures without oxidant and their effective adsorption of lead ions, Journal of Materials Chemistry C, 21 (2011) 6683-6689.

[22] F. Cataldo, On the polymerization of p-phenylenediamine, European polymer journal, 32 (1996) 43-50.

[23] S. Sayyah, S. Abd El-Rehim, M. El-Deeb, S. Kamal, R. Azooz, Electropolymerization of p-phenylenediamine on Pt-electrode from aqueous acidic solution: Kinetics, mechanism, electrochemical studies, and characterization of the polymer obtained, Journal of applied polymer science, 117 (2010) 943-952.

[24] P. Chandrasekhar, R.W. Gumbs, Electrosyntheses, Spectroelectrochemical, Electrochemical, and Chronovoltabsorptometric Properties of Family of Poly (Aromatic Amines), Novel Processible Conducting Polymers I. Poly (Benzidines), Journal of the Electrochemical Society, 138 (1991) 1337-1346.

[25] D.-M. Zhou, Y.-Q. Dai, K.-K. Shiu, Poly (phenylenediamine) film for the construction of glucose biosensors based on platinized glassy carbon electrode, Journal of applied electrochemistry, 40 (2010) 1997-2003.

[26] Y.-Q. Dai, D.-M. Zhou, K.-K. Shiu, Permeability and permselectivity of polyphenylenediamine films synthesized at a palladium disk electrode, Electrochimica Acta, 52 (2006) 297-303.

[27] I. Tapsoba, S. Bourhis, T. Feng, M. Pontie, Sensitive and Selective Electrochemical Analysis of Methyl-parathion (MPT) and 4-Nitrophenol (PNP) by a New Type p-NiTSPc/p-PPD Coated Carbon Fiber

Microelectrode (CFME), Electroanalysis: An International Journal Devoted to Fundamental, 21 (2009) 1167-1176.

[28] J.G. Bruno, J.L. Kiel, Synthesis of diazoluminomelanin (DALM) in HL-60 cells for possible use as a cellular-level microwave dosimeter, Bioelectromagnetics: Journal of the Bioelectromagnetics Society, 15 (1994) 315-328.

[29] J. Maddaluno, K. Faull, Inhibition of mushroom tyrosinase by 3-amino-L-tyrosines: Molecular probing of the active site of the enzyme, Experientia, 44 (1988) 885-887.

[30] E. Grandmougin, Ber. dtsch. chem, 39 (1906) 2494.

[31] W. Lee, M.g. Kasanmascheff, M. Huynh, A. Quartararo, C. Costentin, I. Bejenke, D.G. Nocera, M. Bennati, C. Tommos, J. Stubbe, Properties of site-specifically incorporated 3-aminotyrosine in proteins to study redox-active tyrosines: Escherichia coli ribonucleotide reductase as a paradigm, Biochemistry, 57 (2018) 3402-3415.

[32] R.L. McCreery, Advanced carbon electrode materials for molecular electrochemistry, Chemical reviews, 108 (2008) 2646-2687.

[33] P. Hashemi, E.C. Dankoski, J. Petrovic, R.B. Keithley, R. Wightman, Voltammetric detection of 5-hydroxytryptamine release in the rat brain, Analytical chemistry, 81 (2009) 9462-9471.

[34] N. Nakatsuka, M.M. Hasani-Sadrabadi, K.M. Cheung, T.D. Young, G. Bahlakeh, A. Moshaverinia, P.S. Weiss, A.M. Andrews, Polyserotonin Nanoparticles as Multifunctional Materials for Biomedical Applications, ACS nano, 12 (2018) 4761-4774.

[35] N.m. Elgrishi, K.J. Rountree, B.D. McCarthy, E.S. Rountree, T.T. Eisenhart, J.L. Dempsey, A practical beginner's guide to cyclic voltammetry, Journal of Chemical Education, 95 (2017) 197-206.

[36] X. Ling, Formation of polymer coatings by electropolymerization, University of Waterloo, 1998.

[37] MSU, Experiment 5: Cyclic Voltammetry

[38] https://www.tek.com/blog/performing-cyclic-voltammetry.

[39] J. Szelwicka, Herstellung und Charakterisierung von Polydopamin-Hybrid-Filmen für Photokatalyse, Max Planck Institute for Polymer Research, Mainz, 2018.

[40] K. Weil, E. Gileadi, E. Kirowa-Eisner, and J. Penciner: Interfacial Electrochemistry–An Experimental Approach, Addison-Wesley, Advanced Book Program, Reading, Massachusetts 1975, 525 Seiten, Preis: US $19.50, Berichte der Bunsengesellschaft für physikalische Chemie, 80 (1976) 826-826.

[41] A.J. Bard, L.R. Faulkner, J. Leddy, C.G. Zoski, Electrochemical methods: fundamentals and applications, Wiley New York1980.

[42] K.Q. Ding, Q.F. Wang, M. Zhao, Cyclic Voltammograms of Ferrocene on Multi-Walled Carbon Nanotubes (MWCNTs)-Modified Edge Plane Pyrolytic Graphite (EPPG) Electrode in Room Temperature Ionic Liquids (RTILs) of 1-Ethyl-3-Methylimidazolium Tetrafluoroborate (EMIBF4), Journal of the Chinese Chemical Society, 54 (2007) 723-730.

[43] M. Matsumiya, M. Terazono, K. Tokuraku, Temperature dependence of kinetics and diffusion coefficients for ferrocene/ferricenium in ammonium-imide ionic liquids, Electrochimica Acta, 51 (2006) 1178-1183.

[44] T.V. Vorburger, J. Raja, Surface Finish Metrology, American Society for Precision Engineering, 1988.

[45] G. Haugstad, Overview of Atomic Force Microscopy, 2015.

[46] U.o. Utah, Lecture 10: Basics of Atomic Force Microscope.

[47] C.L. Texts, How an FTIR Spectrometer Operates 2015.

[48] B. Lindberg, K. Hamrin, G. Johansson, U. Gelius, A. Fahlman, C. Nordling, K. Siegbahn, Molecular spectroscopy by means of ESCA II. Sulfur compounds. Correlation of electron binding energy with structure, Physica Scripta, 1 (1970) 286.

[49] M.P. Seah, D. Briggs, Practical Surface Analysis: Auger and X-ray Photoelectron Spectroscopy, John Wiley & Sons1990.

[50] Lab Manual: XPS, Universität Ulm, Ulm, Germany, 2018.

[51] JEOL, Basic Knowledge For Using The SEM, JEOL, Tokyo.

[52] T.F.S.P.-W. BV, Different Types of SEM Imaging – BSE and Secondary Electron Imaging, 2017.

[53] K. GmbH, Contact angle, Hamburg, Germany.

[54] B. Stöckle, D.Y.W. Ng, C. Meier, T. Paust, F. Bischoff, T. Diemant, R.J. Behm, K.E. Gottschalk, U. Ziener, T. Weil, Precise control of polydopamine film formation by electropolymerization, Macromolecular Symposia, Wiley Online Library, 2014, pp. 73-81.

[55] F. Bernsmann, J.-C. Voegel, V. Ball, Different synthesis methods allow to tune the permeability and permselectivity of dopamine–melanin films to electrochemical probes, Electrochimica Acta, 56 (2011) 3914-3919.

[56] G. Tan, Y. Liu, Y. Wu, K. Ouyang, L. Zhou, P. Yu, J. Liao, C. Ning, Electrically reversible redox-switchable polydopamine films for regulating cell behavior, Electrochimica Acta, 228 (2017) 343-350.

[57] N.M. Dimitrijevic, E. Rozhkova, T. Rajh, Dynamics of localized charges in dopamine-modified TiO2 and their effect on the formation of reactive oxygen species, Journal of the American Chemical Society, 131 (2009) 2893-2899.

[58] S. Hong, Y.S. Na, S. Choi, I.T. Song, W.Y. Kim, H. Lee, Non-covalent self-assembly and covalent polymerization co-contribute to polydopamine formation, Advanced Functional Materials, 22 (2012) 4711-4717.

[59] J.H. Kim, M. Lee, C.B. Park, Polydopamine as a biomimetic electron gate for artificial photosynthesis, Angewandte Chemie, 126 (2014) 6482-6486.

[60] F. Tan, M. Liu, S. Ren, Preparation of polydopamine-coated graphene oxide/Fe 3 O 4 imprinted nanoparticles for selective removal of fluoroquinolone antibiotics in water, Scientific reports, 7 (2017) 5735.

[61] M. Amiri, E. Amali, A. Nematollahzadeh, H. Salehniya, Poly-dopamine films: Voltammetric sensor for pH monitoring, Sensors and Actuators B: Chemical, 228 (2016) 53-58.

[62] P. Kanyong, S. Rawlinson, J. Davis, Fabrication and electrochemical characterization of polydopamine redox polymer modified screen-printed carbon electrode for the detection of guanine, Sensors and Actuators B: Chemical, 233 (2016) 528-534.

[63] K. Wu, T. Lian, Quantum confined colloidal nanorod heterostructures for solar-to-fuel conversion, Chemical Society Reviews, 45 (2016) 3781-3810.

[64] Y. Ben-Shahar, U. Banin, Hybrid semiconductor–metal nanorods as photocatalysts, Photoactive Semiconductor Nanocrystal Quantum Dots, Springer2017, pp. 149-174.

[65] M. Ambrico, P.F. Ambrico, A. Cardone, N.F. Della Vecchia, T. Ligonzo, S.R. Cicco, M.M. Talamo, A. Napolitano, V. Augelli, G.M.J. Farinola, Engineering polydopamine films with tailored behaviour for next-generation eumelanin-related hybrid devices, Materials Chemistry C, 1 (2013) 1018-1028.

[66] A.N. Patel, P.R. Unwin, J.V. Macpherson, Investigation of film formation properties during electrochemical oxidation of serotonin (5-HT) at polycrystalline boron doped diamond, Physical Chemistry Chemical Physics, 15 (2013) 18085-18092.

[67] B. Sarada, T.N. Rao, D. Tryk, A. Fujishima, Electrochemical oxidation of histamine and serotonin at highly boron-doped diamond electrodes, Analytical chemistry, 72 (2000) 1632-1638.

[68] G. Loget, J.B. Wood, K. Cho, A.R. Halpern, R.M. Corn, Electrodeposition of polydopamine thin films for DNA patterning and microarrays, Analytical chemistry, 85 (2013) 9991-9995.

[69] V. Ball, D. Del Frari, M. Michel, M.J. Buehler, V. Toniazzo, M.K. Singh, J. Gracio, D. Ruch, Deposition mechanism and properties of thin polydopamine films for high added value applications in surface science at the nanoscale, BioNanoScience, 2 (2012) 16-34.

[70] B.L. Hanssen, S. Siraj, D.K. Wong, Recent strategies to minimise fouling in electrochemical detection systems, Reviews in Analytical Chemistry, 35 (2016) 1-28.

[71] A. Cot, S. Lakard, J. Dejeu, P. Rougeot, C. Magnenet, B. Lakard, M. Gauthier, Electrosynthesis and characterization of polymer films on silicon substrates for applications in micromanipulation, Synthetic Metals, 162 (2012) 2370-2378.

[72] B. Lakard, G. Herlem, S. Lakard, B. Fahys, Ab initio study of the polymerization mechanism of poly (p-phenylenediamine), Journal of Molecular Structure: THEOCHEM, 638 (2003) 177-187.

[73] X. Lu, H. Mao, D. Chao, X. Zhao, W. Zhang, Y. Wei, Preparation and characterization of poly (o-phenylenediamine) microrods using ferric chloride as an oxidant, Materials Letters, 61 (2007) 1400-1403.

[74] G.M. do Nascimento, R.H. Sestrem, M.L. Temperini, Structural characterization of poly-para-phenylenediamine–montmorillonite clay nanocomposites, Synthetic metals, 160 (2010) 2397-2403.

[75] W.M. Haynes, CRC handbook of chemistry and physics, CRC press2014.

[76] T. Huang, Z. Liu, Y. Li, Y. Li, L. Chao, C. Chen, Y. Tan, Q. Xie, S. Yao, Y. Wu, Oxidative polymerization of 5-hydroxytryptamine to physically and chemically immobilize glucose oxidase for electrochemical biosensing, Analytica chimica acta, 1013 (2018) 26-35.

[77] M.Z. Wrona, G. Dryhurst, Interactions of 5-hydroxytryptamine with oxidative enzymes, Biochemical Pharmacology, 41 (1991) 1145-1162.

[78] R. Mrówczyński, R. Markiewicz, J. Liebscher, Chemistry of polydopamine analogues, Polymer International, 65 (2016) 1288-1299.

[79] S. Harvey, D.Y.W. Ng, J. Szelwicka, L. Hueske, L. Veith, M. Raabe, I. Lieberwirth, G. Fytas, K. Wunderlich, T. Weil, Facile synthesis of ultrasmall polydopamine-polyethylene glycol nanoparticles for cellular delivery, Biointerphases, 13 (2018) 06D407.

[80] Y. Li, M. Liu, C. Xiang, Q. Xie, S. Yao, Electrochemical quartz crystal microbalance study on growth and property of the polymer deposit at gold electrodes during oxidation of dopamine in aqueous solutions, Thin Solid Films, 497 (2006) 270-278.

[81] A. De Bruyne, J.-L. Delplancke, R. Winand, Electropolymerization of poly (2-vinylpyridine) films on zinc, Journal of applied electrochemistry, 25 (1995) 284-290.

[82] UCLA, Infrared Spectroscopy Table, 2001.

[83] T. López, P. Quintana, J. Martínez, D. Esquivel, Stabilization of dopamine in nanosilica sol–gel matrix to be used as a controlled drug delivery system, Journal of Non-Crystalline Solids, 353 (2007) 987-989.

[84] X.G. Li, M.R. Huang, R.F. Chen, Y. Jin, Y.L. Yang, Preparation and characterization of poly (p-phenylenediamine-co-xylidine), Journal of applied polymer science, 81 (2001) 3107-3116.

[85] R. Gupta, S. Sanotra, H.N. Sheikh, B.L. Kalsotra, Room temperature aqueous phase synthesis and characterization of novel nano-sized coordination polymers composed of copper (II), nickel (II), and zinc (II) metal ions with p-phenylenediamine (PPD) as the bridging ligand, Journal of Nanostructure in Chemistry, 3 (2013) 41.

[86] I.L. Medintz, M.H. Stewart, S.A. Trammell, K. Susumu, J.B. Delehanty, B.C. Mei, J.S. Melinger, J.B. Blanco-Canosa, P.E. Dawson, H. Mattoussi, Quantum-dot/dopamine bioconjugates function as redox coupled assemblies for in vitro and intracellular pH sensing, Nature materials, 9 (2010) 676.

[87] S. Chumillas, T. Palomäki, M. Zhang, T. Laurila, V. Climent, J.M. Feliu, Analysis of catechol, 4-methylcatechol and dopamine electrochemical reactions on different substrate materials and pH conditions, Electrochimica Acta, 292 (2018) 309-321.

[88] C.D. Motchenbacher, J.A. Connelly, Low noise electronic system design, Wiley1993.

[89] E. Laviron, Electrochemical reactions with protonations at equilibrium: part X. The kinetics of the p-benzoquinone/hydroquinone couple on a platinum electrode, Journal of electroanalytical chemistry interfacial electrochemistry, 164 (1984) 213-227.

[90] D.A. Skoog, D.M. West, F.J. Holler, S. Crouch, Fundamentals of analytical chemistry, Nelson Education2013.

[91] M.D. Ryan, A. Yueh, W.Y. Chen, The electrochemical oxidation of substituted catechols, Journal of The Electrochemical Society, 127 (1980) 1489-1495.

[92] M.R. Deakin, P.M. Kovach, K. Stutts, R.M. Wightman, Heterogeneous mechanisms of the oxidation of catechols and ascorbic acid at carbon electrodes, Analytical chemistry, 58 (1986) 1474-1480.

[93] P. Daubinger, J. Kieninger, T. Unmüssig, G.A. Urban, Electrochemical characteristics of nanostructured platinum electrodes–a cyclic voltammetry study, Physical Chemistry Chemical Physics, 16 (2014) 8392-8399.

[94] B. Iranpour, Gold electrode electrochemistry in protein based solar cells, University of British Columbia, 2012.

[95] V. Bhanu, K. Kishore, Role of oxygen in polymerization reactions, Chemical Reviews, 91 (1991) 99-117.

[96] R.A. Zangmeister, T.A. Morris, M.J. Tarlov, Characterization of polydopamine thin films deposited at short times by autoxidation of dopamine, Langmuir, 29 (2013) 8619-8628.

[97] D. Belanger, J. Pinson, Electrografting: a powerful method for surface modification, Chemical Society Reviews, 40 (2011) 3995-4048.

[98] N. Singh, J. Nayak, K. Patel, S.K. Sahoo, R. Kumar, Electrochemical impedance spectroscopy reveals a new mechanism based on competitive binding between Tris and protein on a conductive biomimetic polydopamine surface, Physical Chemistry Chemical Physics, 20 (2018) 25812-25821.

8 LIST OF FIGURES